Morten Hovind
Kjetil Lien

Parametric Study of Mechanical Properties for Saline Frozen Clay

June 2020

NTNU
Norwegian University of
Science and Technology
Faculty of Engineering
Department of Civil and Environmental Engineering

Master's thesis

2020

Morten Hovind, Kjetil Lien

Master's thesis

NTNU
Norwegian University of
Science and Technology

NTNU
Norwegian University of
Science and Technology

NTNU

Norwegian University of
Science and Technology

Parametric Study of Mechanical Properties for Saline Frozen Clay

Morten Hovind
Kjetil Lien

Civil and Environmental Engineering
Submission date: June 2020
Supervisor: Rao Martand Singh, IBM
Co-supervisor: Chuangxin Lyu, IBM

Norwegian University of Science and Technology
Department of Civil and Environmental Engineering

Abstract

Frozen ground is soil or rock below 0 °C and a natural composite of solid particles, ice, water and air. When the soil freezes, the ice cements the soil particles together, leading to increased strength and lowered permeability. Temperature, salinity, strain rate and soil composition control the mechanical behaviour of frozen soil. The mechanical behaviour is particularly susceptible to alteration at temperatures near the point of thaw, where phase changes occur. Thawing ground may initiate landslide, increased frost heave and additional settlements. Thus, understanding the effect of each parameter on soil strength is important for geotechnical engineering in cold regions.

Numerous studies have been conducted to investigate which parameters impact the behaviour of frozen soil. However, the amount of research on saline frozen clay is limited, especially at subzero temperatures close to 0 °C. Additionally, few studies have been performed on pore water response in frozen fine-grained soils. This thesis conducts triaxial testing on frozen saline Onsøy clay to examine the effects of different parameters on soil strength and pore water response.

The results show that temperature is the most important factor considering both soil strength and pore water response in frozen soil. Strength increases linearly with decreasing temperature in the tested temperature range. Furthermore, salinity, strain rate and mean effective stress was found to influence soil strength. Pore water measurements recorded suction in several tests, reasons for suction in frozen soil is proposed and discussed. Lastly, a regression analysis is constructed to summarize the parametric effects on saline frozen clay.

Sammendrag

Frossen grunn er jord eller stein med temperatur under 0 °C og betegnes som et naturlig kompositt bestående av mineralkorn, is, vann og luft. Når jorden fryser, sementerer isen jordpartiklene sammen, noe som fører til økt styrke og senket permeabilitet. Temperatur, saltinnhold, tøyningshastighet og jordsammensetning kontrollerer den mekaniske oppførselen til frossen jord. Den mekaniske oppførselen er spesielt utsatt for forandring ved temperaturer nær tinepunktet, hvor faseendringer finner sted. Tining av frossen grunn kan føre til skred, telehiv og ytterligere setninger. Det er derfor viktig å forstå påvirkningen til de ulike parametrene på den frosne jordens styrke.

En rekke studier har blitt utført for å undersøke hvilke parametere som påvirker den mekaniske oppførselen til frossen jord. Det er derimot kun utført et begrenset antall studier på saltholdig frossen leire, spesielt ved temperaturer nært tinepunktet. I tillegg er det utført få studier på oppbyggingen av poretrykk i finkornet frossen leire. Denne oppgaven utfører treaksialforsøk på frossen saltholdig leire fra Onsøy for å undersøke hvordan styrke og poretrykk påvirkes av ulike parametere.

Resultatene viser at temperatur er den mest avgjørende faktoren når det kommer til styrke og oppbygging av poretrykk i frossen jord. Styrken i jorda øker lineært med avtagende temperatur i det testede temperaturområdet. Videre er det bevist at saltinnhold, tøyningshastighet og gjennomsnittlig effektivspenning påvirker den mekaniske oppførselen til frossen jord. Porevannsmålinger registrerte sug for flere tester, og det blir diskutert hvorfor dette kan oppstå i frossen jord. Til slutt er det utført en regresjonsanalyse for å oppsummere de parametriske effektene på saltholdig frossen leire.

Preface

This master thesis is written in conjunction with the course *TBA 4900 Geotechnical Engineering, Master Thesis*. It is written as a part of a 5 year MSc in Civil and Environmental Engineering at the Norwegian University of Science and Technology (NTNU). The thesis was carried out during the spring of 2020, and is connected to a science project called Nunataryuk.

First and foremost, we would like to thank PhD Candidate Chuangxin Lyu, who in addition to developing this thesis, has helped us with laboratory work and academic knowledge. We would also like to give our gratitude to our supervisors, first Prof. Gudmund Reidar Eiksund, later Prof. Rao Martand Singh, for their guidance throughout the whole working period. Finally, we would like to thank our fellow students for all the good advice, help and memories you have given us.

It is further assumed that the reader has basic knowledge of classic geotechnics.

Table of Contents

List of Tables

List of Figures

Abbreviations

ε_a	=	axial strain
ε_v	=	volumetric strain
$\dot{\varepsilon}$	=	strain rate
σ_1	=	axial pressure
σ_3	=	confining pressure
θ	=	temperature in °C
ϕ	=	friction angle
A	=	cross-section area
A_0	=	initial cross-section area at zero strain
A_{piston}	=	cross-section area of piston
a	=	attraction
i_r	=	iceness ratio
p'	=	effective mean stress
p_w	=	pore water pressure
p_0	=	preconsolidation pressure
q	=	deviatoric stress
R^2	=	coefficient of determination
S_n	=	salinity
T	=	temperature
T_c	=	temperature where all the unbound water is frozen
T_f	=	freezing temperature
T_{sc}	=	supercooled temperature
ΔT	=	temperature shift
u	=	pore pressure
V_v	=	volume of voids
V_s	=	volume of solids
w	=	water content
w_u	=	unfrozen water content
w_i	=	ice content
w_L	=	liquid limit
w_P	=	plasticity limit

Chapter 1

Introduction

1.1 Background

Frozen ground is soil or rock below 0 °C, and the definition is merely based on temperature. Natural frozen soil is usually found in colder climates, and most often as permafrost. Permafrost is defined as an area where the ground temperature inferior 0 °C two years in a row.

Frozen soil is a natural composite consisting of solid particles, ice, water and air. Together, these components constitute a complex material, where the mechanical properties are highly dependent on temperature and stress level. When the soil freezes, the ice binds the soil particles together. The strength of the soil increases while permeability decreases. These attributes allow, for instance, ground freezing to be used to overcome structural problems such as excavations, structural underpinning and to control groundwater flow.

Over the last decades, global warming and increased human activity in cold regions have led to thawing of permafrost and increased soil temperature. United Nations' climate report claims that high altitude permafrost areas are particularly vulnerable to climate change, and are currently experiencing a temperature change twice the global average (Hock and Rasul, 2019). Hanssen-Bauer et al. (2019) has calculated the air temperature on Svalbard to rise 6.2 °C until the next decade, given that the current emission level continues to grow until 2040. This may create geotechnical challenges, and the need for knowledge of frozen ground technology is increasing.

Construction work in cold regions has become more common in recent decades, and along with the construction of more advanced structures, the interest relative to frozen ground engineering has greatly increased (Jean-Sebastien L'Heureux, 2020). This has led to significant advances being made in frozen ground technology, and the application of ground freezing in geotechnical projects continues to grow.

Several studies have been carried out to investigate which parameters influence the behaviour of frozen soil (Hivon and Sego, 1995; Li et al., 2004; Yamamoto and Springman, 2014). Several calculation models have been proposed, but there is currently no common agreement on which of these models to be used (Tsegaye, 2014; Ghoreishian Amiri et al., 2016). The phase relationship between ice and water makes frozen soil a complex material, which has to add some extra parameters compared to unfrozen soil, regarding design. Especially temperature and salinity are parameters that control the phase relation happening in the soil at subzero temperatures and need to be accounted for when working with unfrozen soil.

The amount of unfrozen water in frozen soil has proven to be an important factor when calculating soil response. Presence of solutes, such as different types of salts in the pore water, alters the unfrozen water content and is thus of interest when investigating frozen soil. The number of studies performed on saline frozen clay is limited, and it is therefore considered necessary to further investigate which parameters alters the behaviour of this material.

1.2 Objectives

The main objectives of this master thesis are:

1. To study pore water response in saline frozen clay and its correlation to different parameters.
2. To investigate which parameters affect the mechanical behaviour of saline frozen clay, and the effect of these parameters.
3. To present a regression analysis to summarize the parametric effects on saline frozen clay.

1.3 Approach

To achieve the objectives of this thesis, a literature study describing factors affecting the mechanical behaviour of frozen soil shall be performed. Furthermore, a series of undrained

shear tests shall be carried out on artificially frozen Onsøy clay. The tests will be performed on -3 °C, -5 °C and -10 °C with varying test parameters to ensure a broad set of data. The tests will be carried out using a specialized triaxial cell with temperature control. Lastly, the test results will be analysed and compared with relevant literature along with a regression analysis. This will form the basis of understanding which parameters affect the mechanical behaviour of saline frozen clay and the effect of each parameter.

1.4 Limitations

Due to limited time and equipment, this master thesis deals only with shear tests on saline frozen clay at three different temperatures. Ideally, it would be useful to investigate several soil types along with more varied temperatures to obtain a broader set of data.

1.5 Outline

The thesis is structured as follows:

Chapter 2 provides a brief introduction to the basic theory that deals with frozen ground mechanics. The chapter starts by presenting the characterization of frozen soil, along with a brief description of some calculation models used to predict the unfrozen water content in the soil. Lastly, settlements due to thawing of frozen ground are presented.

Chapter 3 is a literature review that deals with the mechanical behaviour of frozen soil. Relevant test data from parametric studies are presented, and observations regarding various parameter effects are discussed and analyzed. Lastly, the theory regarding area correction is presented to be used in the treatment of this thesis´ test results.

Chapter 4 introduces the testing procedure. The test plan is presented and the triaxial equipment is illustrated and described. Lastly, a standardized test procedure is presented and possible errors are described.

Chapter 5 describes the Onsøy soil through index parameters and deposition history.

Chapter 6 presents results from the triaxial testing and discuss these in the aim of the objectives.

Chapter 7 finishes the discussion and states the conclusions that are drawn. Lastly, recommendations for future work on the subject is suggested.

Chapter 2

Basic Theory

This chapter briefly introduces basic theory considering frozen soil mechanics and is based on the book *Frozen Ground Engineering* by Andersland and Ladanyi (2004). The topics reviewed are chosen to give an insight into frozen soil behaviour and which parameters that affect the strength of the frozen soil.

2.1 Frozen Ground

Frozen ground is defined as soil or rock below 0 °C and is merely based on temperature. It is well known that frozen soil is stronger than unfrozen soil due to ice cementing the soil or rock particles together. Additionally, ice reduces permeability rendering the soil impervious to water seepage. Frozen ground support systems are applied worldwide to solve a variety of construction problems in a cheap and effective manner. Freezing of soil may, for example, be used as temporary earth support or to control groundwater in challenging areas.

Frozen soil is a system consisting of four components: soil particles, ice, water and gas, as illustrated by Figure 2.1. Due to intermolecular forces between water and solids, unfrozen water may exist in the soil for temperatures way below 0 °C. The amount of unfrozen water depends on the capillary forces, absorption forces, temperature and presence of dissolved solutes in the soil. The soil particles vary in size and shape and are surrounded by a thin film of unfrozen water. The water film around the soil particles are considered as bound

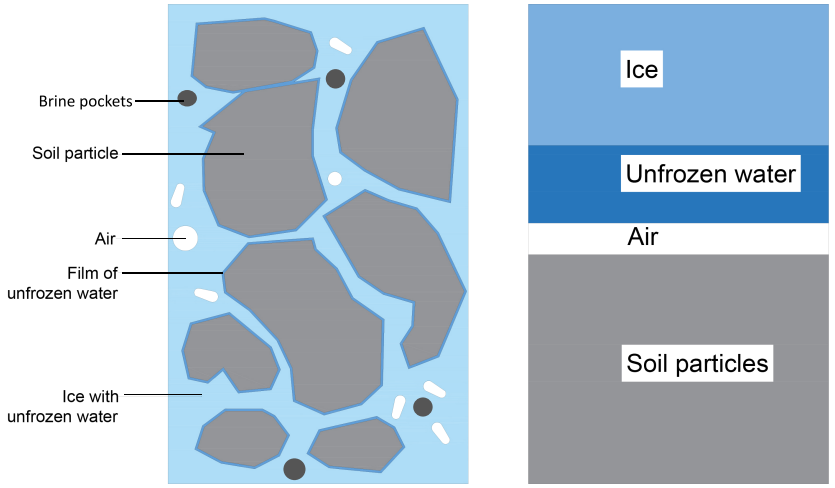

Figure 2.1: Components of unsaturated ice rich frozen soil. Modified after Ting et al. (1983).

water. The voids are filled with air, unfrozen water and ice. As the frozen soil experiences thawing, ice will melt, making the soil a system of three components instead of four.

A typical freezing process of soil is shown in Figure 2.2. Ice formation in a soil involves freezing of pore water starting at a supercooled temperature, T_{sc} below 0 °C. At this temperature, the water is in a metastable equilibrium until some of the water is transformed into ice triggered by nucleation centres. The phase transition from water to ice releases latent heat causing freezing of unbound water to stabilize at the freezing point T_f. The freezing point is usually close to 0 °C, but can be as low as -5 °C for fine-grained soils with large specific surface areas. The release of latent heat, as water freezes, continues to slow the cooling process until temperature T_e is reached. At temperature T_e, all of the unbound water is frozen along with most of the bound water. This temperature is usually as low as -70 °C, and the frozen soil can hold a significant amount of unfrozen water down to this point.

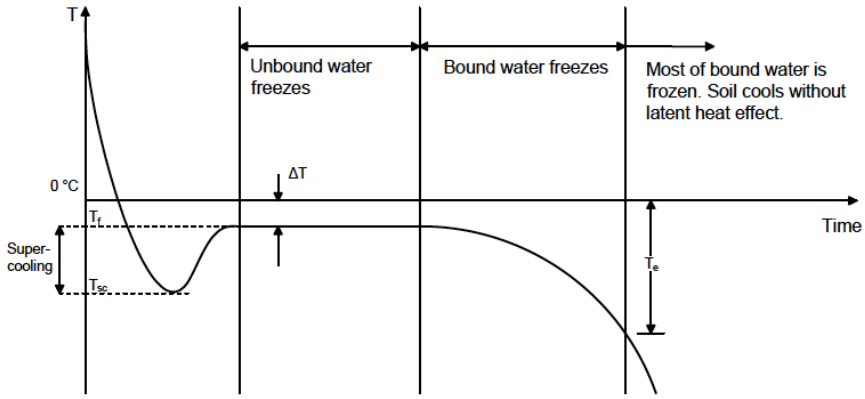

Figure 2.2: Cooling curve for water in soil. Modified after Andersland and Ladanyi (2004).

2.2 Unfrozen Water Content

The water-ice relationship varies with mineral composition, specific surface area of the particles, the presence of solutes and temperature. Fine-grained soils with large surface areas have a greater quantity of unfrozen water than soil consisting of coarser grains. Water present in the soil is divided into two categories: unfrozen water, w_u, and ice, w_i, as shown in Equation 2.1.

$$w = w_u + w_i \tag{2.1}$$

To calculate unfrozen water content Tice et al. (1976) produced the expression shown in Equation 2.2, which is derived from a large amount of experimental data for several soil types.

$$w_u = \alpha\theta^{\beta} \tag{2.2}$$

where α and β are characteristic soil parameters and θ is temperature as positive numbers in °C below the freezing point.

The amount of unfrozen water decreases rapidly at subzero temperatures close to 0 °C, as the unbound water in the voids freezes. However, freezing of bound water requires significantly lower temperatures, and may reach temperatures down to -70 °C before all the bound water is frozen. Some typical phase composition curves are shown in Figure 2.3, displaying the rapid decrease of unfrozen water just below the freezing point, followed by a stabilization at colder temperatures.

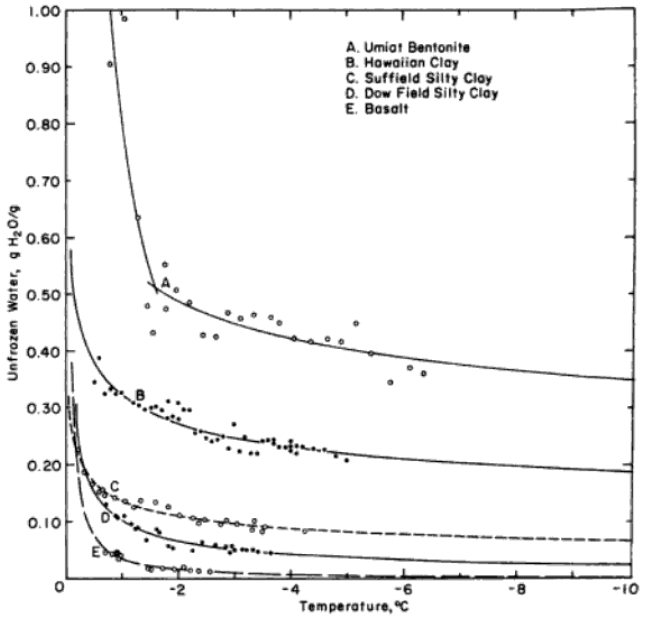

Figure 2.3: Phase composition curves for five different soils. (Anderson and Morgenstern, 1973)

Numerous methods have been developed to estimate the unfrozen water content in frozen soils. Nuclear magnetic resonance, time-domain reflectometry and dilatometry are examples of experimental tests to determine unfrozen water content (Patterson and Smith, 1985; Flerchinger et al., 2006; Tang et al., 2018). The methods vary in complexity, accuracy and rapidity, and they all use different boundary conditions and assumptions. In addition to this, researchers have attempted to produce empirical expressions to predict the unfrozen water content for different soils, given temperature and salinity. For example, Equation 2.2 uses the liquid limit to determine tabulated parameters, α and β, which are used to calculate the unfrozen water content, w_u (Andersland and Ladanyi, 2004). In the next section, another example including salinity is introduced, see Equation 2.7.

For most engineering applications the liquid limit method is widely accepted, however other procedures should be applied for saline soils.

2.3 Salinity

Unfrozen water content varies with the presence of solutes. Dissolved salts within the soil pores is an example of this phenomenon. The presence of dissolved salts in the soil decreases the freezing point of the pore water, resulting in greater amounts of unfrozen water below freezing temperatures. The effect varies with the types of solutes. For instance, the eutectic point for an $H_2O-NaCl$ system is -21.2 °C ($\simeq$ 23,3 % NaCl), while it is -51 °C for an $H_2O-CaCl_2$ system. Figure 2.4 shows the phase diagram for sodium chloride and water. At temperatures colder than the eutectic point, the solution consists of merely ice and hydro halite, which means that no liquid is present.

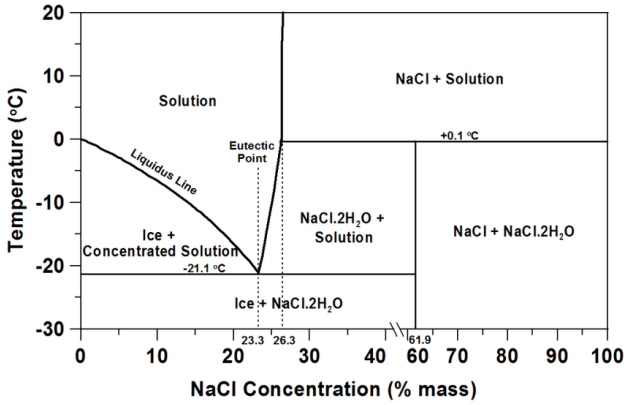

Figure 2.4: Phase diagram for a $H_2O-NaCl$ solution. (Farnam et al., 2014)

Banin and Anderson (1974) researched how salinity in soil affects the freezing temperature of the pore water. As pore water freezes, the salt solutes are forced into a smaller and smaller volume since the soluble salts are excluded from the ice matrix. This leads to an increasing salt concentration in the remaining pore water, resulting in a lowered freezing point for the remaining solute. The freezing temperature, T_f, accounting for salt content, can be calculated using the following expression (Patterson and Smith, 1983).

$$T_f = T_i + \frac{S_n}{A(\frac{w_u}{w})} \tag{2.3}$$

where S_n is the salinity in ppt NaCl, A is a constant equal to -17.04 g/L°C^{-1}, T_i is the temperature at which unfrozen water content in nonsaline soil equals w_u and w is the total water content. This is a useful method if the relationship between w_u and temperature is known for the given soil. However, if the relationship between w_u and temperature is unknown, Velli and Grishin (1983) developed an empirical equation calculating temperature

shift, ΔT, due to salinity by applying Equation 2.4.

$$\Delta T = T_k(\frac{S_n}{1000 + S_n}) \tag{2.4}$$

where S_n is salinity in ppt NaCl and T_k is a reference temperature dependant on the type of salt, see Table 2.1.

Table 2.1: Reference temperature, Velli and Grishin (1983).

Salt type	T_k
Sea salt	57.0 °C
NaCl	62.0 °C
$CaCl_2$	32.5 °C

The ice fraction (or iceness ratio), i_r, is defined as the ratio of ice to the total water in the soil.

$$i_r = \frac{w_i}{w} = 1 - \frac{w_u}{w} \tag{2.5}$$

For saline soil, the ice fraction may be derived based on temperature and salinity as shown in Equation 2.6 (Ono, 1975):

$$i_r = 1 - \frac{S_n}{1000}\left(1 - \frac{54.11}{T}\right) \tag{2.6}$$

Combining Equation 2.5 and 2.6 gives the expression of unfrozen water content ratio, w_u/w:

$$\frac{w_u}{w} = \frac{S_n}{1000}(1 - \frac{54.11}{T}) \tag{2.7}$$

Using Equation 2.7, the unfrozen water content may be estimated given temperature and salinity. Furthermore, by constraining the water content ratio to equal 1, the initial freezing point of the soil may be calculated.

2.4 Thawing

Thawing of frozen ground is an important aspect when designing structures in cold regions. When frozen ground thaws, the ice will melt and the soil skeleton must adapt to a new void ratio equilibrium, resulting in settlements as illustrated by Figure 2.5.

Settlements in unfrozen ground are often results of weak bearing soils, changes in moisture content, maturing of vegetation or dissipation of excess water (consolidation). A new aspect is introduced in designing for settlements in frozen soil, specifically melting of ice. The volume change due to thawing of soil depends on consolidation and structural changes that occurred during the last freezing cycle.

A simple procedure to roughly measure the thaw settlement is to place a frozen soil sample in a container and allow it to thaw in an uncontrolled manner. The excess water collected corresponds to the thaw settlement. Another rough estimation of the thaw settlement may be based on observation of the ice content in the soil, but this method may lead to considerable errors. The most reliable method to calculate the thaw settlements is to conduct a triaxial test, where field environment is matched and in-situ conditions are achieved.

Figure 2.5: Settlements due to thawing of ice-rich permafrost in Fairbanks. Photo by Romanovsky (2018).

A typical void ratio, V_v/V_s, vs. pressure curve are shown in Figure 2.6. When the soil is frozen, the void ratio will slowly decrease with increasing pressure (from *a* to *b*). As the soil sample starts to thaw, around 0 °C at pressure σ_0, the void ratio will drop significantly due to phase change, ice to water. Thus, drainage of excess unfrozen water (*b* to *c*) occurs. The overburden pressure, σ_0, is commonly based on the in-situ stresses in the test sample. Stresses beyond the overburden pressure cause water to slowly dissipate (*c* to *d*). As presented in Figure 2.6, a large amount of volume change occurs around 0 °C, making it an important aspect to consider when designing for frozen soil.

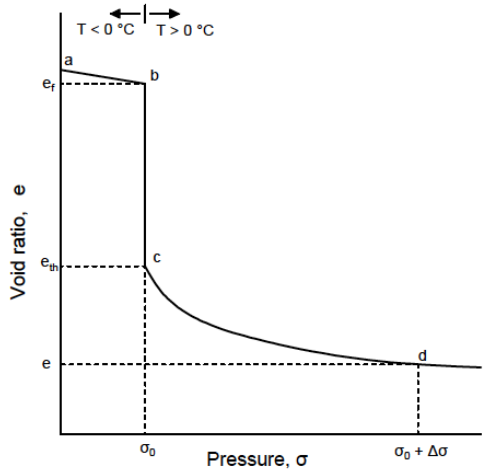

Figure 2.6: Common void ratio vs. pressure curve for thawing frozen soil. Modified after Andersland and Ladanyi (2004)

Chapter 3

Literature Review

The following chapter presents a literature review on parametric studies of frozen soil. Results from laboratory work found in relevant literature are presented and discussed to gain a broad knowledge about which parameters that affect pore water pressure and shear strength in frozen soil. Lastly, literature upon area correction are presented.

3.1 Pore Water Pressure in Partially Frozen Soils

Pore water pressure measurements in partially frozen soil is required to apply reliable effective stress based constitutive models or similar concepts for geotechnical analysis and design. According to Kia (2012), previous analysis' has mainly treated frozen soil as a Tresca or frictional-cohesive material, both of which use total stress concepts. A total stress approach does not represent the actual stresses when a water phase is present.

Unfrozen saturated soil is composed of soil grains and water. Without soil grains, water will carry the entire load. Without water, the soil skeleton carries total load. Equations including pore water pressure determine what part of the load is carried by water. Similarly, a partially frozen soil is a multi-phase coupled system consisting of ice, water and soil particles. Therefore, a more realistic rendition may be to conduct an effective stress analysis using effective stress material properties. This requires measurements of pore-pressure distribution in the soil.

Furthermore, analysing creep in frozen soils should consider pore-water generation and dissipation. Frozen soils with a continuous water phase has long term resistance and the deformation is governed by effective stress material properties. Again, assessing pore pressure distribution is needed.

3.1.1 Measuring Pore Water Pressure

When a saturated soil freezes, hydraulic and mechanical properties change as pore water freezes to ice. The ice matrix increases cohesion and tensile strength, while hydraulic conductivity and compressibility is reduced. This provides challenges in measuring pore water pressure. A range of methods has been used to study pore water in partially frozen soils.

Kia (2012) developed a Filter-less Rigid Piezometer (FRP) as a method to measure pore water pressure. With FRP, the interface between the piezometer fluid and pore water is within the soil, avoiding the use of a filter. The device is saturated with mineral oil. Furthermore, the PhD thesis states that flexible piezometers modify measured pressure due to softening of the pore fluid phase. FRP shall also be able to measure the pore pressure when only a small volume of unfrozen pore water is present.

Arenson and Springman (2005) used pore pressure transducers at the top and bottom of the triaxial test apparatus to test ice-rich permafrost. In these tests, about 20% showed a slight difference in behaviour between the top and bottom, or sudden pore pressure changes. Some of the test specimens had high air content, and air voids seemed to contribute to this behaviour.

Wang and Nishimura (2017) conducted tests on high-plasticity Kasaoka clay. The study assumed that the effective stress path for a frozen sample is the same as for an unfrozen sample if consolidation and shear strain history is similar. By using this idea, it is possible to avoid the challenges of experimentally measurements of pore pressure in frozen samples.

A miniature pore pressure transducer was used by Zhang et al. (2016). This small transducer has a porous tip filled with antifreeze-liquid and may be inserted into the sample. Before employing this method, two other methods were attempted. (1) In the first attempt, a pressure device was used to measure pore water pressure in the porous stone at the specimen base. (2) The second method installed pressure transducers connected to a porous tip along the height of the sample. The paper explained that attempt (1) and (2) failed due to a freezing film forming and hindering pressure transmission. Meanwhile, the miniature

pore pressure transducer produced satisfactory results.

3.1.2 Variables Affecting Pore Water Pressure

At low temperatures, frozen soil can be characterized as a solid material, since most of the water is frozen to ice. Because of this, most researchers have considered the deformation of frozen soil under external load to be attributed to creep. However, even below the freezing point a considerable amount of unfrozen water still exists. Investigating pore water response is important as it is closely connected to soil deformation, especially during the consolidation phase. Studies performed by Zhang et al. (2016) show that the pore water behaviour of frozen soil at subzero temperatures close to 0 °C differs significantly from unfrozen soil. Some test results from triaxial testing on silty clay are shown in Figure 3.1, where pore pressure and strain are presented by pink and blue lines respectively. The tests allowed drainage from the top during testing.

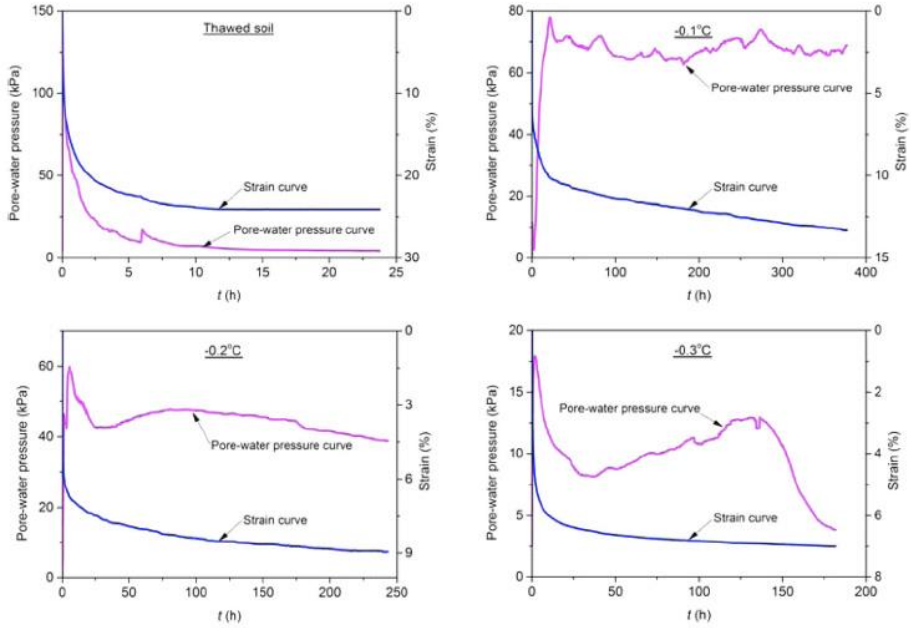

Figure 3.1: Pore water pressure at subzero temperatures close to 0 °C. (Zhang et al., 2016)

The results from Zhang show that for unfrozen soil the pore pressure slowly decreases over time. However, for tests performed at subzero temperatures, the pore pressure shows a fluctuation phenomenon. Zhang believes this is connected to the combined influence of solid matrix deformation and the migration of unfrozen water. Zhang also states that

an exponential relationship between the soil temperature and pore water pressure exists, where decreasing temperature lower the peak pore water pressure until it reaches a stable value.

Hazirbaba et al. (2011) investigated pore water pressure response in silt subjected to strain-controlled undrained cyclic triaxial testing. The study is of significance because it recorded very little to negative pore pressure at -0.2 °C. The suction appears when a thermal gradient is applied. Hazirbaba believes the interaction between frozen and unfrozen water near freezing temperatures causes suction, as water migrates through soil pores to the growing ice lens. Redistribution of unfrozen pore water may depend on shear strain level since suction occurred for certain strain levels, as argued by Hazirbaba.

3.2 Parameters Affecting Undrained Shear Strength

This section gives a literary review of different effects which influences the strength of frozen soil. The goal is to isolate each one to understand trends and its relations to different parameters.

3.2.1 Confining Pressure and Mean Effective Stress

Chamberlain et al. (1972) performed triaxial tests on Ottawa sand at -12 °C with a strain rate of 1.6 %/h. This study showed that confining pressure, σ_3, greatly influenced shear strength. Furthermore, Wang and Nishimura (2017) carried out triaxial testing of frozen and unfrozen silty clay and found a linear dependency between strength and confining pressure. The clay samples were fully saturated and isotropic normally consolidated to 100, 200 or 400 kPa. Results from Wang are presented in Figure 3.2.

Additionally, it is of interest to review the behaviour of ice under confining pressure to better understand the behaviour of frozen soil. Studies of confining pressure on poly-crystalline ice by Sego and Morgenstern (1985) show that compressive strength does not change with confinement stress for strain rates in the ductile range. However, in the brittle range and under specific loading conditions, confinement stress may influence the compressive strength (Smith and Schulson, 1993).

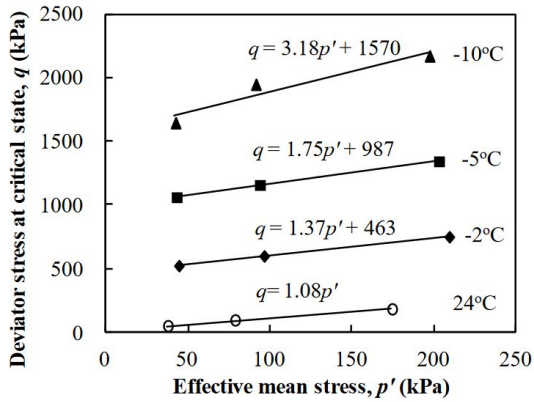

Figure 3.2: Linear dependency between q and p'. Tested with a strain rate of 0.6%/h. (Wang and Nishimura, 2017)

3.2.2 Unfrozen Water Content and Salinity

Frozen soil contains a sizeable amount of liquid water in bound form. Yong (1965) related unfrozen water content to initial water content through experimentation. Results show that clay has more unfrozen water than silt at similar initial water content and temperature. It is expected for sand to have even less than silt.

Salinity alters the mechanical properties of frozen soil. Studies on the effect of increased salinity and temperature show that the soil experiences a significant loss of strength (Hivon and Sego, 1995), which is related to the increasing unfrozen water content. Figure 3.3 shows the distribution of volumetric unfrozen water content for a frozen silty sand. Furthermore, saline pore water has been identified to reduce the rate of frost heave in fine-

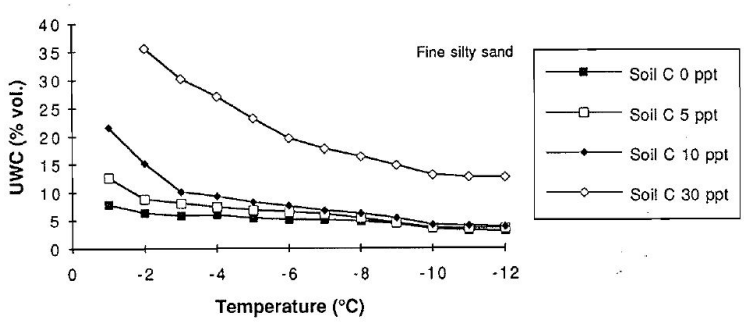

Figure 3.3: Volumetric unfrozen water content vs. temperature for a fine silty sand. (Hivon and Sego, 1995)

grained soils (Chamberlain, 1983). Nixon (1988) did a literature review on Soviet laboratory and field testing which indicates that soils with salinity exceeding 10-20 ppt. may reduce the foundation bearing capacity by a factor of 2-3.

Figure 3.4 shows experimental data from Ogata et al. (1983), Hivon and Sego (1995) and Pharr and Merwin (1985). The figure displays that the relationship between strength and salinity strongly depends on the soil type. Fine-grained soils exhibit a linear reduction in strength as salinity increases. Coarse-grained soils display a proportional reduction in strength as salinity increases. Additionally, strength in coarse-grained soils appears to be more sensitive to salinity than fine-grained soils.

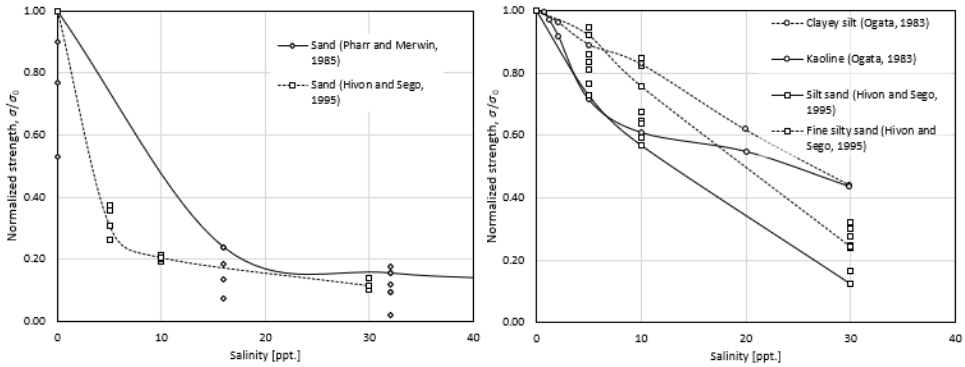

(a) Coarse-grained soils

(b) Fine-grained soils

Figure 3.4: Strength compared to salinity. Strength is normalized by dividing recorded strength at given salinity with strength at zero salinity, $\sigma(S)/\sigma(S = 0)$. Experimental data from Ogata et al. (1983), Hivon and Sego (1995) and Pharr and Merwin (1985).

Konrad and McCammon (1990) studied the relationship between solute rejection and freezing conditions. It was found that no solutes are rejected for a rate of cooling above 3°C/day in a clayey silt. However, for rates lower than 0.1°C/day, more than 90% of the solutes are rejected. An experiment on the freezing process of saline coarse-grained sand conducted by Arenson and Sego (2006), showed pockets of high salinity water trapped in the pores. This indicates that coarse-grained frozen soil has a majority of its unfrozen water in the middle of the pore space, while for fine-grained frozen soil a large amount of the unfrozen water is bound to the soil particles. Hivon and Sego (1995) experienced more ductile deformation in fine-grained frozen soil than for coarse-grained due to water being present between the soil particles during deformation.

3.2.3 Temperature

Temperature dependence is one of the main differences between frozen and unfrozen soil. For instance, permafrost in the Swiss Alps shows rapidly increased deformation during the melting season and a deceleration during the winter (Ikeda et al., 2008). Additionally, from 2001 to 2014, 26% of slope failures happen during the thaw season in Hokkaido, Japan (Ishikawa et al., 2015). This may prove a risk for populations in mountainous areas, as the increased temperature may initiate landslides.

Equation 3.1 is an empirical equation created by Li et al. (2004), to estimate the compressive strength of frozen clay. The equation takes into account temperature and strain rate, both of which are widely known to influence strength.

$$\sigma_m = \sigma_0 \left(\frac{\theta}{\theta_0}\right)^i \left(\frac{\dot{\varepsilon}}{\dot{\varepsilon}_0}\right)^m \tag{3.1}$$

where σ_m is the compressive strength, θ_0 = -1 °C is a dimensionless reference temperature, $\dot{\varepsilon}_0$ = 1 s^{-1} is a dimensionless reference strain rate, σ_0 is the compressive strength at θ = -1 °C and $\dot{\varepsilon}$ = 1 s^{-1} in MPa, and i and m are parameters.

Of these two parameters, temperature proved to be the one that influenced the most. The study also discovered that the compressive strength increases linearly with decreasing temperature, for a constant strain rate. Furthermore, climbing temperature close to the thawing

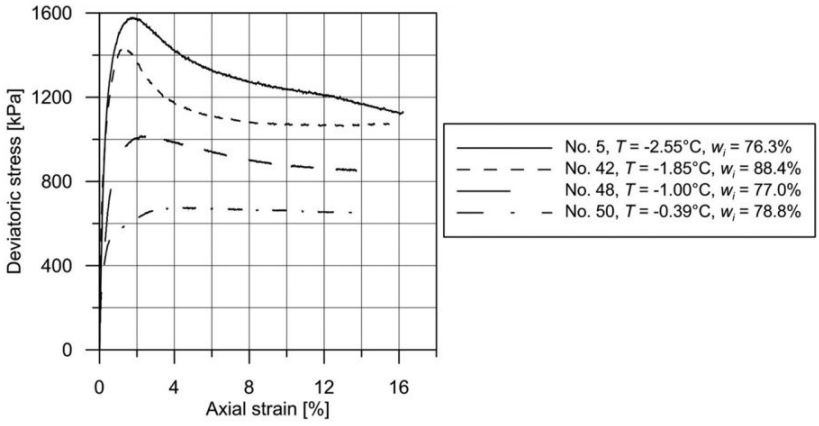

Figure 3.5: Results from triaxial tests performed on ice-rich soil samples with axial strain rate of 0.018 %/h. (Yamamoto and Springman, 2014)

point alters the mechanical behaviour of frozen soil, for instance by increasing the ductility (Yamamoto and Springman, 2014; Rist and Murrell, 1994). Stress-strain curves from tests performed by Yamamoto is shown in Figure 3.5.

Altered mechanical behaviour due to temperature increase is mainly a consequence of phase change between ice and water. When ice melts, the amount of unfrozen water raises, which permits significant plastic deformations (Nixon and Lem, 1984). This effect is more prominent for saline soil than non-saline soil, given the same water content and temperature.

Hivon and Sego (1995) tested uniaxial strength for silty sand with different salinity ranging from 0 to 30 ppt. The results from this paper are shown in Figure 3.6, and exhibit a linear dependency between temperature and peak strength. The same linear relationship is shown in Figure 3.7, displaying results from triaxial testing of frozen clay performed by Wang and Nishimura (2017).

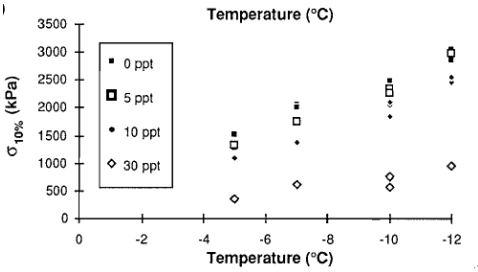

Figure 3.6: Results from uniaxial testing on frozen silty sand showing compressive strength vs. temperature at 10 % strain. (Hivon and Sego, 1995)

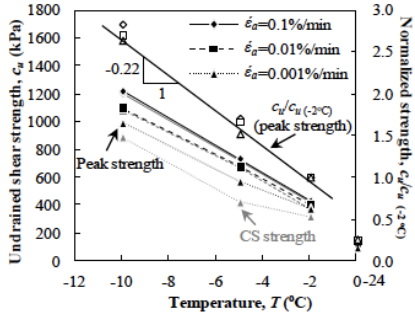

Figure 3.7: Results from triaxial testing on frozen clay preconsolidated to 400 kPa. Showing undrained shear strenght vs. temperature. (Wang and Nishimura, 2017)

3.2.4 Strain Rate

Several studies show that increased strain rate, $\dot{\varepsilon}$, increases the compressive strength of frozen soil (Chamberlain et al., 1972; Sayles and Haines, 1974; Parameswaran and Jones, 1981; Li et al., 2004). Bragg and Andersland (1981) uniaxially loaded frozen sand samples at different strain rates and found that the applied strain rate controls the deformation mode of the soil. Results from this study show a more brittle behaviour for higher strain rates, which is characterized by the soil reaching peak strength at low strain values. This is also referred to as strain softening. For lower strain rates, a more ductile behaviour is observed, resulting in plastic strain hardening. See Figure 3.8.

Figure 3.9 shows the relationship between strength and strain rate for four different temperatures. Note that the test performed on unfrozen soil is not affected by a change in strain rate. The main reason that the strain rate effect is present in frozen soil, and not observable in unfrozen soil, is the presence of ice. A study performed by Mellor and Cole (1982) shows that axial stress in ice is highly influenced by the strain rate.

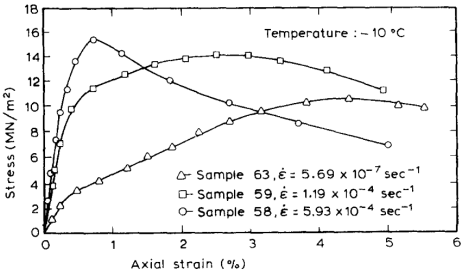

Figure 3.8: Stress-strain curves for sand with different applied strain rates at -10 °C. (Bragg and Andersland, 1981)

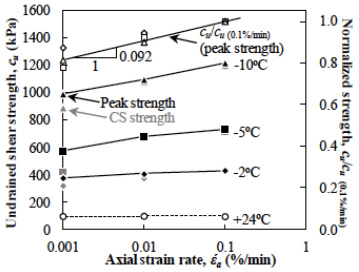

Figure 3.9: Log-log relationship between shear stress and axial strain rate for varying temperatures. (Wang and Nishimura, 2017)

Furthermore, the shear strength of frozen clay tends to increase log-linear to the axial strain rate, which has been proven by several different studies, including Li et al. (2004) and Wang and Nishimura (2017). The log-linear relation can potentially be described, by rewriting equation 3.1, which was presented in a regression analysis performed by Li et al. (2004):

$$ln\left(\sigma_m\right) = b_0 + b_1 ln\left(\frac{\theta}{\theta_0}\right) + b_2 ln\left(\frac{\dot{\varepsilon}}{\dot{\varepsilon}_0}\right) \tag{3.2}$$

where b_0 = ln(σ_0), b_1 = i and b_2 = m (Li et al., 2004).

The results from the regression analysis performed by Li showed that parameter b_2 depends upon dry density which means that the strain effect may vary with respect to the soil composition.

3.3 Area Correction

Calculations of deviatoric stress in triaxial testing normally require a set of corrections to be correctly represented. Area correction is among one of these, especially if the test is run for large deformations which highly influence the geometry of the test specimen. The

deviatoric stress is defined as the piston load transferred to the specimen cross-section, σ_1, minus the cell pressure, σ_3. While it is easy to measure the load applied by the piston, it is more complicated to record the specimen cross-section as the specimen normally does not deform isotropic.

Area correction is normally divided into two steps: the simple area correction (before failure), and advanced area correction based on the rupture surface. The simple area correction depends on how the specimen deforms. Some common deformation modes are shown in Figure 3.10.

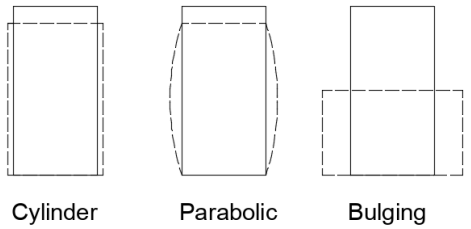

Figure 3.10: Typical deformation modes during triaxial testing. (Mulabdic´, 1993)

.

Baldi et al. (1988) proposed the following expressions to calculate the specimen area correction associated with the three deformation modes shown:

Cylindrical

$$A = A_0 \frac{1 - \varepsilon_v}{1 - \varepsilon_a} \tag{3.3}$$

Parabolic

$$A = A_0 \left(-\frac{1}{4} + \frac{\sqrt{25 - 20\varepsilon_a - 5\varepsilon_a^2}}{4\left(1 - \varepsilon_a\right)} \right)^2 \tag{3.4}$$

Bulging

$$A = A_0 \frac{1 - \varepsilon_v}{1 - a\varepsilon_a} \tag{3.5}$$

where compressive deformations are positive and

A_0 = initial cross-section area at zero strain

a = experimental constant, normally between 1-2

ε_a = vertical strain

ε_v = volumetric strain

Chapter 4

Experiment

When investigating the behaviour of frozen soil, it is important to have equipment that is compatible with the research objective. Measurement of pore pressure in frozen soil has proven to be challenging, and the use of normal triaxial equipment is not sufficient. The triaxial equipment used in this thesis, shown in Figure 4.1, is specially designed to test frozen soil, and was purchased by NTNU from GDS Instruments in 2017. Artificial frozen clay from Onsøy has been used in the testing. The clay is extracted by NGI, and bought by NTNU for academical purposes. Index testing has been conducted on the unfrozen Onsøy clay to classify material parameters, namely salinity and water content. This thesis also presents a new set of procedures to standardize testing with the given equipment, and how to present test data.

4.1 Index Testing

The following index tests have been carried out for each specimen of unfrozen Onsøy soil.

- **Natural water content:** Three measurements of in situ water content, w, after manual by Norwegian Public Roads Administration (2014).
- **Salinity:** Two measurements of salt content.

4.2 Performed Triaxial Tests

Table 4.1: Test overview.

Test no	Date	Temp (°C)	w (%)	Salinity (ppt)	$\dot{\varepsilon}$ (%/h)	p' (kPa)
1	01/09	-5	68	35	1	100
2	01/14	-5	71	29	1/10	200
3*	01/17	-5	73	25	—	—
4	01/20	-5	68	26	1	400
5	01/23	-3	47.5	18	1/0.2/5	100
6	01/27	-3	48	18	1/5	200
7	01/30	-3	52	20	1	400
8	02/03	-5	52	23	1	100
9	02/07	-5	42.5	19	1/0.2/5	200
10	02/10	-5	48.5	35	1	200
11	02/13	-5	40	28	1	400
12	02/17	-5	50	28	1	200
13	02/20	-10	46.5	28	0.33/1/3	200
14	03/05	-10	48.4	21	1/0.2/5	200
15	03/09	-10	37.9	21	1/0.2/5	400
17**	05/18	-3	55.9	26	1/0.2/5	20

* Membrane leak, removed from thesis.
** Late conducted test added in Appendix B, not discussed in results.

A thorough predetermined test-plan is necessary to collect enough and relevant data to compare for results. The authors' goal is to achieve enough data so that trends and parameter effects may be observed and investigated. Its importance also shows when selecting test conditions, as choosing a similar framework as other researchers allow easier comparison with experimental results found in the literary review. The test plan is presented in Table 4.1.

Temperature is tested at -3, -5 and -10 °C. Literature presented that -5 and -10 °C are common test temperatures among other researchers. There may be several reasons for this. The authors believe it is regarded as problematic to test frozen soil close to thawing temperature as phase change may cause fluctuating results. Furthermore, small temperature variations are negligible at colder temperatures as most of the free water is transformed to ice. In order to investigate soil behaviour close to thawing, the authors decided to conduct tests with -3 °C.

During testing, the strain rate is varied by firstly running 1 %/h, followed by a raised or lowered rate. This technique is beneficial as the authors are limited by a small time frame,

and enables the possibility to extract more data from each test.

Confining pressure is chosen in regards to soil response, equipment capability and realistic encounters. High pressure should be avoided as pressure melting and ice fracture is unwanted. Furthermore, confinement stress in the range 300 to 600 kPa has been known to occur in projects, i.e. tunnel excavations (Wang and Nishimura, 2017).

4.3 Equipment

The triaxial cell is placed in the cold laboratory in the basement of Lerkendalsbygget at Gløshaugen Campus, Trondheim, Norway. Temperature is regulated by fans maintaining a cold climate during testing. Meanwhile, temperature in the testing cell is controlled by a circulation thermostat, circulating refrigerated oil around the specimen.

4.3.1 Cold Laboratory

The lab climate should be cold and dry so that the sample does not thaw during build in and keeps cold during tests. Cooling is supplied by eight cooling fans, controlled by a panel placed outside the lab. Maintenance and de-icing of the system is carried out if needed.

The laboratory is designed with a sluice room to avoid warm humid air entering. This is both to keep a constant temperature and to avoid the formation of ice on the cooling fans, which makes them less effective.

4.3.2 Cell

The triaxial cell is insulated by metal plates and polystyrene, and the cell temperature is mainly controlled by a coil which is installed in the cell wall as shown in Figure 4.2. The coil is filled with refrigerated oil, where the oil temperature is controlled by a circulation thermostat. The cell is filled with oil during testing, which is pumped into the system by a compressor. During testing, the cell oil temperature is measured by two thermistors placed in the top and bottom of the cell.

4.3.3 Pore Pressure Measurements

Pore pressure is recorded by opening a valve connected to the bottom of the sample which is wired to a pore pressure transducer. The transducer is placed outside the cold laboratory

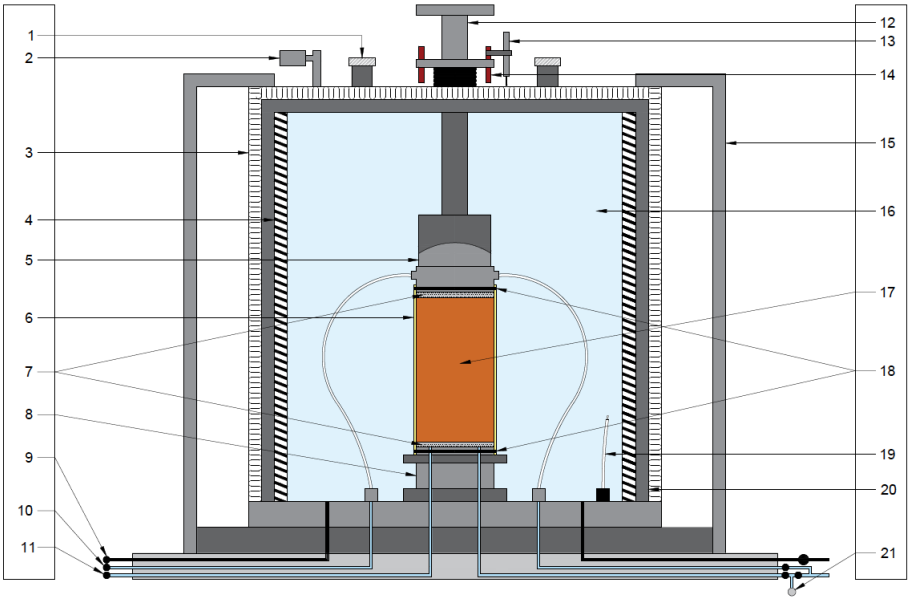

Figure 4.1: Schematic diagram of the triaxial cell with built-in soil sample.

1 Fluid Circulation Valve	8 Bottom Pedestal	15 Metal Insulation Panel
2 Air Valve	9 Cell Valve	16 Cell Fluid
3 Cell Wall Insulation	10 Bottom Cap Valve	17 Test Sample
4 Coil	11 Top Cap Valve	18 O-ring
5 Top Cap	12 Loading Rod	19 Thermometer
6 Rubber Membrane	13 Local LVDT	20 Cell wall
7 Porous Stone	14 Plastic Cylinder	21 Pore Pressure Sensor

Figure 4.2: Coil system inside the triaxial cell.

to avoid pore water freezing and breakage of the instrument. Figure 4.4 gives an overview of some of the valves. By closing the valve marked in red the system is undrained, but still measures pore pressure as the middle valve is connected to the transducer.

4.3.4 Circulation Thermostat

The circulation thermostat is delivered by JULABO (model FP51-SL). The JULABO system has a working temperature range of -51 °C to +200 °C, and a temperature stability of $\pm$ 0.05 °C.

During testing the circulation thermostat uses internal or external temperature control, chosen by the user. With internal control, the oil is set to a fixed temperature by the user. With external control the oil is regulated by a thermistor in the cell, keeping a desired constant temperature. By using external control it is possible to counteract the heat from the hydraulic system and temperature differences in the cold laboratory as oil temperature is based on the cell temperature. In this thesis, external control is used for all tests.

4.3.5 Freezing Liquid and Cell Oil

The freezing liquid, used in the back pressure piston and to freeze the soil samples, is a solution of ethylene glycol and air-free water. The freezing point of the solution is controlled by the mixture ratio of water to ethylene glycol. It should be noted that water drained from the soil sample will lower the freezing point of the solution. The cell oil is Thermal H5 delivered by JULABO and has a working temperature of -50 °C to +105

°C. Furthermore, it is chosen as it wears little on the equipment and is not particularly corrosive.

4.3.6 Cell and Back Pressure Piston

The cell and back pressure is applied by two pistons placed outside the cold laboratory, which are manually controlled from the GDSLAB software or panels shown in Figure 4.5. The piston volume and piston pressure are monitored in the GDSLAB software. The capacity of the pistons is 20 MPa. The cell pressure piston is filled with the same oil as the triaxial cell. The back pressure piston is filled with a solution of ethylene glycol and air-free water, which main task is to ensure that the water drained from the soil will not freeze in the filter or the hose.

4.3.7 LVDT

The deformation measurements are monitored by an LVDT (*Linear Variable Differential Transformer*) delivered by GDS Instruments. The LVDT is manually mounted on the cell before testing. The LVDT has a deformation range up to 10 mm and a working temperature of -50 °C to +85 °C.

4.3.8 Software

The software LabVIEW and GDSLAB are used to control and monitor the tests. LabVIEW is used to control the test rig during experimentation, and to monitor deformation, load, pore pressure and temperature with time. GDSLAB is used to control the cell and back pressure pistons, and to monitor the volume and pressure in the pistons.

4.3.9 Emergency Stop

An emergency stop is installed on the test rig to ensure that the load piston stops when deformation reaches a certain value. This is a safety measure to avoid damage to equipment and lab personnel.

4.4 Procedure for Triaxial Testing

The following procedure is based on the procedure described by Østbye (2018), with some minor changes due to different equipment being used. The steps are described in detail

so that it can be used as an aid for future testing of frozen soil. The method is merely a recommended procedure pro 2020 worked out by the authors of this thesis, and each step may be changed or optimized as one gain more experience. It is recommended to be at least two technicians working in the cold laboratory during sample build in, due to practical reasons and to ensure a safe working environment. The testing form is attached in Appendix D.

The procedure for triaxial testing is divided into 6 steps:

1. Sample preparation
2. Equipment preparation
3. Sample build in
4. Isotropic consolidation
5. Main testing
6. Build out sample

4.4.1 Sample Preparation

1. Slide the sample out of the sampling tube by using a hydraulic extruder machine.
2. Cut and trim a soil sample with height at least twice the size of the cross-section diameter by using a thread saw.
3. Measure the mass and the dimensions of the soil sample.
4. Make sure the membrane is intact by filling it with water and check for leaks. Thread the waterproof rubber membrane over the sample. Attach the rubber skin to the top and bottom piece with two O-rings on each side. Figure 4.3 shows a sample prepared for freezing.
5. Immerse the sealed sample in ethylene glycol and place it in the cold box. The liquid provides a slow freezing process.
6. Set the cold box temperature to 4 °C, and let the sample cool for a minimum of two hours to ensure homogeneous temperature in the soil.
7. Set the target temperature which the soil sample is tested at. Keep the specimen freezing in the cold box for at least 36 hours.
8. Put the sample in the cold room.

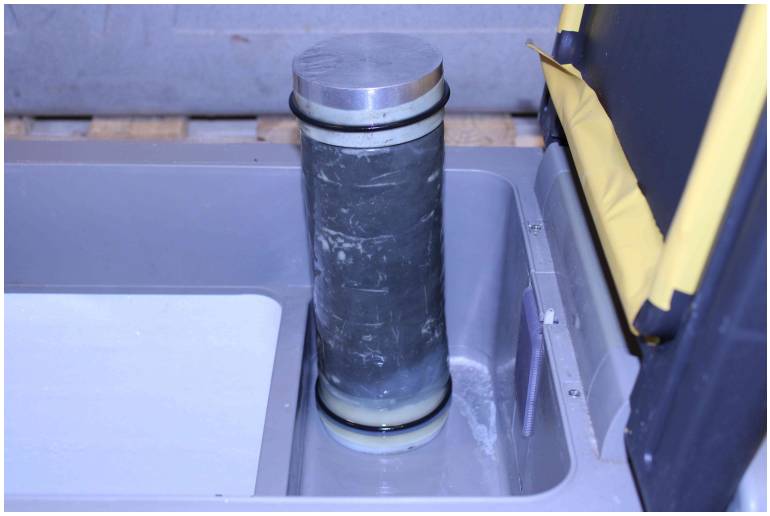

Figure 4.3: Sample set up before artificial freezing.

4.4.2 Equipment Preparation

1. Saturate the porous stones with ethylene glycol mixture.
    - Place the porous stones in a glass jar filled with ethylene glycol.
    - Use a vacuum desiccator to extract any air from the porous stones. Let it stand for 1 hour.
2. Make sure all the valves are closed.
3. Mix ethylene glycol and air-free water in a container.
    - Adjust the mixture ratio so that the freezing point of the mixture is below the test temperature.
4. Make sure the back pressure pump volume is sufficient to saturate the system by opening the bottom valve, and check if liquid seeps out of the bottom cap.
5. If the volume of the back pressure pump is insufficient, refill the back pressure pump with ethylene glycol and air-free water.
    - Disconnect the hose marked in Figure 4.4 from the cell and place it in the container with ethylene glycol mixture.
    - Control the back pressure piston from the panel shown in Figure 4.5 or the GDSLAB software. Use *Target volume* to fill the piston approximately half full.

- Reconnect the hose to the cell.
- Open the *bottom* valve.
- Use the *fast empty*-function to saturate the bottom of the cell. Close the *bottom* valve when all the air is cleared out of the system and only ethylene glycol mixture comes out of the hose.
- Set the back pressure piston to *hold*.
- Use a syringe to saturate remaining hose parts with ethylene glycol mixture.

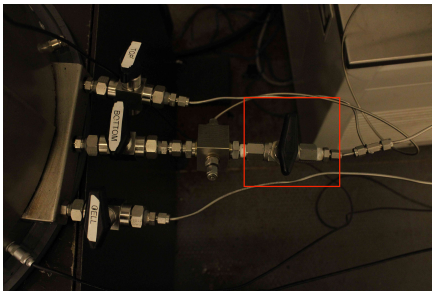

Figure 4.4: Valves when closed.

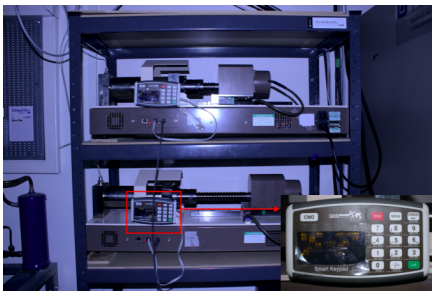

Figure 4.5: Cell pressure piston (bottom) and back pressure piston (top) is regulated from panels or GDSLAB software.

4.4.3 Sample Build In

1. Remove the rubber membrane and o-rings from the frozen sample.
2. Clean rubber membrane and make sure it is not leaking by filling it with water and look for holes.
3. Insert the test sample to the triaxial cell.
   - Clean the bottom and top cap surfaces.
   - Lubricate the sides of the top and bottom cap with silicon to ensure a tight seal between the metal and rubber membrane.
   - Saturate the bottom cap.
   - Gently slide the porous stone at the bottom cap and apply saturated filter paper on top of it. Make sure to remove any air in the filter paper.
   - Place the sample on the filter paper and install the rubber membrane on the sample.

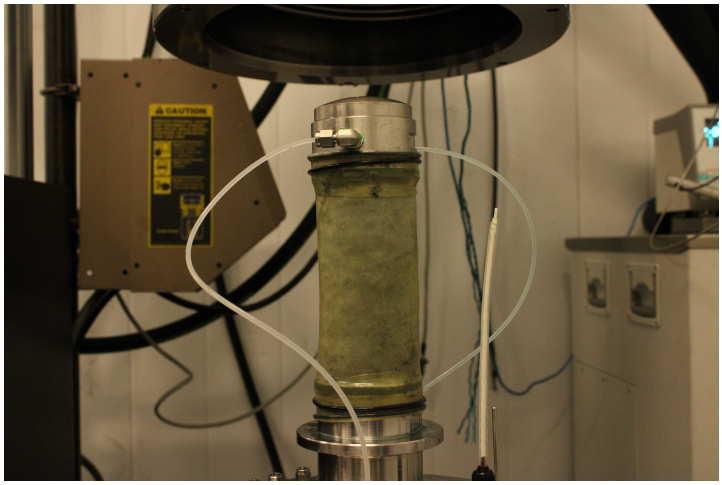

Figure 4.6: Sample with membrane and o-rings.

- Wrap the rubber membrane down on the bottom cap and apply an o-ring. Wrap the rubber membrane around the o-ring and apply a second o-ring.
- Place saturated filter paper and porous stone on top of the sample.
- Open *top* valve slightly to avoid air from entering, and place the top cap on top of the sample.
- Wrap the rubber membrane on the top cap and apply two o-rings. Figure 4.6 shows how the set up should be.

4. Raise the bottom part of the cell and connect with the top part.
5. Slowly lower the load cell to contact the sample and check the length between cell and load cell.
    - The length should be at least 5-6 cm longer than the test sample.
6. Place wooden plate under the cell and move the cell to the rig. Carefully shake the cell so it fits the rig.
7. Remove wooden plate.
8. Install metal insulation panel and LVDT, and put rubber between rig and cell.
9. Apply the fluid circulation wires.
10. Fill the cell with oil.
    - Turn on the air pressure system outside the cold lab.

Figure 4.7: Set up for filling the cell with oil.

- Connect air tube to the oil tank.
- Adjust the air pressure.
- Connect the tube to the top of the cell and place the bottom part of the tube in an empty can. The cell is filled when oil starts entering the empty can. Figure 4.7 shows how the setup should be.
- Close the cell valve and disconnect the tube connected to the top part of the cell
- Open the cell valve, increase the pressure and let it circulate for 2 hours to get rid of air bubbles.

4.4.4 Isotropic Consolidation

1. Start logging of cell and back pressure piston in GDSLAB.
   - Open LABview and fill the *File Name* and *Operator*. See upper-left in Figure 4.8 marked with red squares.
   - Adjust *Piston servo voltage*, as marked by a yellow square in Figure 4.8, to zero by rotating the *zero* button on the panel. The zero button is marked with red in Figure 4.9.
   - Press *Reset* on the panel and then press *High* for the hydraulic pressure, shown by the blue square in Figure 4.9.

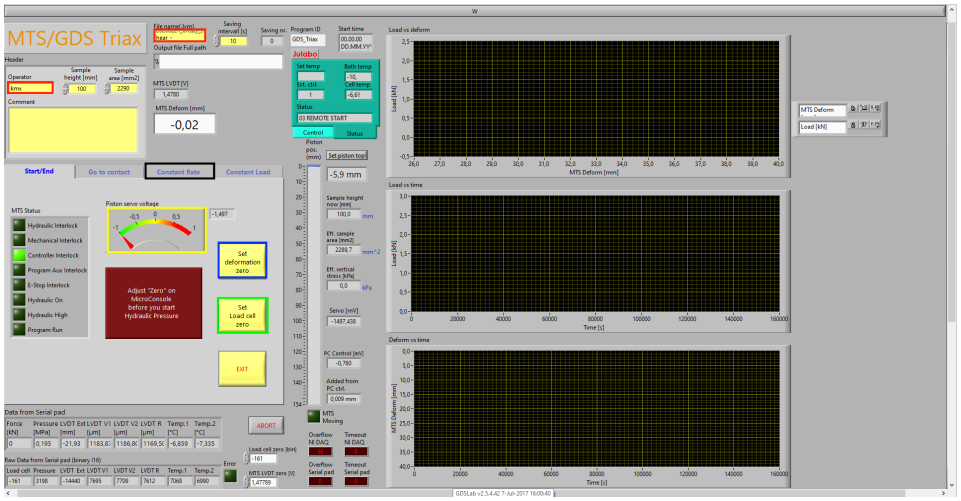

Figure 4.8: LabVIEW: Start/End tab.

Figure 4.9: Load cell panel.

- Go to LABview, press the *Set Load Cell Zero* button as marked with green in Figure 4.8.
- Adjust the piston to almost contact the system using the zero button on the panel.
- Go to the *Constant Rate* tab, marked with black in Figure 4.8, and adjust *Max load* to 0.1 kN. Click *Press to start* to contact the piston and sample, as shown in Figure 4.10.
- Go to Start/End tab and click *Set deformation zero*. This button is marked with

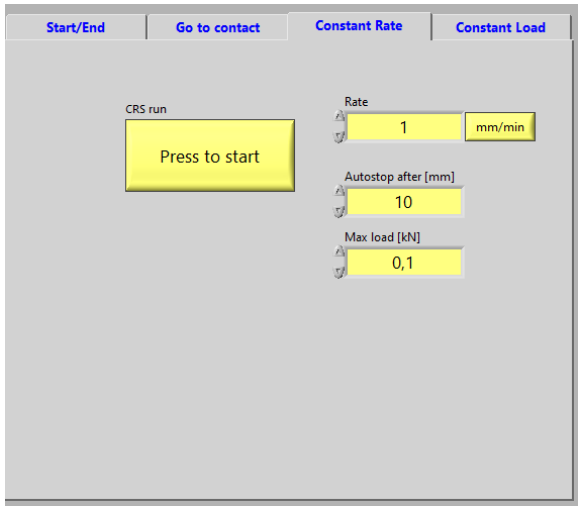

Figure 4.10: Constant rate tab in LABview.

a blue square in Figure 4.8.

- Open the GDSLAB software on the monitor.
- Choose station 2 and press *Data Save*. Press *Choose Data File* and choose *Single Directory*. Press *Next* twice and name the file appropriately. See Figure 4.11.
- Press *Sample* and *Setup Sample Details*. Press *Yes* twice and then *Ok*.
- Press *Add Test* and *Create New Test Stage*. Choose *Just Log!* as test type, press *Next* and then *Yes*. See Figure 4.12.
- Press *Test List* and *Go to Test*.
- The window now shows the test plan as in Figure 4.13. Click *Start Test* to start recording.

2. Turn on the cell and back pressure.

   - Control the cell pressure from GDSLAB on the monitor or from the separated control panel as shown in Figure 4.5.
   - Set *Target Pressure* to adjust cell pressure on the cell pressure piston.
   - Open the *cell* valve.
   - Set *Target Pressure* to adjust back pressure on the back pressure piston.
   - Open the *bottom* and *top* valve.

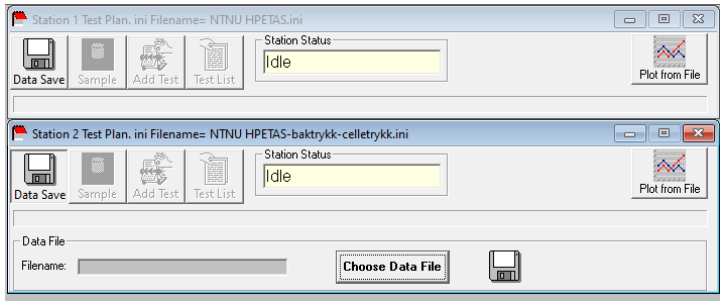

Figure 4.11: GDSLAB opening window.

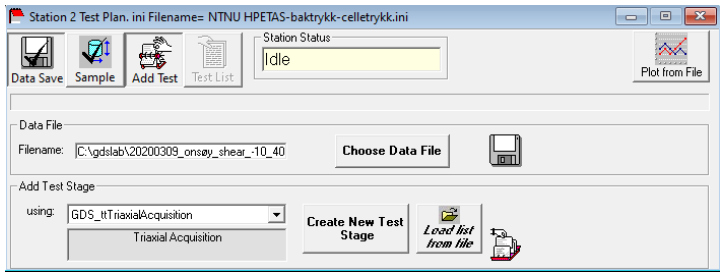

Figure 4.12: GDSLAB *Add Test* tab.

- Adjust the cell pressure to the piston area. Go to the *Constant Load* tab in LabVIEW and apply a constant load calibrated to the equation below.

$$Load_{const} = \sigma_3 \cdot A_{piston}$$

- If the process of building up the cell is too time demanding, it is recommended to apply the load in several steps.

3. Observe the logging of volume and pore pressure. The sample is consolidated when the back pressure piston volume is stabilized. Close the valve to the back pressure piston.

4.4.5 Main Testing

1. Shear test
   - The shear test is controlled from the *Constand Rate* tab.
     (a) Set the strain rate and maximum deformation. The maximum deformation should be high enough for the test to not end prematurely.
     (b) Press *Press to start*.

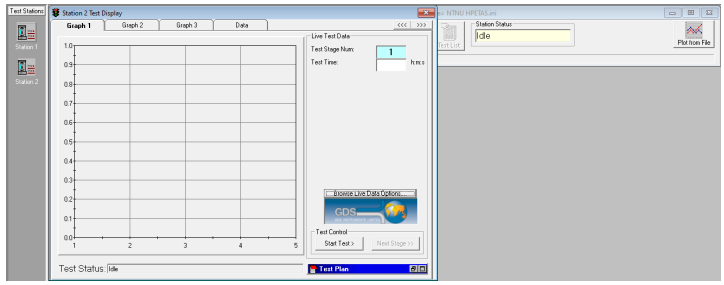

Figure 4.13: GDSLAB window showing test graphs.

2. Creep test

    - The creep test is controlled from the *Constant Load* tab.
        (a) Set the desired load level in the *Load* field.
        (b) Press *Press to start*.

4.4.6 Build Out Sample

1. Dismantle LVDT.
2. Refill the cell pressure pump with oil by using the separate control panel shown in Figure 4.5

    - Press *Menu*, *Set*, *lock/unlock* and *Unlock Device*.
    - Click *Fill empty* and *Fast Fill*

3. Empty the cell for oil.

    - Turn on the air pressure system outside the cold lab.
    - Connect air tube from the oil tank to the cell valve and open the cell valve to allow the oil to flow out.
    - Connect air tube from the air pressure system to the top of the cell and increase pressure. Let the pressurized chamber extract oil until air appears through the pipes.
    - Close the air pressure valve outside the cold room.
    - Reduce the air pressure.
    - Disconnect air tube from the top of the cell.
    - Close the cell valve.

- Disconnect the air tube between oil tank and cell.

4. Lift the loading rod and tighten the support rod.
5. Remove the metal insulation panel and the rubber between cell and piston.
6. Disconnect the fluid circulation wires.
7. Lift the cell and place the wooden plate.
8. Move the cell out of the system and remove the wooden plate.

4.5 Source of Errors

4.5.1 Temperature

The cold laboratory have issues maintaining a consistent room temperature during testing, mainly due to the hydraulic system generating heat during testing. It is not known if this affects the temperature in the cell or the how much this influences the test results. Precautions are taken by giving the machine time to cool down after a test and the room temperature is observed, and verified, with a thermometer.

During testing the laboratory temperature is set 2 °C below wanted test temperature to account for this heat. Also, readings from the external temperature control show that the bath temperature holds the desired test temperature. As a consequence, the lab climate is deemed acceptable on these accounts, but it is unknown if it has any other influence on the tests.

4.5.2 Artificial Freezing

The test samples collected from Onsøy are artificially frozen before testing. A mixture of ethylene glycol and water function as anti-freezing liquid. In preparation, the antifreeze is kept refrigerated at around 4 °C. The sample is then placed in the solution and temperature is lowered below soil freezing point in a fan-cooled, insulated container. Test 1 to 5 was kept in the liquid until the test date, but due to the ethylene glycol 's ability to diffuse the rubber membrane and seep into the test specimen, this procedure was changed. No notable effects on the test results was detected by the authors, because of this. From test 6 and onward, the test samples were removed from the anti-freezing liquid after it had reached the desired temperature and then placed into the cold laboratory.

Isotropic freezing is difficult to achieve as pore water will flow towards the freezing surface, allocating pore water from the centre to the surfaces. Therefore, attempts of cooling and freezing the sample uniformly are made by keeping the freezing temperature high, while still below the freezing point.

Inspection of the horizontal cross-section display a fairly even distribution of ice, as shown in Figure 4.14.

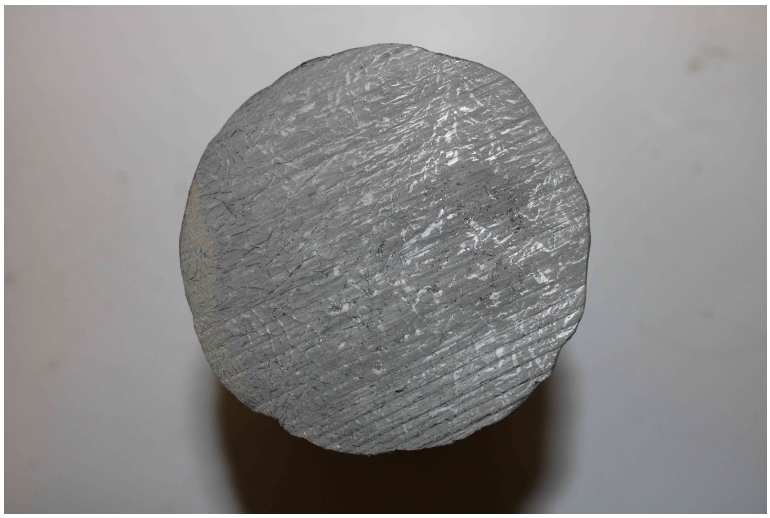

Figure 4.14: Cross-section of artificial frozen clay at -5 °C.

4.5.3 Deformation Mode

The deformation mode of the test samples vary from test to test. The most common deformation mode is cylindrical as shown in Figure 4.15. Some test samples tend to form other deformation modes where the cross-section differs across the height. An example of this is shown in Figure 4.16, showing an hourglass deformation mode. Expression 3.3 is used to correct the test sample area during testing. The expression averages the cross-section over the entire height, meaning that for hourglass deformation, the vertical stresses are underestimated in the middle and overestimated in top and bottom because of the area enlargement.

Figure 4.15: Cylindrical deformation mode.

Figure 4.16: Hourglass deformation mode.

Chapter 5

Soil Description

This chapter describes the soil samples that are used in the triaxial testing performed in this thesis. The first part characterizes the soil by presenting index properties and notable observations. Furthermore, the Onsøy test site is presented and shown with an overview map. Lastly, the methods of how some of the test specimens were remoulded are presented.

Gundersen et al. (2019) performed extensive field and laboratory work on soil from the same site. Findings from this study are compared to this thesis and soil characterization is concluded on validated results.

5.1 Soil Characterization

Soil was sampled with a ⌀72 mm sampler by NGI. Samples show a homogeneous clay. Fragments of marine shells have been found in specimens. The samples are obtained from two different boreholes.

	Unit	Depth	Name	Location
•	BH2 PS3	6.6-8.0 meter	Borehole I	South Central
•	BH-ONS7-02	10.0-12.0 meter	Borehole II	South East

*Location of each borehole is presented in Figure 5.1.

Index tests performed by Gundersen et al. (2019) show a grain size distribution of about 68 % and 50 % clay for borehole I and II respectively. The remaining particles are mainly silt and a very small amount of the soil volume is sand particles. Furthermore, borehole I has water content and unit weight of 70 % and 15.7 kN/m^3 while borehole II have 45 % and 17 kN/m^3, respectively. Salinity is measured from the pore water and are around 30 ppt for borehole I samples and 18 ppt borehole II. Plasticity index, I_p, is about 44 % and 27 %. Some values for each sample are given in Table 4.1 and Table 6.1.

Water content measurements done by the authors match that of Gundersen et al. (2019). Due to this, results from the report is deemed trustworthy for the specimens. Salinity was also tested with two different methods which showed inconsistent results, and it is therefore difficult to conclude on a real value. Thus, the salinity was determined by comparing salinity measurements with those of Gundersen et al. (2019). The entire collection of index values from Gundersen et al. are presented in Appendix A. Index values for each test is given in Table 6.1.

Lastly, Gundersen et al. (2019) show an overconsolidation ratio (OCR) in the range of 1.3 - 1.8, a friction angle, ϕ', of 30 ° and attraction, a, of 5 kPa.

5.2 Site

Due to a growing need of soft clay for research purposes, Onsøy (Fredrikstad, Norway) was determined suitable due to a thick layer of marine deposit and its uniformity. The first site was established by NGI in 1968 and since then two more sites have been founded, namely ”2nd Onsøy test site” and the current ”NGTS Onsøy test site”. The site consists of a homogeneous dark grey soft clay. Silt content increase with depth (Gundersen et al., 2019).

5.2.1 Deposition History

The area has experienced uplift since the last glacier period and the region’s highest former sea level after the ice disappeared (marine limit) is about 170 meters above current sea level (Sørensen, 1979). The present elevation is about 6,5 meters above current sea level.

Quaternary map from (NGU.no, 2020) show thick marine deposits, see Figure 5.2. Furthermore, while working with samples it has been identified fragments of marine shells.

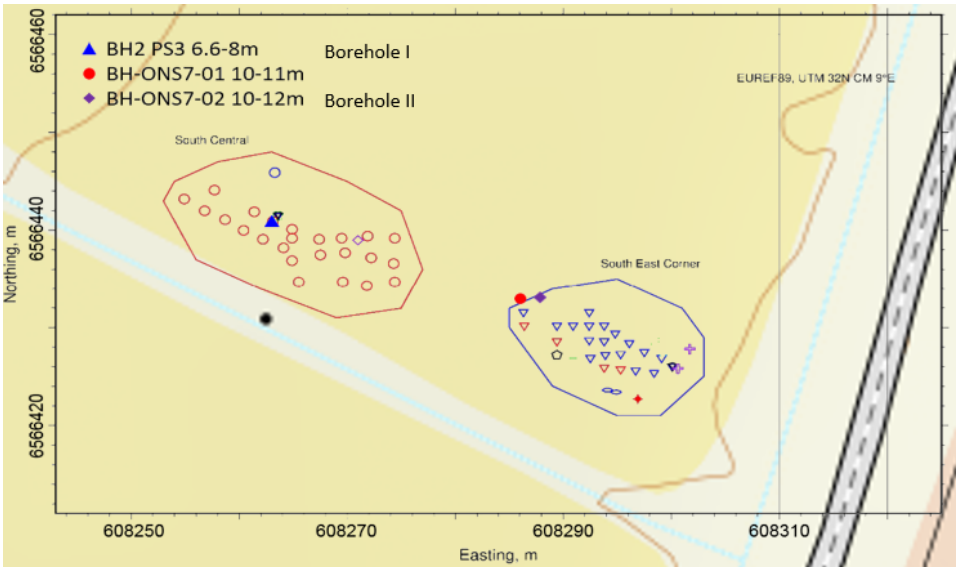

Figure 5.1: Location of boreholes with north and east coordinates in EUREF89 UTM 32N on map. Coordinates from Gundersen et al. (2019); map from Norgeskart (2020).

5.3 Remoulded Samples

To reuse samples, some samples have been remoulded after testing. The remoulding process begins by adding saline water to the soil. The amount of water should result in the water content being just above the liquid limit. Sea salt is used, as this is more consistent with the salt in the natural sample. Salt is added until the brine matches the salinity in the pore fluid. The slurry is then filled into an oedometer mould with an inner diameter of 70 mm. To prevent gas bubbles, a hand-held vibrator is used to release any gas trapped in the soil. The saturated sample is then consolidated with an oedometer apparatus, applying 65 kPa axial pressure. Excess pore water is allowed to drain from the top and bottom. The process is eventually completed when the flow of water stops, usually after 3 days.

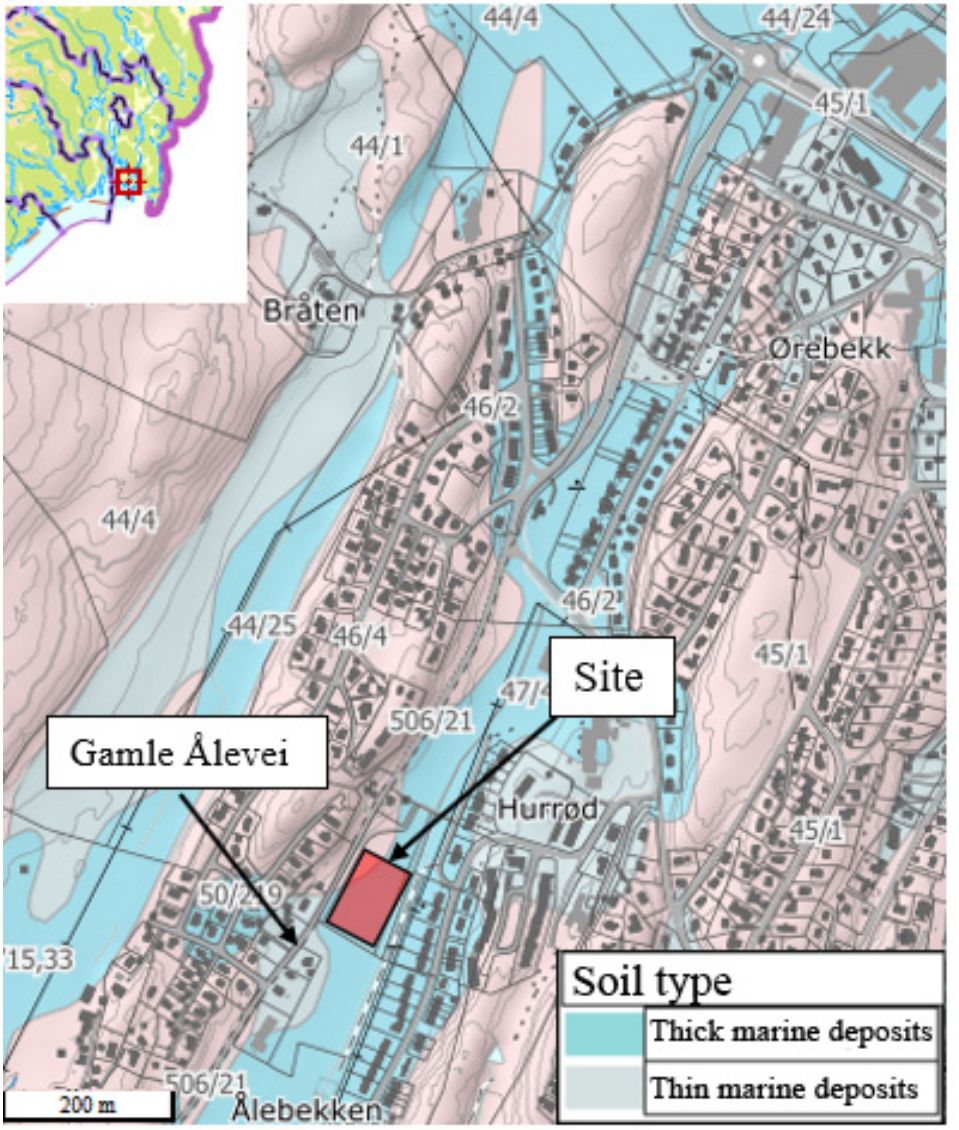

Figure 5.2: Quaternary map showing marine deposits. The red square marks the site. Screenshot from NGU.no (2020) with legend translated to English.

Chapter 6

Results and Discussion of Triaxial Testing

This chapter presents results from the triaxial testing of frozen Onsøy clay. The results are discussed and analyzed in regards to different variables. The parameters studied are unfrozen water content, pore pressure, confining pressure, mean effective stress, water content, salinity, temperature and strain rate. Each discussion is based on results from the present thesis and relevant literature. Introductory, test results are given general comments and errors tied to selected tests are explained. Followed by analysis and discussion. Lastly, regression analysis is performed, and three different empirical equations are presented. Complete collection of test results are attached in Appendix B.

6.1 General Comments on Test Results

Table 6.1 shows the results for each test with given test conditions. Due to tests not reaching maximum resistance, the strength at 10 % accumulated strain was selected. In cases where the experiment was ended early the maximum resistance achieved was chosen. In general, all soils show slight strain hardening and little change after initial yield. Some tests have been subjected to different strain rates after the initial strain rate of 1%/h stabilized. This was done to investigate the effect of strain rate on soil behaviour.

Occasionally samples exposed to low strain rate and cold temperatures showed oscillating resistance. For instance, Figure 6.1 exhibits fluctuations for -5 °C. Regarding these tests, peak strength was determined based on the mean of the curve.

All tests are presented in Appendix B. Shear results are presented using q-p', q-ε_a, u-ε_a and q-σ_3 plots. Consolidation results are shown as back volume change with time, together with other supplementing plots for the consolidation period. Photographs of the deformed sample after the triaxial test are added when available.

6.2 Possible Errors in Some Tests

Three tests experienced issues. Test no. 3 was determined invalid as the membrane leaked, causing the test to become drained. Test no. 8 experienced issues regarding temperature. The soil was heated about 1 °C during 11 hours, corresponding to 11 % accumulated strain. The problem was resolved and temperature stabilized rapidly. Lastly, test no. 14 was mounted for 10 days before running the test due to shortage of oil. During this time, it is presumed that ethylene glycol entered the sample at the specimen ends. Deformation pattern, as shown in Appendix B.13, supports this theory. It is believed that this affects the pore pressure measurements of test no. 14, which also influence both deviatoric and mean stress. Due to a limited time frame, it was decided to include test no. 8 and 14. Reliability on the use of these tests are discussed upon when assessing each parametric effect.

Table 6.1: Overview of test results

Test condition							Result			
No.	T (°C)	p (kPa)	$\dot{\varepsilon}$ (%/h)	w (%)	S (ppt)	$\sigma'_{3.0}$ (kPa)	p_w (kPa)	q (kPa)	p' (kPa)	σ'_3 (kPa)
1	-5	100	1	68.0	35	200	64.4	170.3	102.2	45.6
2	-5	200	1	71.0	29	300	120.2	264.8	177.2	89.7
			10				194.2	466.3	171.2	15.8
4	-5	400	1	68.0	26	500	128.7	259.2	368.6	281.3
5	-3	100	1	47.5	18	200	59.5	159.2	103.2	50.5
			0.2				-21.4	118.3	171.1	131.4
			5				41.8	282.0	162.1	68.1
6	-3	200	1	48.0	18	300	100.4	213.8	181.1	109.6
			5				128.9	338.9	194.1	81.0
7	-3	400	1	52.0	20	500	140.2	218.8	342.6	269.7
8**	-5	100	1	52.0	23	200	16.4	407.5	236.2	98.3
9	-5	200	1	42.5	19	300	38.4	544.7	342.3	161.6
			0.2				-30.9	469.1	385.4	230.9
			5				-26.2	682.3	453.7	226.2
10*	-5	200	1	48.5	35	300	1.1	255.0	284.4	198.9
			0.2				-47.3	212.4	319.7	247.3
			5				-33.8	393.1	364.8	233.8
11	-5	400	1	40.0	28	450	42.3	544.2	549.6	367.0
12*	-5	200	1	50.0	28	250	13.1	297.4	288.5	189.8
13*	-10	200	1	46.5	28	200	30.1	827.8	440.2	169.9
			0.33				59.2	697.5	362.7	140.8
			3				63.4	890.8	430.4	136.6
14***	-10	200	1	48.4	21	200	38.1	1000.5	470.5	181.3
			0.2				18.7	867.7	495.4	161.9
			5				19.6	1226.4	589.4	180.4
15	-10	400	1	37.9	21	400	13.6	1276.2	816.8	391.4
			0.2				13.1	1110.1	761	391.9
			5				14.8	1484.1	885	390.2

Results for each test is given in Appendix B.
*Remolded sample
**Error in temperature control
***Possibly contaminated with ethylene glycol

6.3 Shear Test

Figure 6.1 presents results from test no. 9 at -5 °C, a typical shear test result from this thesis. Initially it is deformed at a rate of 1 %/h until about 10.5 % vertical strain. Subsequently, the strain rate is changed to 0.2 %/h and lastly 5 %/h. In the elastic range, the stress path slope is $\Delta q/\Delta p' = 3$, similar to that of a standard drained triaxial compression test on unfrozen soil (Nordal, 2019). In frozen soil, this may occur even when the test is run in undrained conditions. The phenomena is further discussed in Section 6.3.1. Unexpectedly high mean effective stress was observed for tests displaying this trend and consequently, a correlation is believed to exist.

The sample behave plastic after about 1.5 % vertical strain. During this time the deviatoric stress increases slightly with strain, as mobilization of interparticle friction develops and strain hardening occurs. This property is strain rate dependent. Higher strain rate is expected to give a brittle behaviour as seen in other literature (Bragg and Andersland, 1981).

Specimen deformation is varied. A majority of the samples show a cylindrical mode, however, some tests bulged at the ends while the middle diameter remained unchanged. Possible diffusion of ethylene glycol to the top and bottom of the specimen would soften it and consequently influence the deformation mode.

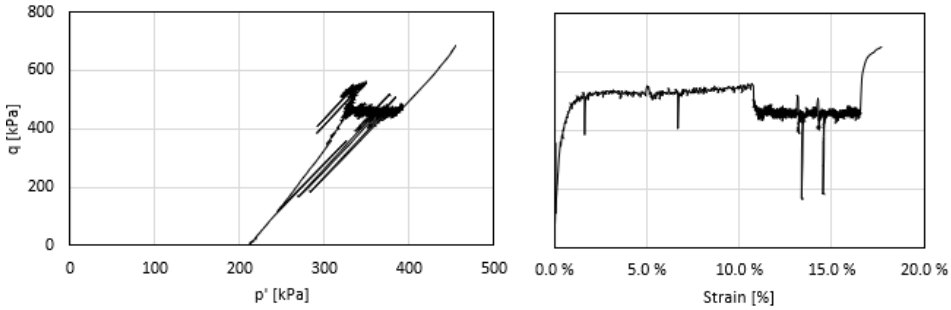

Figure 6.1: Typical shear test results are shown with q - p' and q - ϵ_a. From test no. 9.

6.3.1 Effective and Total Stress

Application of effective stress and total stress concepts is of interest in frozen ground engineering. At a certain level of unfrozen water content, the soil goes from following an effective stress approach to a total stress approach.

As mentioned, the amount of unfrozen water depends on temperature and salinity which in turn determine which concept is most valid. Figure 6.2 illustrates this change in approach based on the unfrozen water content. At a certain amount of UWC marked with ”x”, the design approach best applicable change between an effective and a total stress model.

Test results show that specimens at -3 °C to -5 °C exhibits behaviour close to that of an undrained triaxial compression test on unfrozen soil. As excess pore pressure develops and elastoplastic response is initiated, the requirement of no volume change causes the q-p’ stress path to tilt towards the yield surface.

Colder tests, from -5 °C to -10 °C, exhibit behaviour similar to a drained triaxial compression test on unfrozen soil. The effective stress path for these tests incline 1:3, indicating little to none excessive pore pressure. Cold temperature reduces the amount of free pore water and consequently limits the pore water response. Furthermore, ice is impermeable, suppressing the ability for pore water to flow through the sample. Thus, it is believed by the authors that the absence of excess pore pressure produces ”drained conditions”.

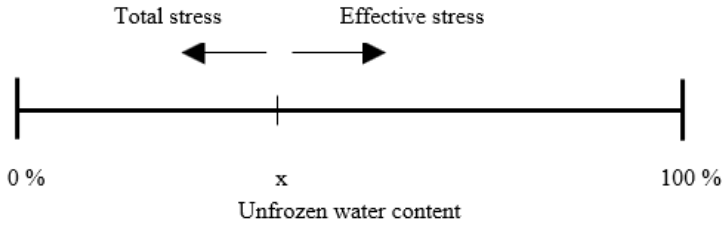

Figure 6.2: Total and effective stress analysis’ dependency on unfrozen water content. A certain UWC, shown with x, marks the change between total and effective stress concepts.

6.4 Pore pressure

To better understand the mechanics of frozen soil, a study on pore pressure behaviour is performed.

6.4.1 Pore Pressure and Temperature

Figure 6.3 shows the relationship between pore pressure and temperature, with data from tests performed on samples from borehole II. Pore pressure data is analysed in the same manner as strength, described in section 6.1. The test results show that pore pressure is highly influenced by temperature, and tends to increase with increasing temperature, which is expected since warmer conditions indicate a more prominent water phase.

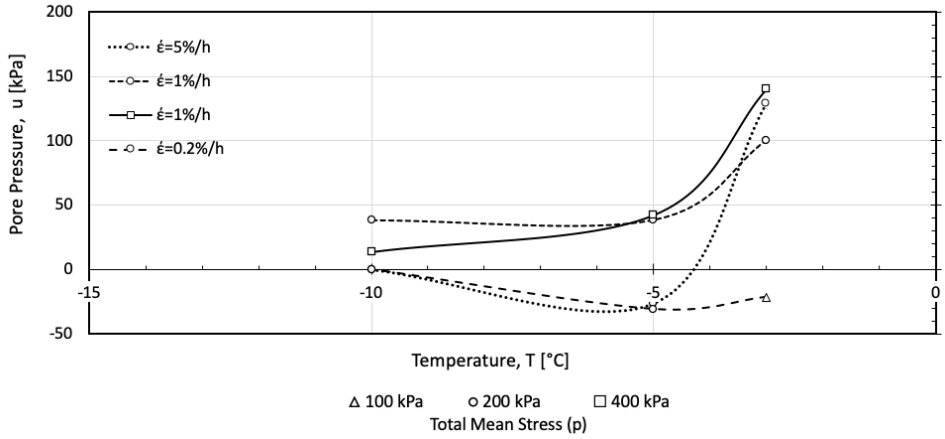

Figure 6.3: Pore pressure vs. Temperature for saline frozen clay with varying strain rate and total mean stress.

The pore pressure also tends to rise with increasing strain rate. This phenomenon is not well presented in Figure 6.3, but is however observable in Table 4.1. It is noteworthy to mention that some of the tests registered negative pore pressure (suction), particularly for tests ran at low strain rates. This is further discussed in section 6.4.3. As for high strain rates (5%/h or higher), test results show that the pore pressure in these tests had insufficient time to stabilize. Some of the tests are run only for 10-20 minutes for higher strain rates. Thus, the authors suspect that the pore pressure in these cases is lower than the real value. Figure 6.4 shows an example of test results for a sample run at different strain rates, and an example of high strain rate being run for a short period.

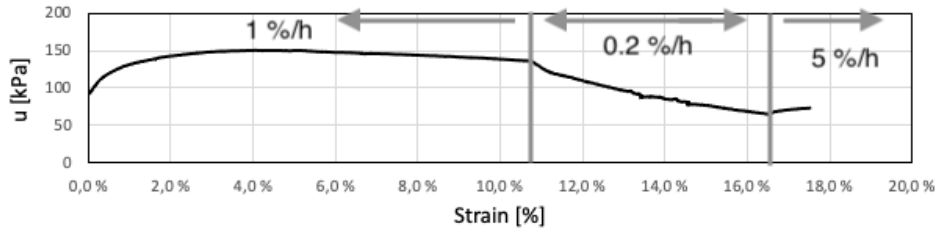

Figure 6.4: Test results from test no. 9 showing pore pressure vs. strain. Change in strain rate are shown to illustrate how testing is performed.

As stated, the pore pressure is connected to the water phase of the test sample. Hence, it is relevant to check how the water content in the frozen soil affects the recorded pore pressure. Results from borehole II is presented in Figure 6.5, run with 1 %/h strain rate. The water content varies from 37.9 % to 52 %. It is observable that higher water content leads to higher pore pressure measurements for all tests, except test no. 8 (-5 °C and 52 % water content). However, test no. 8 was exposed to temperature problems as mentioned in section 6.2, and might be unreliable.

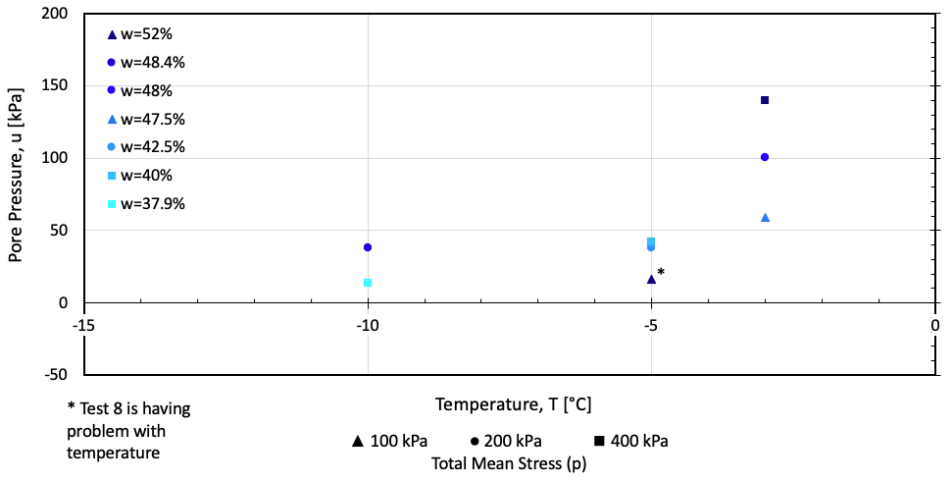

Figure 6.5: Pore pressure vs. Temperature distribution for saline frozen clay run at 1 %/h strain rate showing the effect of water content.

6.4.2 Pore Pressure and Cell Pressure

The connection between pore pressure, u, and cell pressure, σ_3, is presented in Figure 6.6, with each curve showing results with similar temperature, strain rate and salinity. The soil tends to achieve higher pore pressure with increased cell pressure. However, the curve at

-10 °C show decreasing pore pressure and deviates from the trend. A possible reason for this is unexpectedly high pore pressure measurements for test no. 14, which was mounted for 10 days before testing.

The tests run at -5 °C record a high initial slope, followed by a reduced inclination as the cell pressure rises. Similar behaviour is observed for warmer temperatures, however with a steeper slope. A dependency between pore pressure and confining pressure arise. Yet, for lower temperatures, the effect diminishes. A possible cause is the reduction in free pore water.

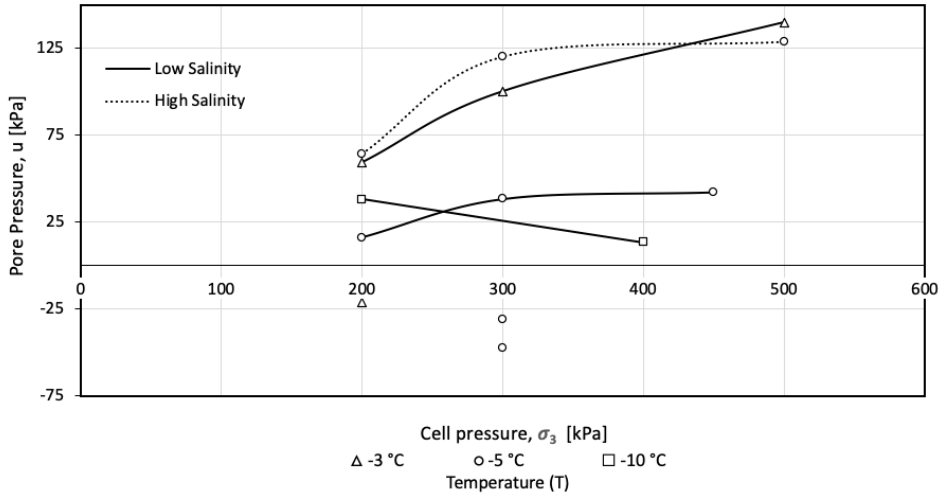

Figure 6.6: Pore pressure vs. confinement pressure. The curves show test results for 1%/h strain rate, and the single points show results for 0.2%/h.

6.4.3 Suction

Some tests showed suction in the range of -47 to -20 kPa. A study performed by Hazirbaba et al. (2011) recorded negative or minimal excess pore water pressure for silt at -0.2 °C. The study suspected that the negative pore pressure was caused by redistribution of pore water as it moved towards growing ice lenses. Similar behaviour may be attributed to the suction recorded in the present thesis. However, the author believes that samples were initiated at equilibrium conditions and therefore a growing ice lens should not be present. Yet, a strain rate of 0.2 %/h may cause a redistribution of pore water.

Another possible explanation may be linked to the fact that the strain rate is altered during testing, as this may allow redistribution of pore water. As the sample is experiencing a

load reduction due to a lower strain rate, suction may be an effect of the previous strain rate. In fact suction is recorded in all tests warmer than -10 °C with a mid-test reduction of strain rate. Since suction may indicate dilative behaviour (Hazirbaba et al., 2011), the temperature effect on dilatancy was further investigated. Li et al. (2018) studied unsaturated frozen silty clay and observed that dilatancy is more visible for lower temperatures, contradicting with the hypothesis of dilatancy causing suction in the present thesis. Returning to the initial idea, at -10 °C, the amount of water able to migrate through the soil is considerably lower than for warmer soils. This supports the theory on redistribution of pore water towards an ice lens being the cause of suction. As a consequence, a dependency on strain rate or a strain rate change seems most likely to cause suction.

Hazirbaba et al. (2011) recorded suction in tests with a thermal gradient, unlike the present thesis where tests are run with a constant temperature. This could contribute to the suction recorded by Hazirbaba. However, triaxial testing in this thesis is done with a constant temperature and a thermal gradient does not explain the suction recorded.

6.5 Deviatoric and Mean Effective Stress

Figure 6.7 shows peak deviatoric stress and mean effective stress from tests with 1 %/h strain rate. Deviatoric stress increases with mean effective stress, however as the mean effective stress rises, the initial slope tends to eventually reach an upper level. This is inconsistent with results from Wang and Nishimura (2017), which show a linear relationship between deviatoric stress and mean effective stress. A reason for the differences in the findings might be the scientific approach. As described earlier in the present thesis, Wang did not measure pore pressure, but did rather use an assumption described in section 3.1.1. Thus, possibly making the results difficult to compare. Furthermore, p'-values in Figure 6.7 are significantly higher than that of Wang. A potential cause for this may be linked to the fact that for cold temperatures the test acts as if it was drained conditions, as described in section 6.3.1. Cold temperatures leads to a small amount of unfrozen water in the test, which again leads to small pore pressure measurements. As present thesis measures pore pressure directly it is affected by this phenomena, however, Wang is not. The cold temperatures causes the effective stress path to continuously increase with an inclination of 1:3, leading to high p' values. An example can be seen in Figure 6.1. For tests with warm temperatures or high salinity, the p'-values are as expected.

Furthermore, data from Wang have a steeper inclination, q/p', compared to this thesis. The present thesis uses saline frozen soil which should be taken into consideration when comparing strength. As stated in the literary review, section 3.2.2, pore water salinity exceeding 10-20 ppt may drastically reduce the strength, which is also observed in the

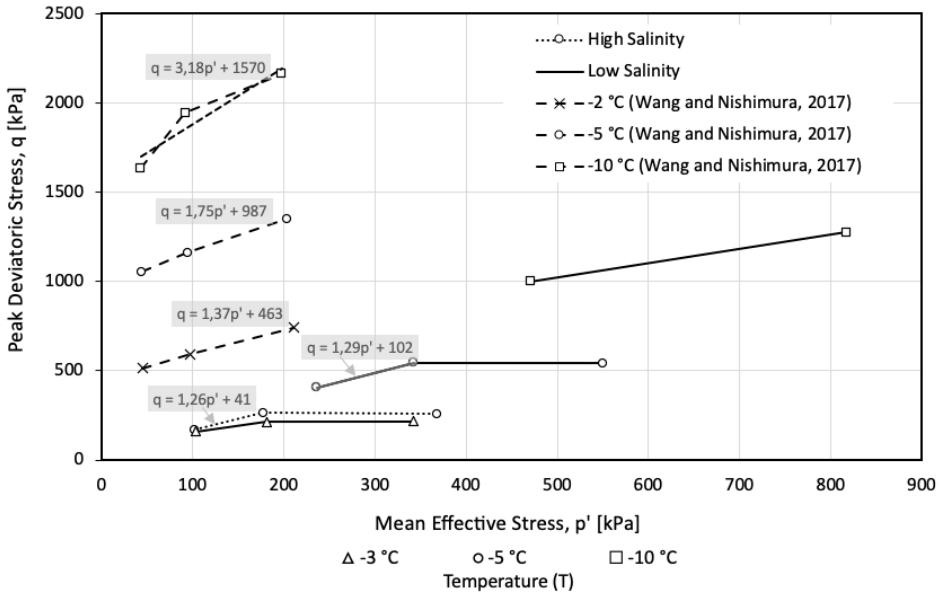

Figure 6.7: Mean effective stress vs. Peak deviatoric stress. Strain rate of 1 %/h. Compared with data from Wang and Nishimura (2017).

present thesis. Thus, salinity is considered a cause for a more gradual strength increase.

From a statistical point of view, Figure 6.7 raises some questions on the reliability of the data size. Removing one point on a curve changes the trend noteworthy. By ignoring the first point, the curve becomes flat. By removing the midpoint the slope is significantly reduced. Lastly, by removing the third point, the slope is increased. Hence it becomes clear that the data set is possibly inadequate.

6.6 Water Content and Salinity Effect

6.6.1 Water Content

Water content in frozen soil influences strength either as water in the pores or ice. Water in the pores reduces strength while water in the phase of ice increases strength. Figure 6.8 presents water content measured in the index test together with peak deviatoric stress. The figure indicates that increased water content decreases strength, but a clear trend is not observable. Hence, studying the strength effect of water content alone is of little use, especially since salinity and temperature greatly influences the state of the water.

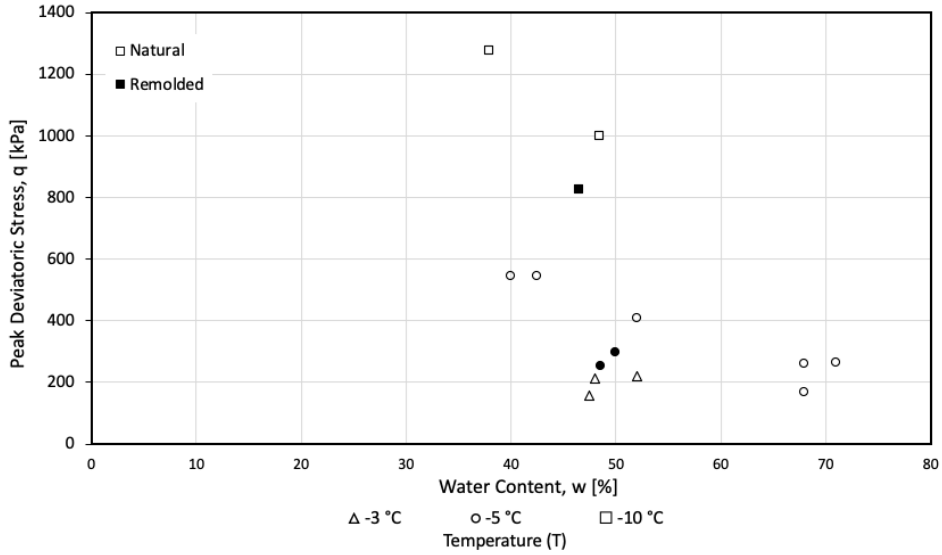

Figure 6.8: Water content vs. peak deviatoric stress. Strain rate of 1%/h. Hollow symbols are natural whereas filled symbols are remoulded samples.

However, it has been proved that studying the strength effect of unfrozen water content is more relevant. When including salinity and temperature it is possible to calculate unfrozen water content, by using the empirical Equation 2.7. Figure 6.9 shows the calculated volumetric UWC with deviatoric stress. This shows a clear trend of strength being lowered for rising unfrozen water content. Compared to Figure 6.8, it is observable that considering UWC rather than WC when discussing strength, is of higher relevance.

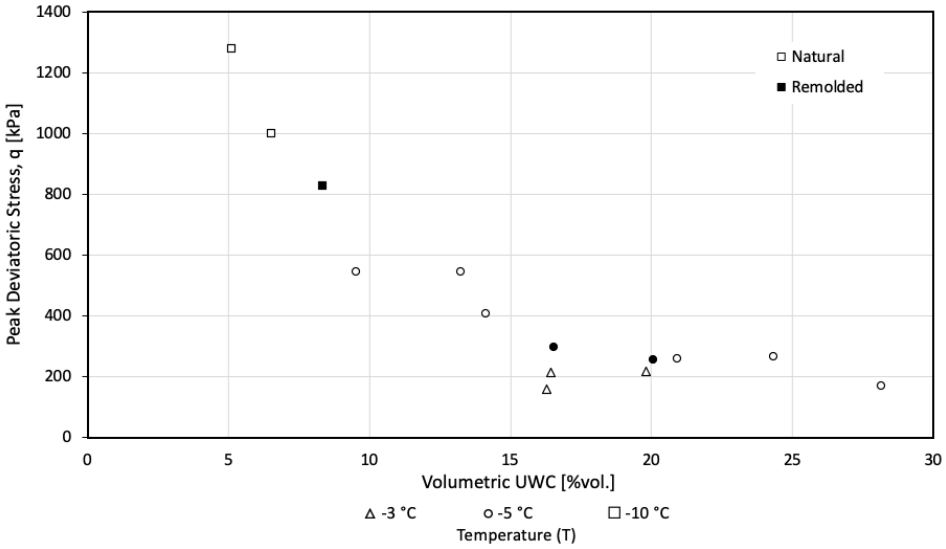

Figure 6.9: Volumetric unfrozen water content with deviatoric stress. Strain rate of 1 %/h.

6.6.2 Salinity

Figure 6.10 shows deviatoric stress compared to salinity in ppt. The soil strength decreases for samples with high salinity, which is expected since salinity alters the unfrozen water content. At a salinity of 26 ppt and above, with the temperature of -5 °C, the strength reduction appear to halt and the curve levels out. Few tests have been carried out for samples with salinity below this, but these tests fit both a linear and exponential trend.

Data from the literature review with a focus on salinity are summarized in Figure 3.4. It shows test results from several different soil types acquired from three studies (Ogata et al., 1983; Hivon and Sego, 1995; Pharr and Merwin, 1985). The figure shows that for fine-grained soils, for instance, clayey silt from Ogata et al. (1983) or fine silty sand from Hivon and Sego (1995), the salinity forms a linear relationship to normalized strength. Meanwhile, the strength in coarse-grained soils relates proportional to salinity, as seen for sand from Pharr and Merwin (1985) and Hivon and Sego (1995). Thus, a linear relationship between strength and salinity is expected for the clay tested in the present thesis. As mentioned above, indications of linear dependency are observed in Figure 6.10, but since the present study has not conducted experiments on specimens with salinity below 18 ppt, a reasonable conclusion can not be made.

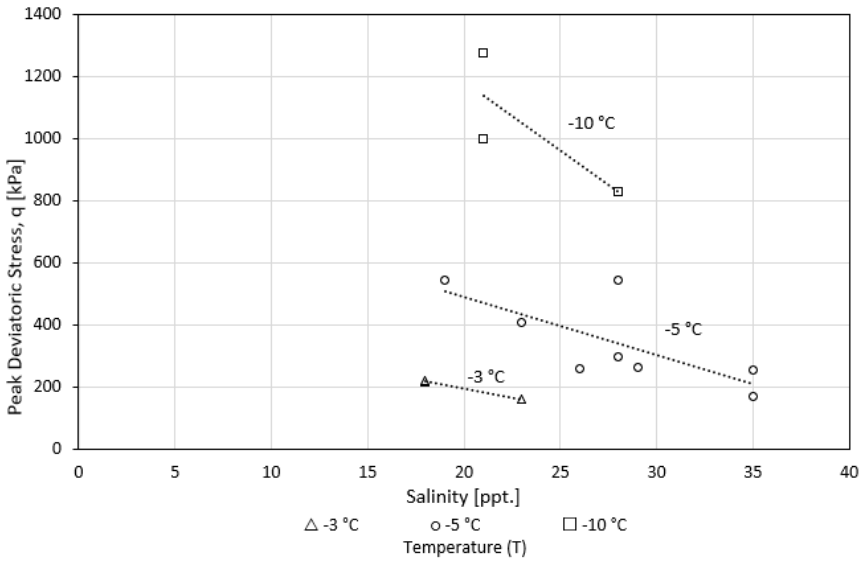

Figure 6.10: Salinity with deviatoric stress. The strength decreases for high salinity samples.

The exponential and linear correlation in coarse and fine-grained soils, respectively, is believed to be caused by a difference in pore water properties. As mentioned in Section 3.2.2, unfrozen pore water in coarse soils may be trapped in the middle of the pore space. Because of this, the introduction of salt inclusions traps pockets of high salinity water in the soil. Contrary to fine-grained soils, where a large proportion of the unfrozen water is located as a film surrounding the soil particles. This film is a result of the polarity of water together with the negatively charged clay particles, forming a covalent bond and lowering the pore water freezing point. Thus, clay is less sensitive to a change in salinity compared to sand, due to the unfrozen water content in clay being affected by both salt inclusions and interparticle bonds.

6.7 Temperature Effect

One of the most important differences when working with frozen clay compared to unfrozen clay is the dependency on temperature. As mentioned earlier, temperature highly influences both strength and pore pressure in the frozen soil. This is a consequence of water transitioning to ice which cements the soil skeleton, creating a more solid mass.

6.7.1 Peak Deviatoric Stress vs. Temperature

Figure 6.11 shows the relationship between temperature and peak deviatoric stress, for three different strain rates along with various mean stress applied. As expected the peak deviatoric stress is highly influenced by temperature, as it increases with descending temperature. This phenomenon is widely accepted, and probably linked to the unfrozen water content being lowered with descending temperature, which again corresponds to a higher content of ice.

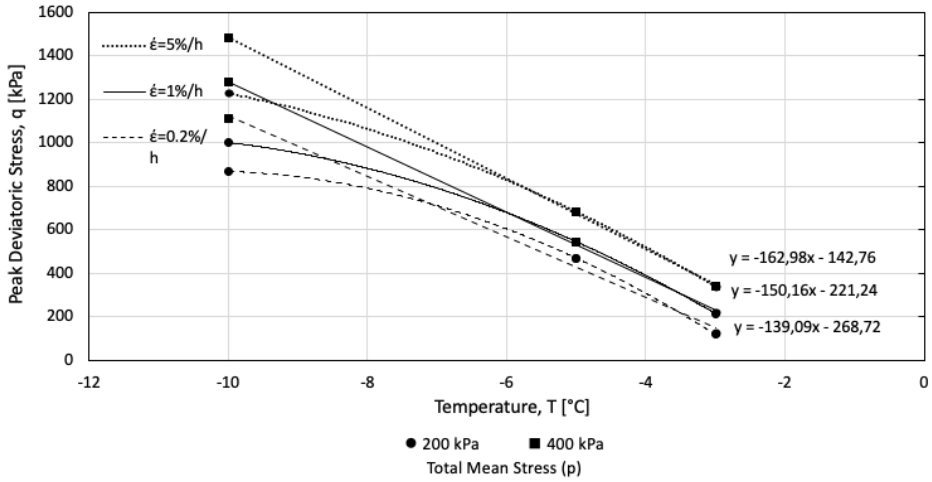

Figure 6.11: Peak deviatoric stress vs. temperature with varying strain rates and mean effective stress.

Figure 6.11 also shows that for temperatures warmer or equal to -5 °C, the soil strength seems to merely depend on the strain rate, which will be discussed later in this thesis. However, for cold temperatures (-10 °C) the soil strength seems to be affected by the mean stress in addition to the strain rate. This phenomenon is observed regardless of the strain rate applied, and the soil strength tends to increase with increasing mean stress. It is also noted that high mean stress, p = 400 kPa, seems to be creating a linear relationship between the peak deviatoric stress and the temperature. The slope of the linear dependency is fairly similar regardless of the strain rate, but seems to be showing a minor decrease for slower strain rates. The difference quotient is 17.2 % larger for 5 %/h strain rate compared to 0.2 %/h.

As mention in Section 3.2.3, Hivon and Wang recorded a linear relationship between temperature and shear strength. The strain rates applied in the two studies are 0.8 %/h and ranging from 0.06 to 6 %/h, for Hivon and Wang respectively. Hence, of a magnitude

comparable to the strain rate used in this thesis. It should be mentioned that results from Hivon are computed from uniaxial tests, and thus behave drained, in addition to being silty sand and not clay. The magnitude of the results are not very comparable, but the authors believe it is still interesting to investigate for similar trends and tendencies. The same goes for results from Wang. These are computed from triaxial testing on clay, but the soil samples do not contain any salt, resulting in peak deviatoric stress 2-3 times larger than for present study. Comparison of test results is shown in Table 6.2.

Author	S [ppt]	T [°C]	$\dot{\varepsilon}$ [%/h]	q [kPa]
Present study	19-28	-5	0.2-5	470-680
	26-35	-5	0.2-10	170-470
	21-28	-10	0.2-5	700-1490
Hivon and Sego (1995)*	0-30	-5	0.8	349-1543
	0-30	-10	0.8	575-2500
Wang and Nishimura (2017)	0	-5	0.06-6	1200-1600
	0	-10	0.06-6	2000-2440

Table 6.2: Comparison of test results with relevant literature.
*Uniaxial compressive strength

Test results from both Hivon and Wang show a linear relationship between strength and temperature, in other words, the same as the test results in this thesis with mean stress equal to 400 kPa. It is also notable that the difference quotient of the linear relation seems to experience a minor reduction with reducing strain rate for results from Wang, which was also the case for the present study. Thus, it seems like the soil strength is more sensitive for temperature change when subjected to higher strain rates. The tendency of reduced strength due to change in mean stress for low temperatures is not observed in the relevant literature, and differ from the linear temperature - deviatoric stress trend which was expected in advance of testing.

The data used for -10 °C with a mean stress of 200 kPa are all recorded from the same test sample (no. 14). This may be an explanation of why the soil experiences a reduced strength compared to the results recorded with mean stress of 400 kPa. As mentioned in section 6.2, test no. 14 experienced bulging during testing, along with potential contamination of ethylene glycol, and the reliability of the test data should thus be questioned.

Another explanation of the strength reduction, may be linked to the test conditions going from effective stress approach to total stress approach at low temperatures. At -10 °C, most of the water has frozen to ice ($i_r \simeq 85\%$), making the test sample behave drained.

Since the amount of unfrozen water is significantly lower at cold temperatures along with being less accessible, the water phase is close to negligible. This may be observed in the p'-q-plots found in Appendix B.

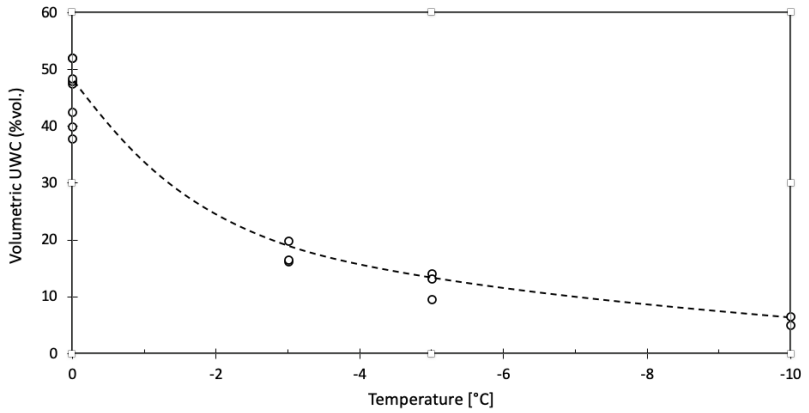

Figure 6.12: Distribution of volumetric unfrozen water content.

As mentioned, the reduction of strength due to decreasing temperature may be explained by examining the unfrozen water content. Figure 6.12 shows the volumetric UWC distribution from borehole II. It should be mentioned that the unfrozen water content in this thesis is not measured manually, but calculated by using Equation 2.7. The graph shows a typical freezing behaviour of soil, where temperature close to 0 °C initiates rapid freezing of unbound water, followed by a slower freezing process as colder temperatures are required to freeze the bound water. This creates an exponential decrement of UWC with decreasing temperature.

It is logical to think that the strength is more affected by temperature changes near 0 °C than at colder temperatures, as the change in unfrozen water content is greater. However, studying the relationship between UWC and peak deviatoric stress (Figure 6.13), it is observed that the trend between strength and UWC is similar to the trend between UWC and temperature. This may explain the observations of a linear trend between peak deviatoric stress and temperature.

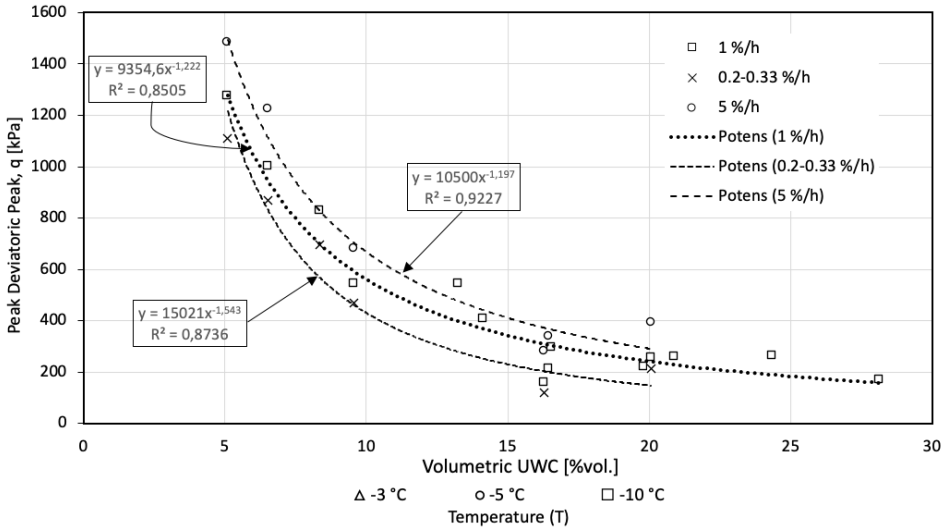

Figure 6.13: Relationship between volumetric unfrozen water content and peak deviatoric stress with varying strain rates.

6.8 Strain Rate Effect

Figure 6.14 shows the relationship between strain rate and peak deviatoric stress, q, for four different tests. All tests show a clear tendency of increasing strength with increasing strain rate, regardless of the sample temperature. Furthermore, the shear strength tends to increase log-linear to the strain rate, consistent with results from Li et al. (2004) and Wang and Nishimura (2017). It is also observed that a soil sample subjected to low strain rate tends to fail in a ductile manner, while failure in soil subjected to high strain rate tends to be more brittle.

The log-linear relationship seems more distinct for colder conditions. This is consistent with results obtained by Li et al. (2004), but does not appear in test results from Wang and Nishimura (2017). The reason for this is unclear, but may be linked to the fact that frozen soil behaves more ductile at higher temperatures, and have a lower ice content. In that case, when altering the strain rate for a warm frozen soil the failure mechanism may change from ductile to brittle. Contrary to a colder soil where the failure mechanisms may be more similar regardless of the applied strain rate.

The log-linear trend appears unaffected by confining stress and salinity. Note that all the tests in this thesis failed in a ductile manner regardless of applied strain rates. That means that no clear shear bands were recorded, and failure mode was observed as bulging.

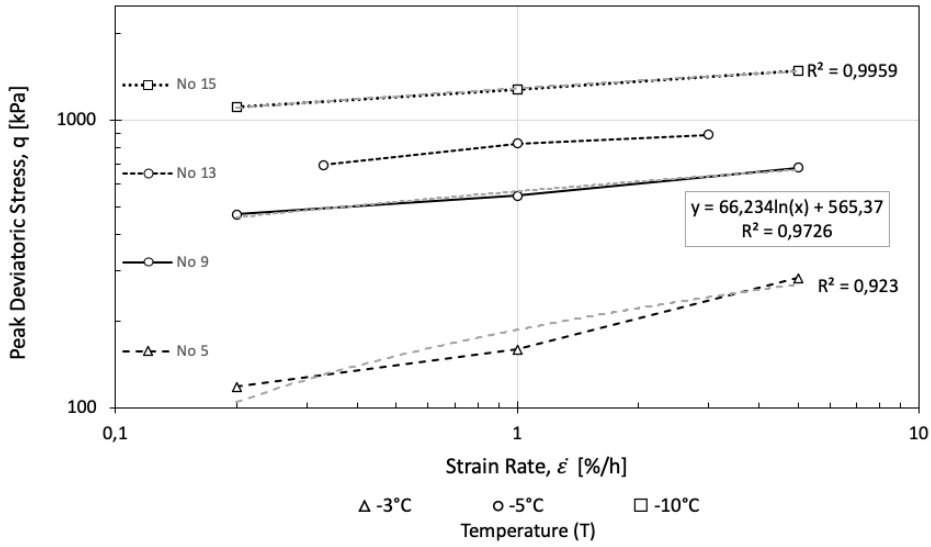

Figure 6.14: Peak deviatoric stress vs. strain rate in a log-log scale for triaxial tests on frozen clay. Showing log-linear relationship.

6.9 Regression Analysis

Regression analysis has been utilized to give a quantitative study, relating empirical observations to a mathematical expression. The method employed gives each parameter an exponent and aims to achieve the most accurate expression based on experimental results. Its usefulness becomes prominent when comparing test results with relevant literature, as soil parameters are fairly similar and often stated. However, the resulting constants are adapted to an experiment with a specific soil type which may not be comparable with other soils or experimental conditions. Still, it is a useful tool which offers insight about the significance of each parameter.

Two equations have been used to estimate peak deviatoric strength, q. Each are further explained in Subsection 6.9.1 and 6.9.2. The exponents have been calculated using the tool "Solver" in Microsoft Excel. Solver works by selecting a cell to strive for a certain value, which is done by changing selected variables and iterating. In this thesis, the method of ordinary least squares was used as the basis for the Solver tool. Firstly, residual between $q_{regression}$ and $q_{laboratory}$ was calculated, then squared. The residual sum of squares (RSS), recognized as the error, was minimized by Solver and exponents was attained. Equation 6.1 expresses the sum of squared residuals.

$$\text{RSS} = \sum_{i=1}^{n} (y_i - f(x_i))^2 \tag{6.1}$$

where y_i is an experimental result and $f(x_i)$ is the fitted regression function.

Resulting q and exponents are presented in Figure 6.15 and Table 6.3. The equations are further studied in Section 6.9.1 to 6.9.3.

As $q_{regression}$ has to be calculated first for Solver to find proper exponents, it is also depended on initial exponents. Errors or inconsistent results emerge based on user input. The Solver iterates by using the first prediction and then continuously improving the prediction each iteration. To counteract inconsistent results, it has been attempted to adjust exponents to fit the optimal solution before Solver calculated. The error associated with this is not certain, however by using R^2 a measurement of how well the regression predicts correctly is achieved.

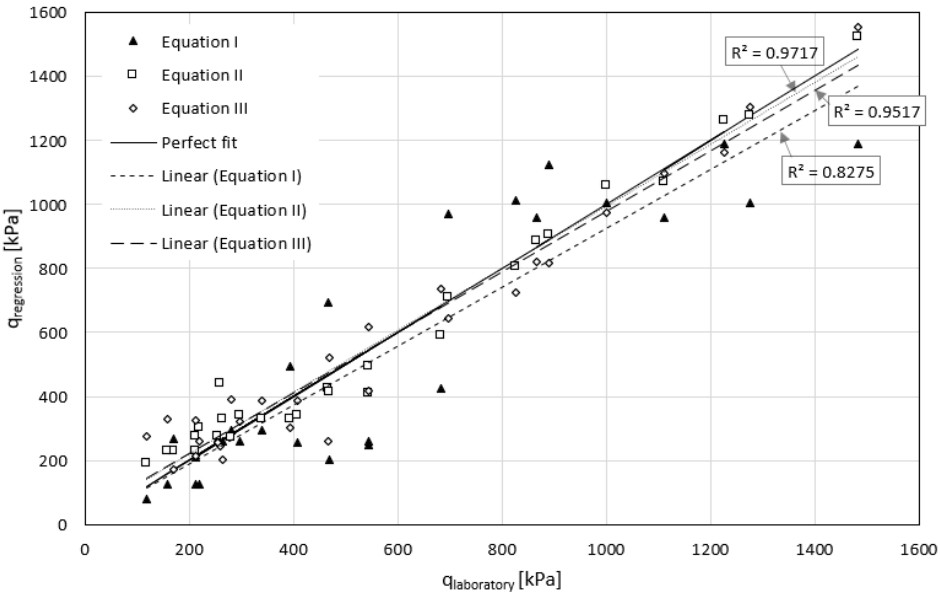

Figure 6.15: Linear regression using three different equations.

6.9.1 Equation I

The first equation tested is presented in Equation 6.2. The form is adopted to make each factor dimensionless by dividing with a reference value. Calculation issues, for instance, division by zero, are avoided as the denominator can not be zero. Preparation for this equation was inspired by Hivon and Sego (1995) and Li et al. (2004). Hivon and Sego used an equation considering strength as a function of temperature. Similarly, Li et al. based their equation on temperature, but added a factor for strain rate. Thus, Equation 6.2 is proposed to add a factor of salinity in addition to temperature and strain rate.

$$q = A\left(1 + \frac{T}{T_0}\right)^m \left(\frac{\dot{\varepsilon}}{\dot{\varepsilon}_0}\right)^n \left(1 + \frac{S}{S_0}\right)^t + B \tag{6.2}$$

where $T_0 = -1$°C is a reference temperature, $\dot{\varepsilon}_0 = 10^{-5}$ s^{-1} is a reference strain rate and $S_0 = 1$ ppt is a reference salinity value. m, n, t, k, A and B are constants derived using Solver.

Filled triangles in Figure 6.15 mark deviatoric stress calculated from Equation 6.2. The coefficient of determination, $R^2 = 0.8275$, is used as a quantity to assess how strong the linear relationship is. This fit is evaluated as a medium fit that needs improvement.

A specific issue with Equation 6.2 is its tendency to create ”staircases”. This effect is observed at $y = 250$ kPa and $y = 1000$ kPa in Figure 6.15 as the data points form a horizontal line. These data points have a common temperature and strain rate. Since two out of three parameters are identical, salinity is needed for a better regression. Yet, probably due to the limited effect of salinity in the equation, a significant number of results form horizontal lines.

Attempts on manually adjusting exponents to avoid and lessen the staircase effect has been done. Firstly, exponents was adjusted to approximately follow the perfect fit, then Solver calculated and refined exponents. Still, the effect is present.

6.9.2 Equation II

The second equation tested is presented in Equation 6.3. Unlike Equation 6.2, this does not use dimensionless references. It continues the use of exponents, with the addition of preconsolidation pressure. This parameter was added due to the author’s desire to add variation, as it may improve accuracy and avoid the staircase effect or similar effects.

$$q = A\left(-T\right)^{m}\left(\dot{\varepsilon}\right)^{n}\left(\frac{1}{S}\right)^{t}\left(p_0\right)^{k} + B \tag{6.3}$$

Hollow squares in Figure 6.15 mark deviatoric stress calculated from Equation 6.3. The achieved coefficient of determination in this regression model, $R^2 = 0.9717$, was superior to that of Equation 6.2. This fit is evaluated as a satisfactory fit.

Soils without salt inclusions would suggest division by zero, which is disallowed. Thus, Equation 6.3 is not valid for non-saline soils.

Table 6.3: Resulting exponents from the regression analysis.

Exponent	Equation I	Equation II
m	2.67	1.24
n	0.84	0.11
t	0.44	0.96
k	-	0.27
A	1.56	271
B	1.68	0

6.9.3 Equation III

Experimental data from this thesis show that the unfrozen water content is close to inverse proportional with the strength, q, see Equation 6.4.

$$q \simeq \frac{a}{w_u^b} \tag{6.4}$$

Implementing Equation 2.7 for unfrozen water, into Equation 6.4 yields an empirical equation for calculating peak deviatoric stress:

$$q = \frac{a}{\left[\frac{S_n}{1000}\left(1 - \frac{54.11}{T}\right) w\right]^b} \tag{6.5}$$

,where a and b are constants, S_n is salinity in ppt and w is water content in %. The peak deviatoric stress is also highly influenced by the strain rate, as stated in section 6.8, and should, therefore, be included in the empirical equation. Inspired by studies from Li et al.

(2004) and Hivon and Sego (1995), in addition to log-linear observations between $\dot{\varepsilon}$ and q, the strain rate is added as follows:

$$q = \frac{a\dot{\varepsilon}^c}{\left[\frac{S_n}{1000}\left(1 - \frac{54.11}{T}\right) w\right]^b} \tag{6.6}$$

The resulting components for Equation 6.6 were calculated to be: $a = 9124$, $b = 1.193$ and $c = 0.108$. Hollow rhombuses in Figure 6.15 mark deviatoric stress calculated from Equation 6.6. The achieved coefficient of determination was calculated to be R^2 = 0.9517, which is evaluated as a fairly satisfactory fit.

This regression model turned out to be surprisingly accurate, considering the regression was based on an empirical equation for unfrozen water content. This may be an indication that calculation models on frozen soil should be based on unfrozen water content.

As UWC has not been measured in this thesis its accuracy is difficult to determine. However, the equation used to calculate UWC is derived from a big sample size with different soil types. Thus, making it reliable.

As mentioned above, the relationship between strength and UWC is estimated to be inversely proportional. As this relationship was observed from experimental recordings it is believed to have some reliability. The good fit obtained by the current regression model may indicate that the assumption is valid. However, it still is an empirical model with limited data size and should be used with caution. Further testing and validation is needed to prove reliability.

Equation 6.6 does not include preconsolidation pressure which proved to be an important factor in Equation II. It is believed that Equation III may also gain a better fit when including preconsolidation pressure.

Chapter 7

Conclusion and Further Work

7.1 Conclusion

The main purpose of this thesis was to study the pore water response and carry out a parametric study of saline frozen soil. Additionally, a regression analysis was to be performed to summarize the parametric effects.

The phase relation between water and ice, highly influenced by temperature, salinity and soil composition, is a major element in frozen soil mechanics. An assembly of test results from Onsøy clay together with results from relevant literature shows the following trends:

- Pore pressure recordings increase with cell pressure, eventually reaching an upper level for high cell pressure values. However, pore pressure is more sensitive to altered temperature, and particularly temperature change close to the thawing point. This is most likely connected to the amount of unfrozen water available.
- Peak deviatoric stress increases with rising mean effective stress, but reaches a plateau at a certain mean effective stress level. This is believed to be caused by different effective stress paths for different levels of unfrozen water content.
- Salinity reduces the strength of frozen clay linearly, eventually reaching a lower limit. The effect of interparticle bonds together with salt inclusions is suspected to produce the linear relationship.

- Temperature has proven to be the main contributor to the mechanical behaviour of frozen soil. The deviatoric stress increases linearly with decreasing temperature. For cold temperatures (-10 °C), it is observed that total mean stress alters the linear trend.
- Strain rate alters the failure mechanism of frozen clay. For low strain rate values, the soil tends to fail in a ductile manner, while for high strain rate values the soil tends to fail in a brittle manner. The deviatoric stress increases log-linearly with increasing strain rate.

Temperature is the most important factor considering both soil strength and pore water response. It shows a linear trend with strength in the tested temperature range of -3 to -10 °C. It is observed that strength is inversely proportional to UWC, and UWC is inversely proportional to temperature, subsequently leading to a linear trend between strength and temperature.

Suction was recorded in several tests. This could be caused by a reduction in strain rate or the application of a low strain rate, believed to redistribute pore water.

Preconsolidation pressure proves to increase the accuracy of the regression model. In total, the best regression was found using temperature, strain rate, salinity and preconsolidation pressure:

$$q = 271\,(-T)^{1.24}\,(\dot{\varepsilon})^{0.11}\left(\frac{1}{S}\right)^{0.96}(p_0)^{0.27}$$

7.2 Recommendations of Further Work

Further work on the topic is needed to confirm trends, ensure reliable data and increase the understanding of frozen soil. Following is recommendations on the subject:

- **Salinity** in the range of 0 - 15 ppt is not tested in the present thesis. To confirm a linear trend, testing of low salinity soil needs to be performed.
- **Different soils** should be tested to study the effect of soil type. Onsøy clay was tested in this thesis which may behave differently to other soils. For instance, naturally frozen clay have different depositional history than artificially frozen clay and thus, may act dissimilar.
- **The freezing process** could be modified. Freezing the sample in confinement stress conditions may prevent the formation of ice crystals and create a more homogeneous

specimen. Furthermore, freezing during in situ environments might better sustain the soil stress history.

- **Effective stress path** and its relation to unfrozen water content needs to be further investigated. Understanding and finding the amount of unfrozen water content that correlates to the change between undrained and drained behaviour is needed to correctly interpret results. Results show that soil behaviour in a triaxial test may be depending on this phenomena.
- **The thawing point** marks a significant change in soil behaviour due to phase transitions. Knowledge on this transformation in frozen saline clay is valuable as degradation of permafrost may prove significant challenges in geotechnical engineering.
- **Pore pressure** measurements need further certification, especially the recorded suction. The authors attempted to find literature that also measured suction, however, these were limited and only one was determined to be comparable. Additional triaxial testing to increase the data size is needed.
- **Creep** is another aspect of soil behaviour not discussed in this thesis, however, it is important in order to fully understand frozen soil. It is the authors recommendations to conduct parametric testing on saline frozen clay regarding parametric effects on creep behaviour.

Bibliography

Andersland, O.B., Ladanyi, B., 2004. Frozen Ground Engineering - Second Edition. John Wiley & Sons, Inc., Hoboken, New Jersey.

Anderson, D.M., Morgenstern, N.R., 1973. Physics, chemistry and mechanics of frozen ground: A review, in: North American contribution to the second international conference on permafrost, pp. 257–288.

Arenson, L., Sego, D., 2006. The effect of salinity on the freezing of coarse-grained sands. *Canadian Geotechnical Journal - CAN GEOTECH J* 43, 325–337. doi:10.1139/t06-006.

Arenson, L.U., Springman, S.M., 2005. Triaxial constant stress and constant strain rate tests on ice-rich permafrost samples. *Canadian Geotechnical Journal* 42, 412–430. doi:10.1139/t04-111.

Baldi, G., Hight, D., Thomas, G., 1988. State-of-the-Art Paper: A Reevaluation of Conventional Triaxial Test Methods. McGraw Hill. doi:10.1520/STP29080S.

Banin, A., Anderson, D., 1974. Effects of salt concentration changes during freezing on the unfrozen water conent of porous materials. *Water Resour. Res.* 10(1), 124–128.

Bragg, R.A., Andersland, O., 1981. Strain rate, temperature, and sample size effects on compression and tensile properties of frozen sand. *Engineering Geology* 18, 35 – 46. doi:10.1016/0013-7952(81)90044-2.

Chamberlain, E., 1983. Frost heave of saline soils, in: Proceedings 4th International Conference on Permafrost, Fairbanks, Alaska, pp. 121–126.

Chamberlain, E., Groves, C., Perham, R., 1972. Discussion: The mechanical behaviour of frozen earth materials under high pressure triaxial test conditions. *Géotechnique* 23, 136–137. doi:10.1680/geot.1973.23.1.136.

Farnam, Y.A., Bentz, D., Sakulich, A., Flynn, D., Weiss, W., 2014. Measuring freeze and thaw damage in mortars containing deicing salt using a low temperature longitudinal

guarded comparative calorimeter and acoustic emission (ae-lgcc). *Advances in Civil Engineering Materials* 3. doi:10.1520/ACEM20130095.

Flerchinger, G.N., Seyfried, M.S., Hardegree, S.P., 2006. Using soil freezing characteristics to model multi-season soil water dynamics. *Vadose Zone Journal* 5, 1143–1153. doi:10.2136/vzj2006.0025.

Ghoreishian Amiri, S.A., Grimstad, G., Kadivar, M., 2016. An elastic-viscoplastic model for saturated frozen soils. *European Journal of Environmental and Civil Engineering* , 1–17doi:10.1080/19648189.2016.1271361.

Gundersen, A., Hansen, R., Lunne, T., L'Heureux, J.S., Strandvik, S., 2019. Characterization and engineering properties of the ngts onsøy soft clay site. *AIMS Geosciences* 5, 665–703. doi:10.3934/geosci.2019.3.665.

Hanssen-Bauer, I., Førland, E., Hisdal, H., Mayer, S., Sandø, A.B., Sorteberg, A., 2019. Atmospheric climate, in: Climate in Svalbard 2100, Miljødirektoratet, Longyearbyen, Svalbard. pp. 49–80.

Hazirbaba, K., Zhang, Y., Hulsey, J.L., 2011. Evaluation of temperature and freeze–thaw effects on excess pore pressure generation of fine-grained soils. *Soil Dynamics and Earthquake Engineering* 31, 372 – 384. doi:10.1016/j.soildyn.2010.09.006.

Hivon, E., Sego, D., 1995. Strength of frozen saline soils. *Canadian Geotechnical Journal* 32, 336–354. doi:10.1139/t95-034.

Hock, R., Rasul, G., 2019. High mountain areas: *Special Report on the Ocean and Cryosphere in a Changing Climate* .

Ikeda, A., Matsuoka, N., Kääb, A., 2008. Fast deformation of perennially frozen debris in a warm rock glacier in the swiss alps: An effect of liquid water. *Journal of Geophysical Research: Earth Surface* 113. doi:10.1029/2007JF000859.

Ishikawa, T., Tokoro, T., Seiichi, M., 2015. Geohazard at volcanic soil slope in cold regions and its influencing factors. *Japanese Geotechnical Society Special Publication* 1, 1–20. doi:10.3208/jgssp.KEY-1.

Jean-Sebastien L'Heureux, T.L., 2020. Characterization and engineering properties of natural soils used for geotesting. *AIMS Geosciences* 6, 35. doi:10.3934/geosci.2020004.

Kia, M., 2012. Measuring Pore-water Pressures in Partially Frozen Soils. Ph.D. thesis. University of Alberta Libraries. Department of Civil and Environmental engineering.

Konrad, J.M., McCammon, A.W., 1990. Solute partitioning in freezing soils. *Canadian Geotechnical Journal* 27, 726–736. doi:10.1139/t90-086.

Li, H., Zhu, Y., Zhang, J., Lin, C., 2004. Effects of temperature, strain rate and dry density on compressive strength of saturated frozen clay. *Cold Regions Science and Technology* 39, 39 – 45. doi:10.1016/j.coldregions.2004.01.001.

Li, Q., Xu, X., Hu, J., Zhou, Z., 2018. Investigation of unsaturated frozen soil behavior:

Phase transformation state, post-peak strength, and dilatancy. *Soils and Foundations* 58, 928 – 940. doi:10.1016/j.sandf.2018.05.003.

Mellor, M., Cole, D.M., 1982. Deformation and failure of ice under constant stress or constant strain-rate. *Cold Regions Science and Technology* 5, 201 – 219. doi:10.1016/0165-232X(82)90015-5.

Mulabdic´, M., 1993. Area correction in triaxial testing. *Swedish Geotechnical Institute* Varia nr 408, 0–21.

NGU.no, 2020. Quaternary map. URL: http://geo.ngu.no/kart/losmasse/.

Nixon, J., 1988. Pile load tests in saline permafrost at clyde river, northwest territories. *Canadian Geotechnical Journal* 25, 24–32. doi:10.1139/t88-003.

Nixon, J.F., Lem, G., 1984. Creep and strength testing of frozen saline fine-grained soils. *Canadian Geotechnical Journal* 21, 518–529. doi:10.1139/t84-054.

Nordal, S., 2019. Geotechnical engineering advanced course lecture notes. *TBA4116 Geotechnical Engineering Advanced Course.* NTNU , Ch. 11.

Norgeskart, 2020. Norgeskart. URL: https://www.norgeskart.no/.

Norwegian Public Roads Administration, 2014. *Håndbok V220 Geoteknikk i vegbygging*. Vegdirektoratet.

Ogata, N., Yasuda, M., Kataoka, T., 1983. Effects of salt concentration on strength and creep behavior of artificially frozen soils. *Cold Regions Science and Technology* 8, 139 – 153. doi:10.1016/0165-232X(83)90005-8.

Ono, N., 1975. Thermal properties of sea ice. iv. thermal constants of sea ice. *U.S. Army Cold Regions Research and Engineering Laboratory TL 467* .

Parameswaran, V., Jones, S., 1981. Triaxial testing of frozen sand. *J. Glaciol.* 27. doi:10.1017/S0022143000011308.

Patterson, D., Smith, M., 1983. Measurement of unfrozen water content in saline permafrost using time domain reflectometry. Canadian Geotechnical Journal , 968–972.

Patterson, D., Smith, M., 1985. Unfrozen water content in saline soils: results using time-domain reflectometry. *Canadian Geotechnical Journal* 22, 95–101.

Pharr, G., Merwin, J., 1985. Effects of brine content on the strength of frozen ottawa sand. *Cold Regions Science and Technology* 11, 205 – 212. doi:10.1016/0165-232X(85)90044-8.

Rist, M., Murrell, S., 1994. Ice triaxial deformation and fracture. *Journal of Glaciology* 40, 305–318. doi:10.3189/S0022143000007395.

Romanovsky, V., 2018. Permafrost thaw building. https://www.newsweek.com/climate-change-permafrost-thawing-arctic-methane-infrastructure-1253152.

Sayles, F.H., Haines, D., 1974. *Creep of frozen silt and clay*. U.S. Army Cold Regions Research and Engineering Laboratory, CRREL Technical Report 252.

Sego, D., Morgenstern, N., 1985. Punch indentation of polycrystalline ice. *Canadian Geotechnical Journal* 22, 226–233. doi:10.1139/t85-030.

Smith, T., Schulson, E., 1993. The brittle compressive failure of fresh-water columnar ice under biaxial loading. *Acta Metallurgica et Materialia* 41, 153–163. doi:10.1016/0956-7151(93)90347-U.

Sørensen, R., 1979. Late weichselian deglaciation in the oslofjord area, south norway. *Boreas* 8, 241 – 246. doi:10.1111/j.1502-3885.1979.tb00806.x.

Tang, L., Wang, K., Jin, L., Yang, G., Jia, H., Taoum, A., 2018. A resistivity model for testing unfrozen water content of frozen soil. *Cold Regions Science and Technology* 153, 55–63.

Tice, A.R., Anderson, D., Banin, A., 1976. *The Prediction of Unfrozen Water Contents in Frozen Soils from Liquid Limit Determinations*. U.S. Army Cold Regions Research and Engineering Laboratory CRREL Report 87-13 .

Ting, J.M., Martin, R.T., Ladd, C.C., 1983. Mechanisms of strength for frozen sand. *Journal of Geotechnical Engineering* 109, 1286–1302. doi:10.1061/(ASCE)0733-9410(1983)109:10(1286).

Tsegaye, A., 2014. Simple Models for Frozen Soil. Modelling the Strength of Saturated Frozen Soil. Technical Report. NTNU. doi:10.13140/RG.2.2.25386.06088.

Velli, Y., Grishin, P., 1983. On the functional dependence of the freezing point of soils on the composition of water-soluble salts in an insterstitial solution. *National Research Council, Canada* .

Wang, J., Nishimura, S., 2017. Interpretation of mechanical behavior of frozen clay through parallel tests of frozen and unfrozen soils. *Japanese Geotechnical Society Special Publication* 5, 155–160. doi:10.3208/jgssp.v05.042.

Yamamoto, Y., Springman, S.M., 2014. Axial compression stress path tests on artificial frozen soil samples in a triaxial device at temperatures just below 0 °c. *Canadian Geotechnical Journal* 51, 1178–1195. doi:10.1139/cgj-2013-0257.

Yong, R.N., 1965. Soil suction effects on partial soil freezing. *Highway Research Record* 68, 31–42.

Zhang, H., Zhang, J., Zhilong, Z., Chai, M., 2016. Investigation of the pore-water pressure of saturated warm frozen soils under a constant load. *Journal of Offshore Mechanics and Arctic Engineering* 138. doi:10.1115/1.4033936.

Østbye, K.S., 2018. Kryp i frossen jord. Master's thesis. Norwegian University of Science and Technology. Department of Civil and Environmental engineering.

Appendix A

Soil characterization

A.1 Map of Site

Figure A.1: Location of site. Retrieved from Norgeskart (2020).

A.2 Water Content, Plasticity, Grain Size and Salinity with Depth

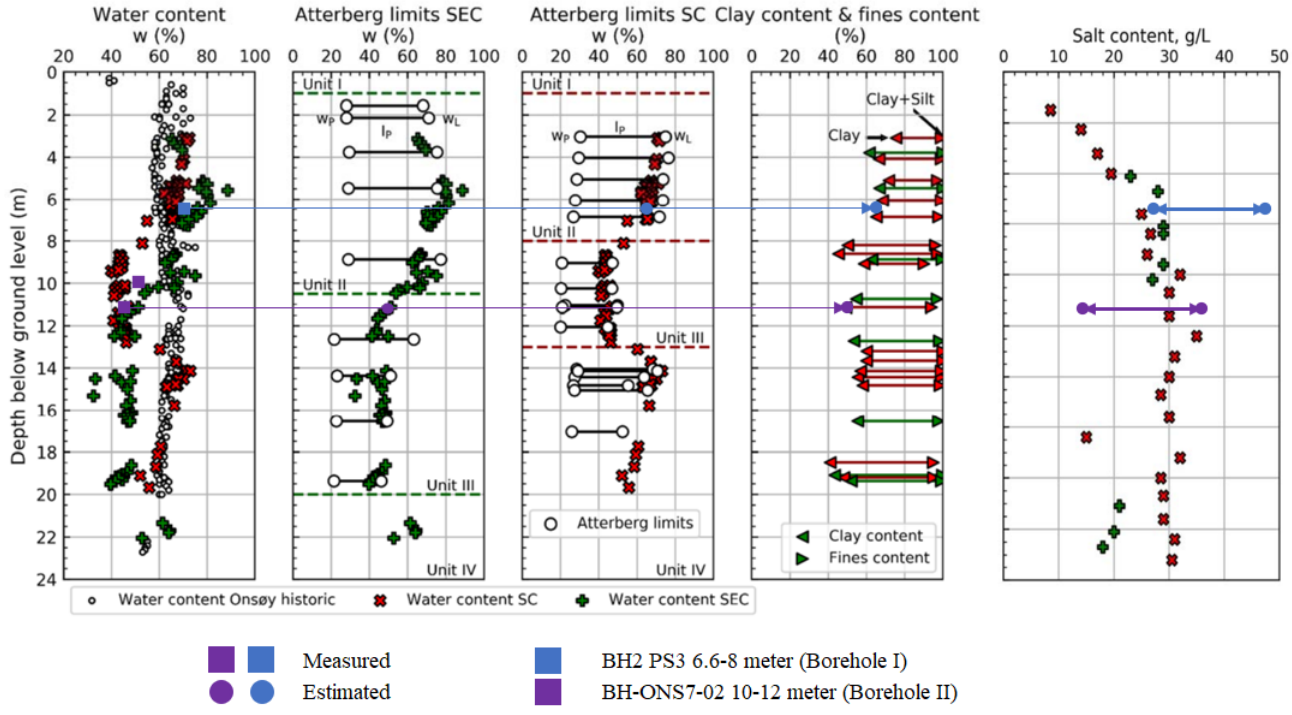

Figure A.2: Properties of the first four samples. Readings compared with Gundersen et al. (2019).

A.3 Unit Weigth, Preconsolidation Stress and Undrained Shear Strength with Depth

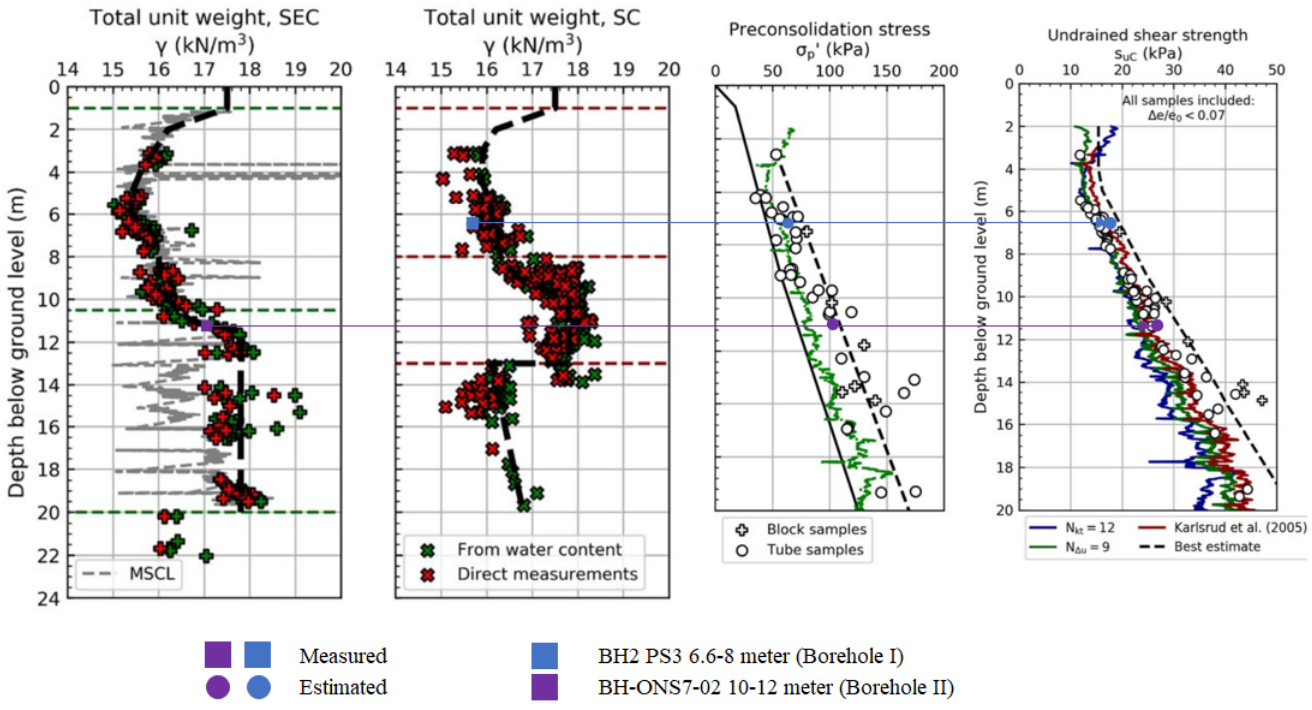

Figure A.3: Unit weigth and engineering properties of the first four samples. Readings compared with Gundersen et al. (2019).

Appendix B

Shear Test

B.1 Test no. 1

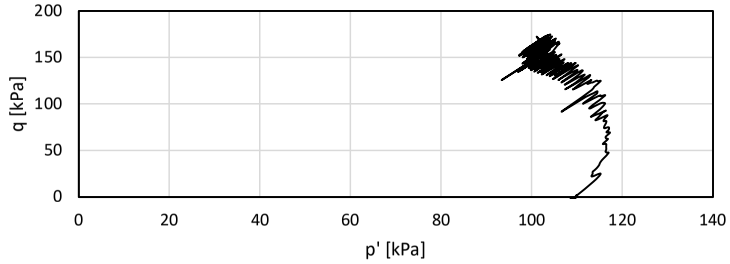

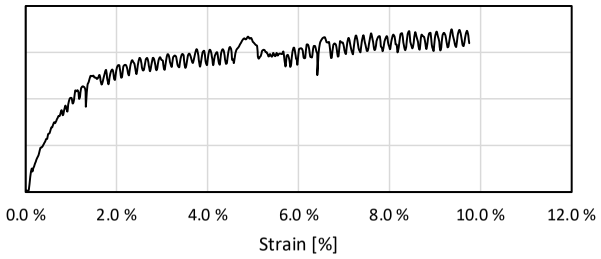

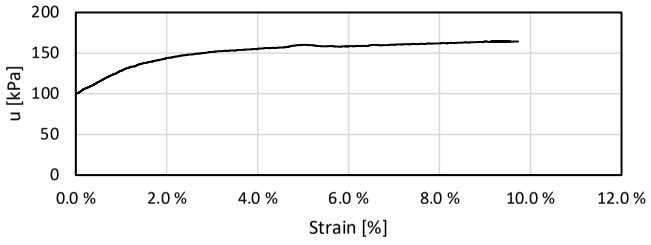

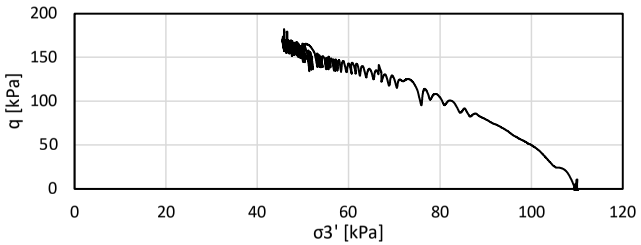

Test	Heigth	Cell pressure	Site
Undrained shear test	135 mm	100 kPa	Onsøy
	Diameter	Strain rate	Date
Test no.	74 mm	1 %/h	09.01.2020
1	Temperature	Depth	Remolded
	-5 °C	7 m	No

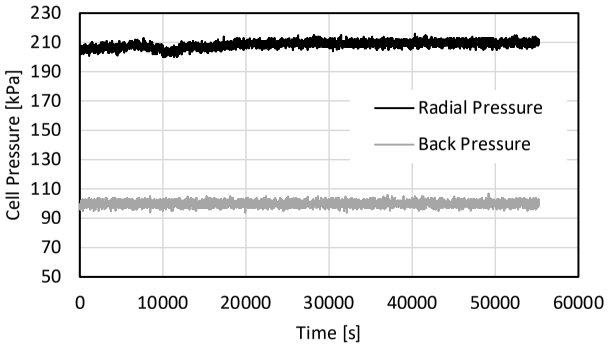

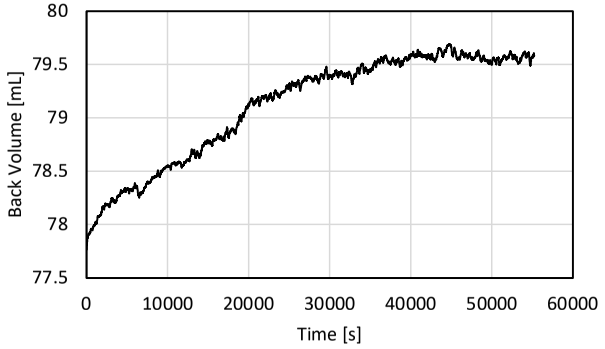

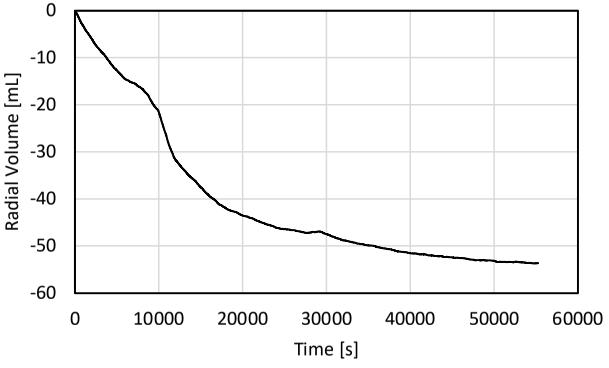

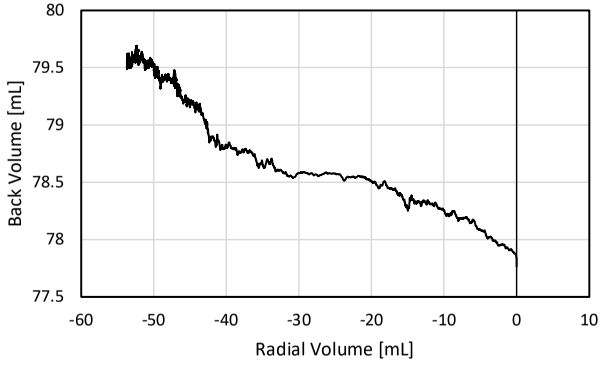

Test	Heigth	Cell pressure	Site
Undrained shear test	135 mm	100 kPa	Onsøy
	Diameter	Strain rate	Date
Test no.	74 mm	1 %/h	09.01.2020
1	Temperature	Depth	Remolded
	-5 °C	7 m	No

B.2 Test no. 2

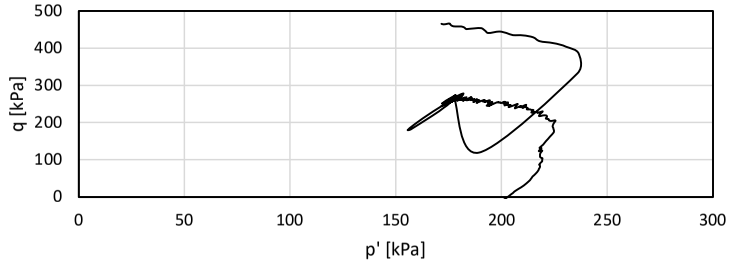

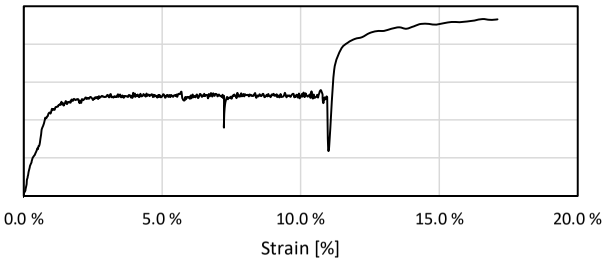

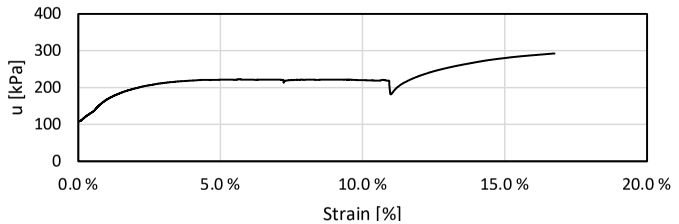

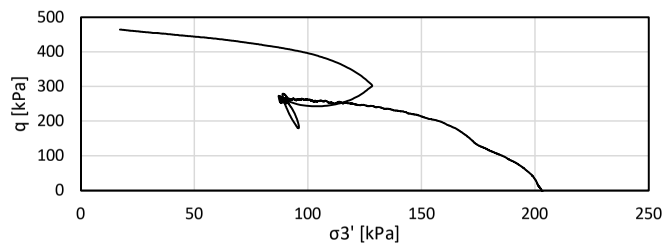

Test	Heigth	Cell pressure	Site
Undrained shear test	147 mm	200 kPa	Onsøy
	Diameter	Strain rate	Date
Test no.	73 mm	1 / 10 %/h	14.01.2020
2	Temperature	Depth	Remolded
	-5 °C	8 m	No

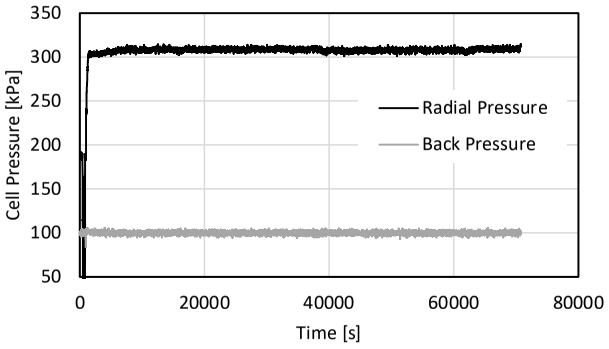

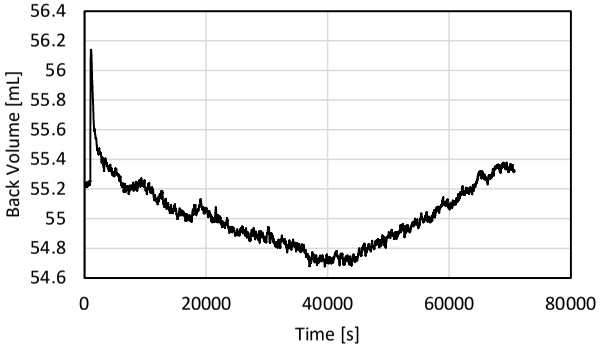

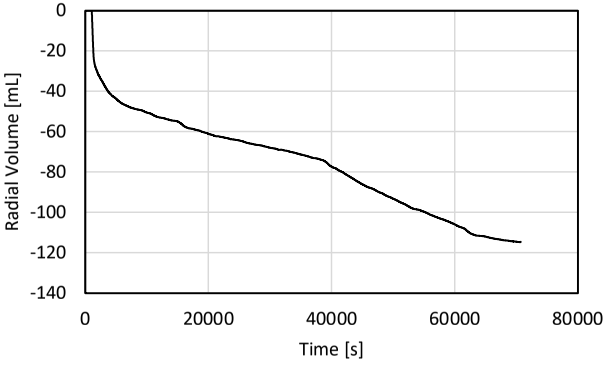

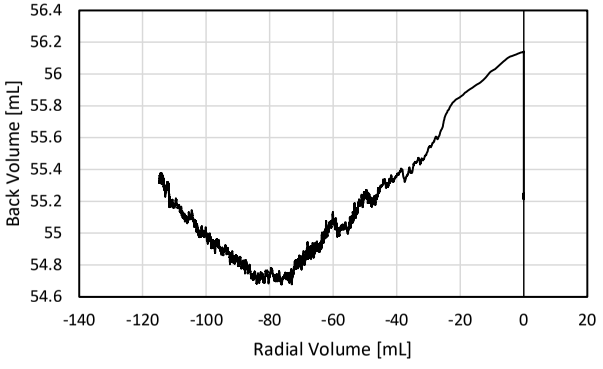

Test	Heigth	Cell pressure	Site
Undrained shear test	147 mm	200 kPa	Onsøy
	Diameter	Strain rate	Date
Test no.	73 mm	1 / 10 %/h	14.01.2020
2	Temperature	Depth	Remolded
	-5 °C	8 m	No

B.3 Test no. 4

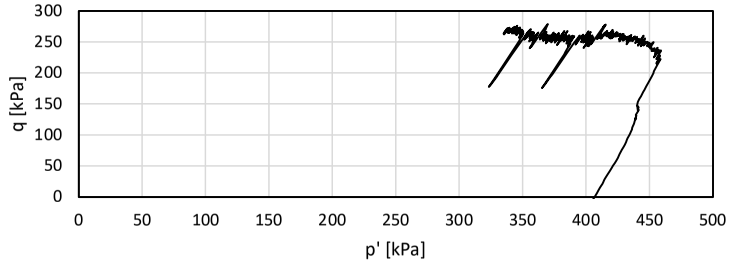

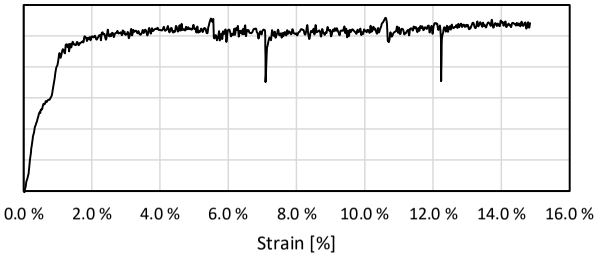

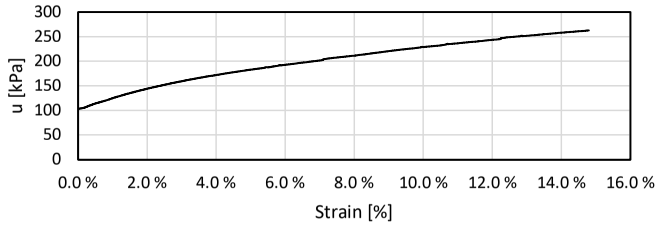

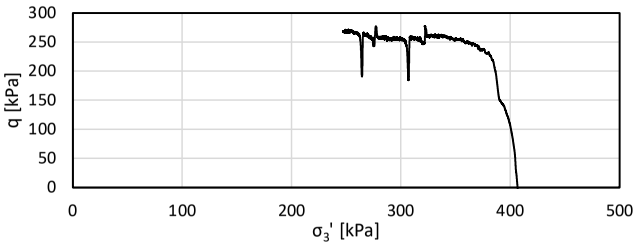

Test	Heigth	Cell pressure	Site
Undrained shear test	145 mm	400 kPa	Onsøy
	Diameter	Strain rate	Date
Test no.	73 mm	1 %/h	20.01.2020
4	Temperature	Depth	Remolded
	-5 °C	8 m	No

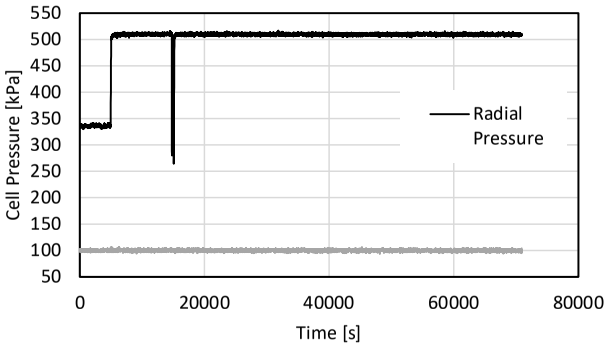

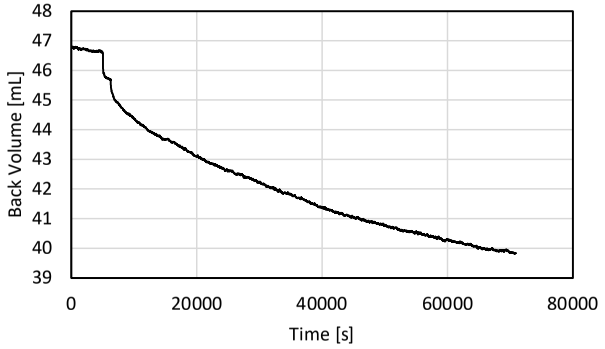

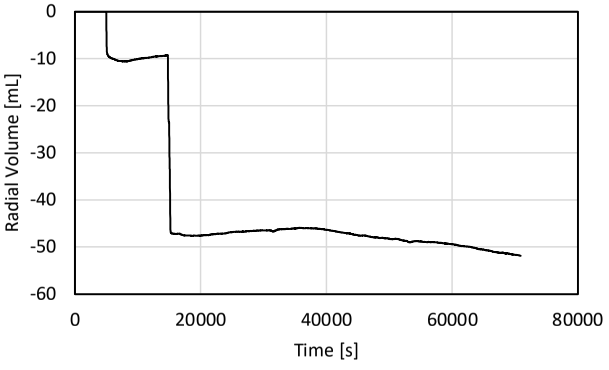

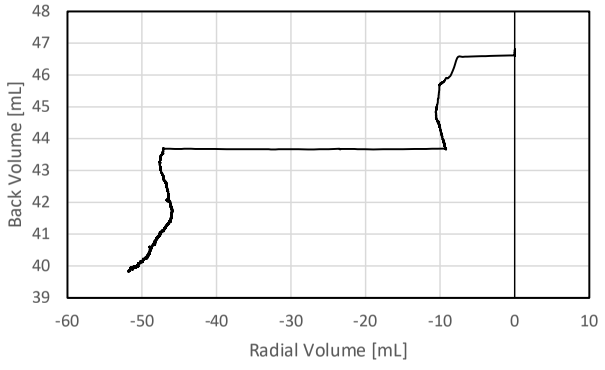

Test	Heigth	Cell pressure	Site
Undrained shear test	145 mm	400 kPa	Onsøy
	Diameter	Strain rate	Date
Test no.	73 mm	1 %/h	20.01.2020
4	Temperature	Depth	Remolded
	-5 °C	8 m	No

B.4 Test no. 5

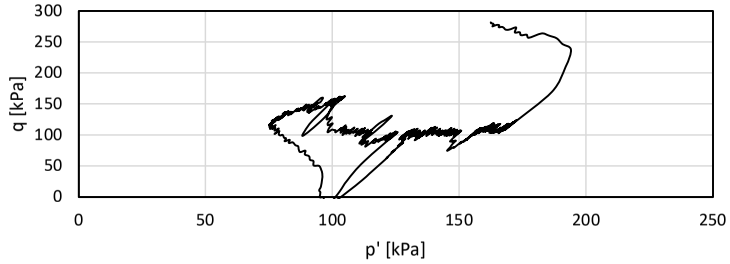

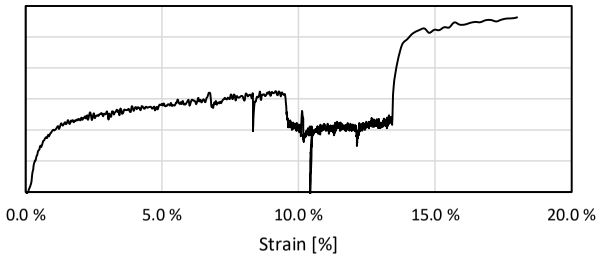

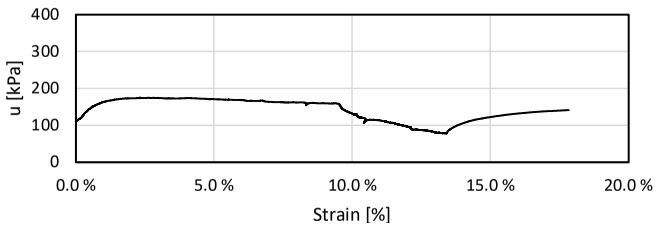

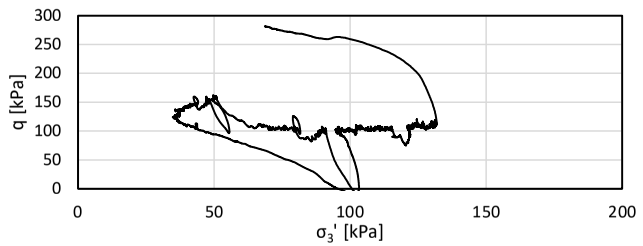

Test	Heigth	Cell pressure	Site
Undrained shear test	135 mm	100 kPa	Onsøy
Test no.	Diameter	Strain rate	Date
5	73 mm	1 / 0,2 / 5 %/h	23.01.2020
	Temperature	Depth	Remolded
	-3 °C	11 m	No

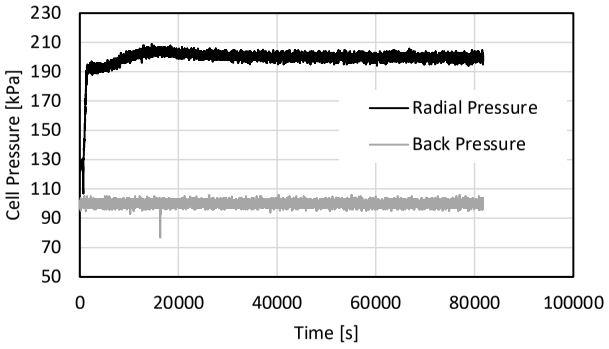

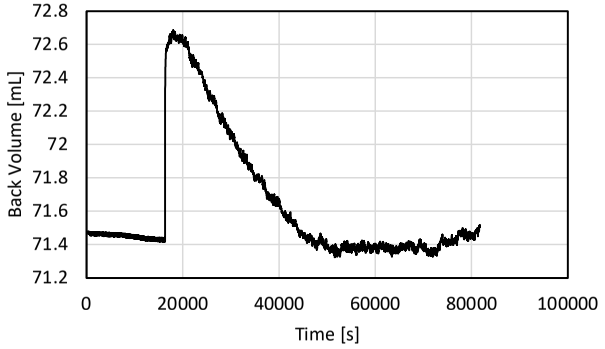

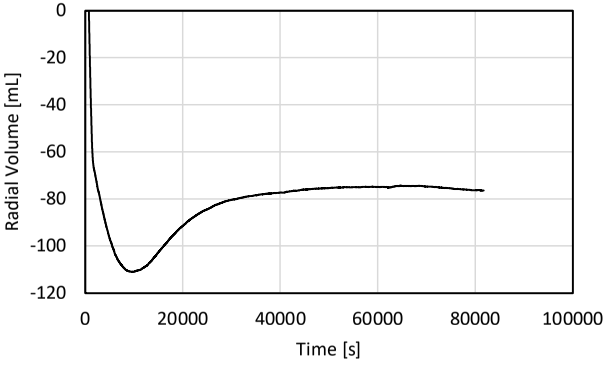

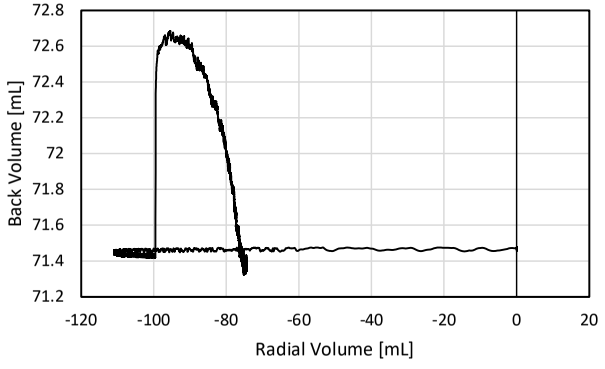

Test	Heigth	Cell pressure	Site
Undrained shear test	135 mm	100 kPa	Onsøy
	Diameter	Strain rate	Date
Test no.	73 mm	1 / 0,2 / 5 %/h	23.01.2020
5	Temperature	Depth	Remolded
	-3 °C	11 m	No

B.5 Test no. 6

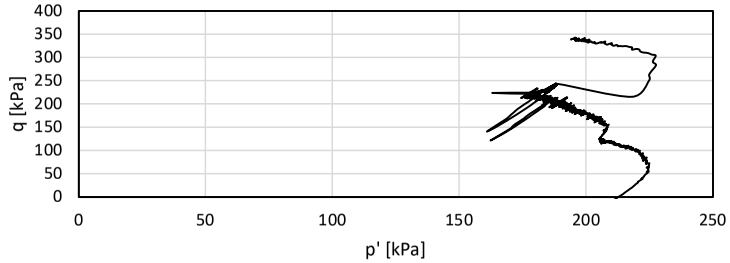

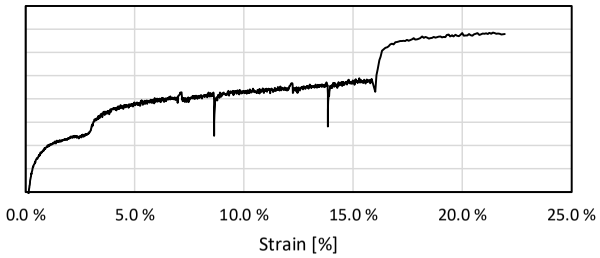

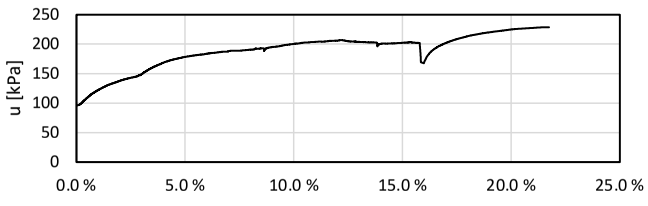

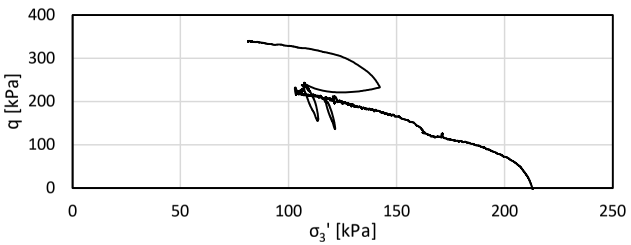

Test	Heigth	Cell pressure	Site
Undrained shear test	144 mm	200 kPa	Onsøy
	Diameter	Strain rate	Date
Test no.	73 mm	1 / 5 %/h	27.01.2020
6	Temperature	Depth	Remolded
	-3 °C	10 m	No

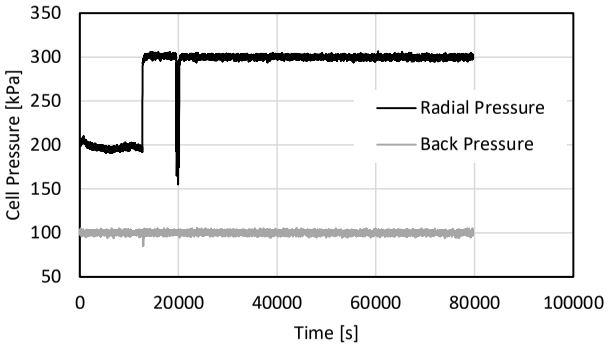

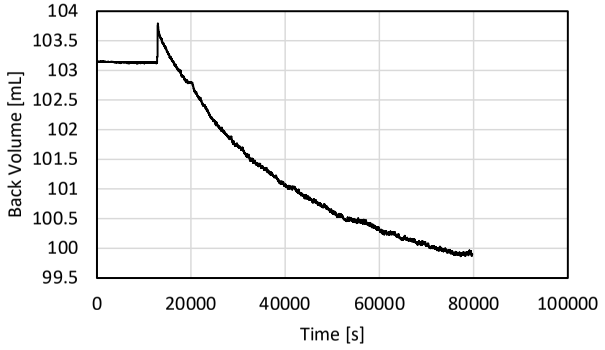

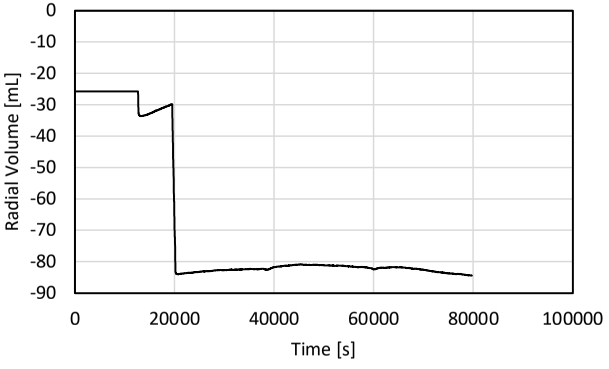

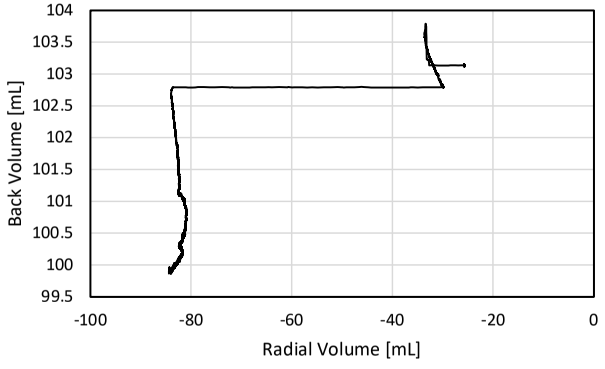

Test	Heigth	Cell pressure	Site
Undrained shear test	144 mm	200 kPa	Onsøy
	Diameter	Strain rate	Date
Test no.	73 mm	1 / 5 %/h	27.01.2020
6	Temperature	Depth	Remolded
	-3 °C	10 m	No

B.6 Test no. 7

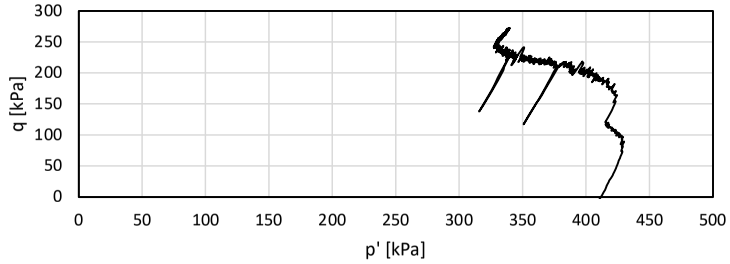

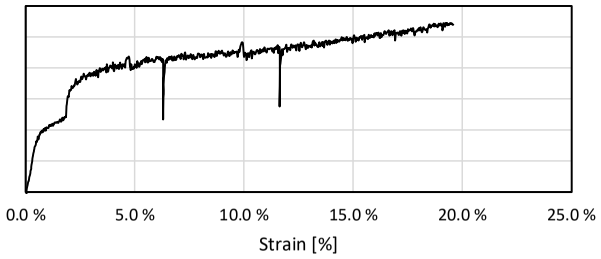

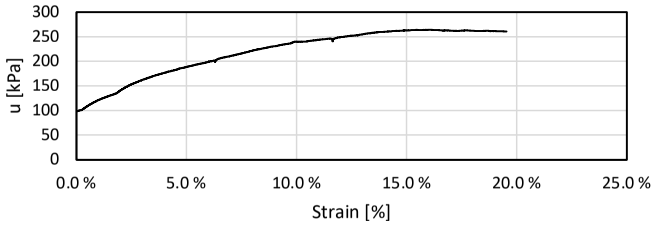

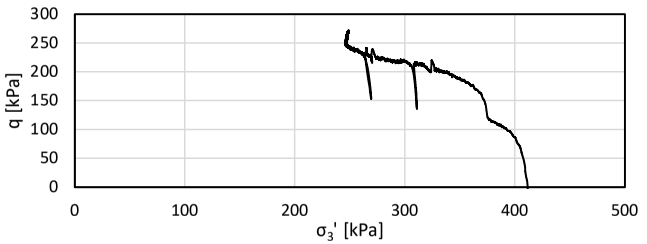

Test	Heigth	Cell pressure	Site
Undrained shear test	137 mm	400 kPa	Onsøy
	Diameter	Strain rate	Date
Test no.	73 mm	1 %/h	30.01.2020
7	Temperature	Depth	Remolded
	-3 °C	10.5 m	No

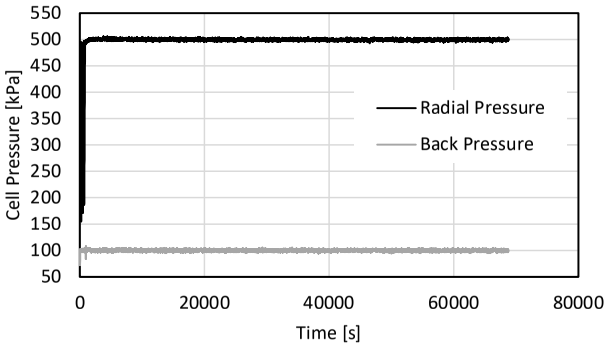

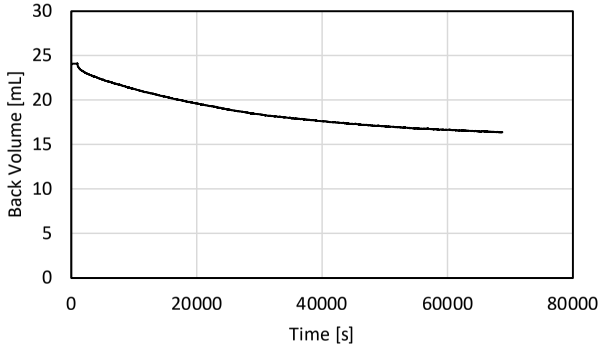

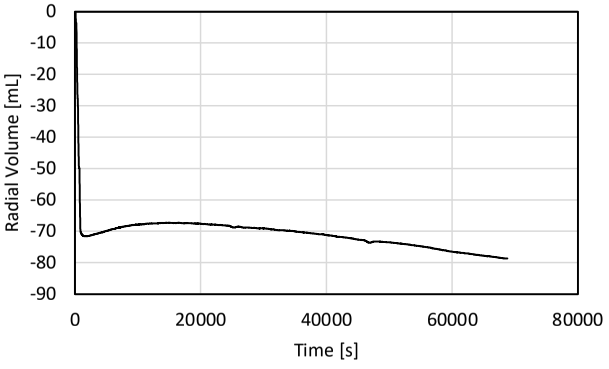

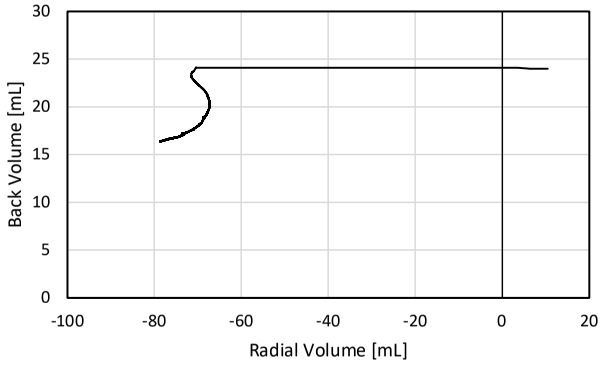

Test	Heigth	Cell pressure	Site
Undrained shear test	137 mm	400 kPa	Onsøy
Test no.	Diameter	Strain rate	Date
7	73 mm	1 %/h	30.01.2020
	Temperature	Depth	Remolded
	-3 °C	10.5 m	No

B.7 Test no. 8

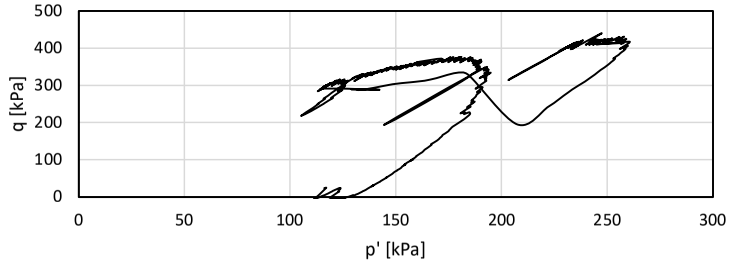

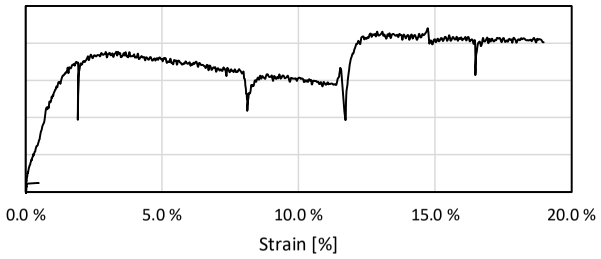

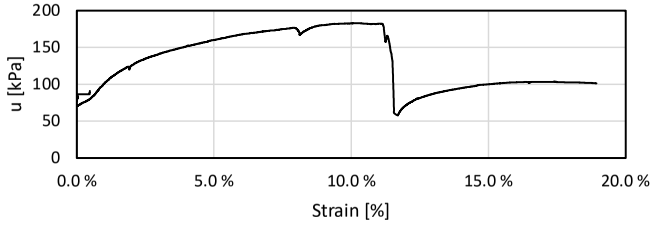

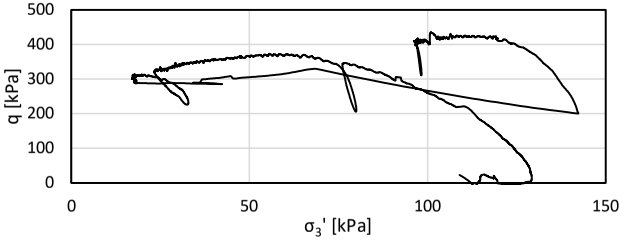

Test	Heigth	Cell pressure	Site
Undrained shear test	135 mm	100 kPa	Onsøy
Test no.	Diameter	Strain rate	Date
8	73 mm	1 %/h	04.02.2020
	Temperature	Depth	Remolded
	-5 °C	11 m	No

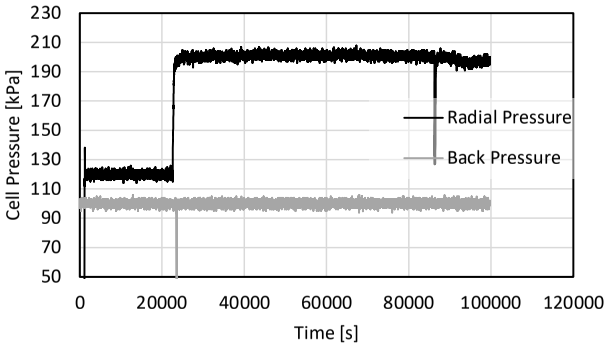

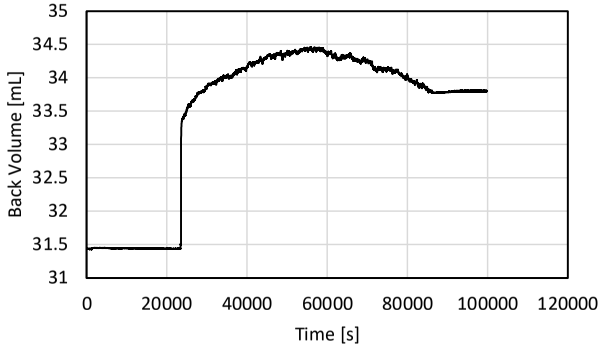

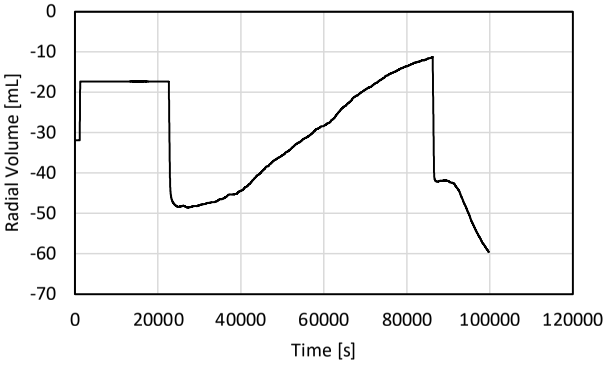

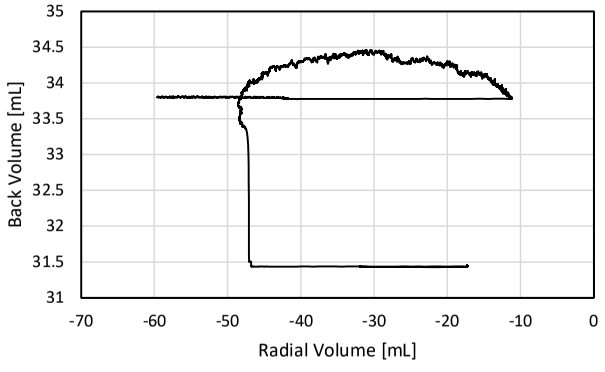

Test	Heigth	Cell pressure	Site
Undrained shear test	135 mm	100 kPa	Onsøy
	Diameter	Strain rate	Date
Test no.	73 mm	1 %/h	04.02.2020
8	Temperature	Depth	Remolded
	-5 °C	11 m	No

B.8 Test no. 9

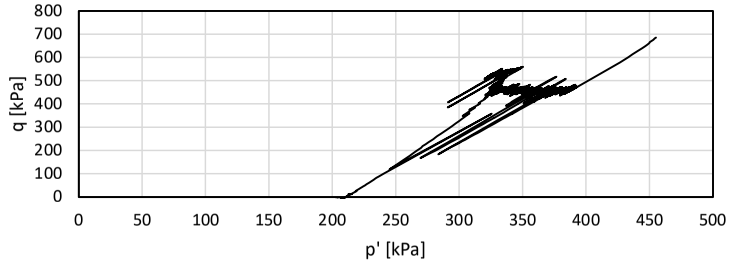

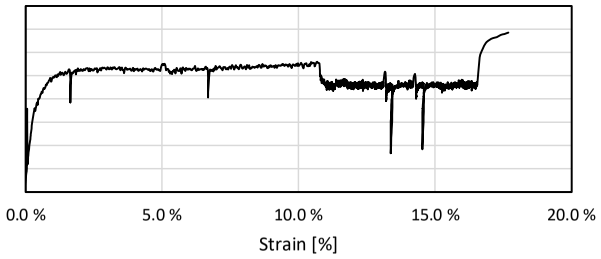

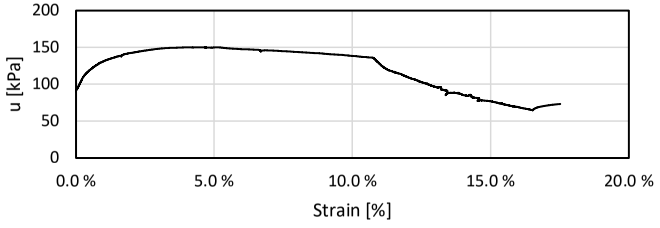

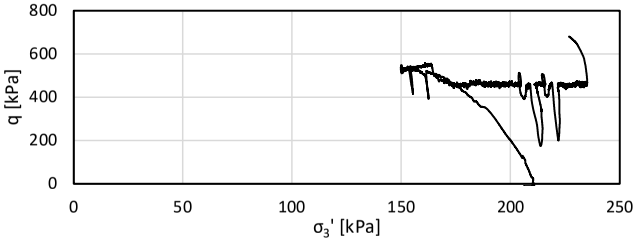

Test	Heigth	Cell pressure	Site
Undrained shear test	138 mm	200 kPa	Onsøy
	Diameter	Strain rate	Date
Test no.	73 mm	1 / 0.2 / 5 %/h	07.02.2020
9	Temperature	Depth	Remolded
	-5 °C	12 m	No

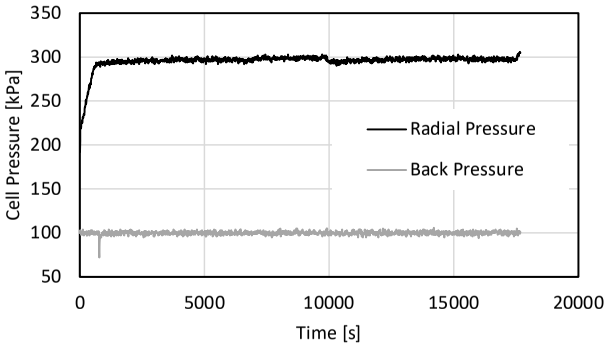

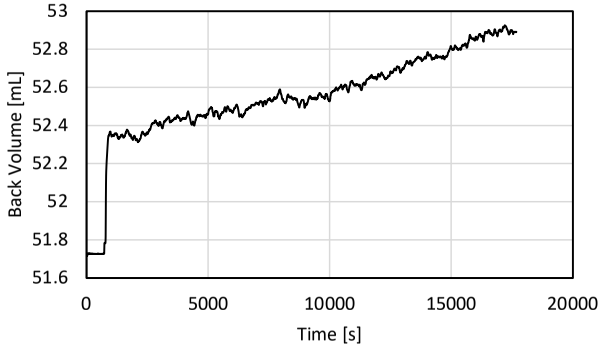

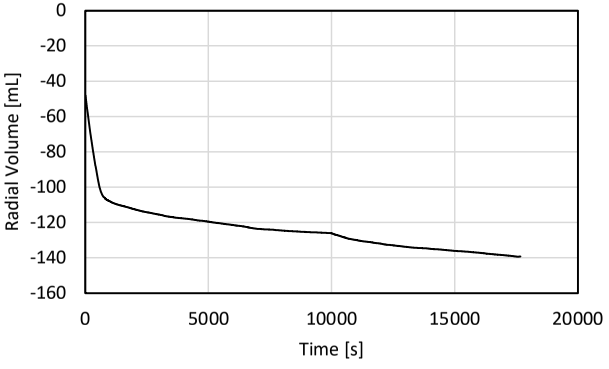

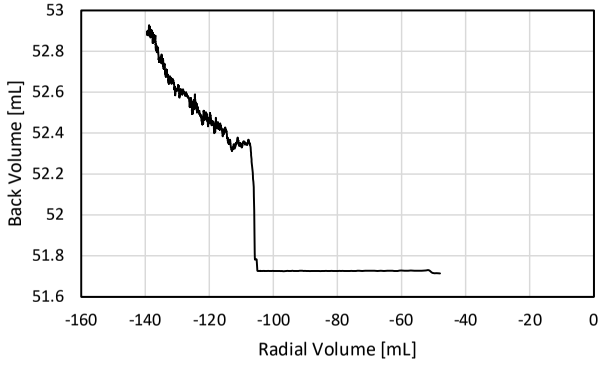

Test	Heigth	Cell pressure	Site
Undrained shear test	138 mm	200 kPa	Onsøy
	Diameter	Strain rate	Date
Test no.	73 mm	1 / 0.2 / 5 %/h	07.02.2020
9	Temperature	Depth	Remolded
	-5 °C	12 m	No

B.9 Test no. 10

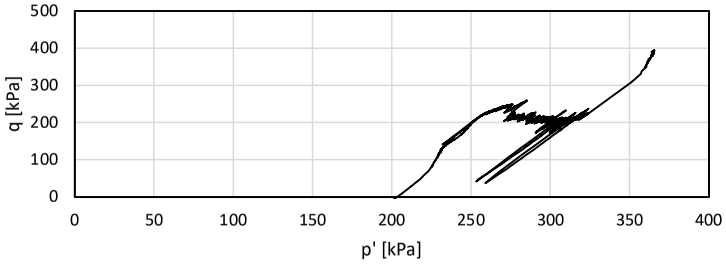

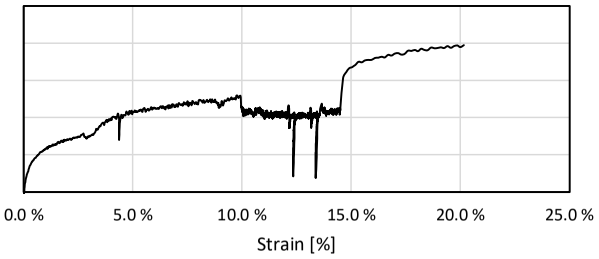

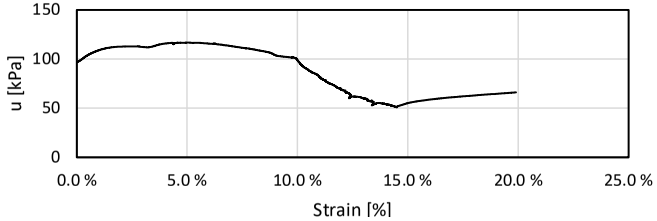

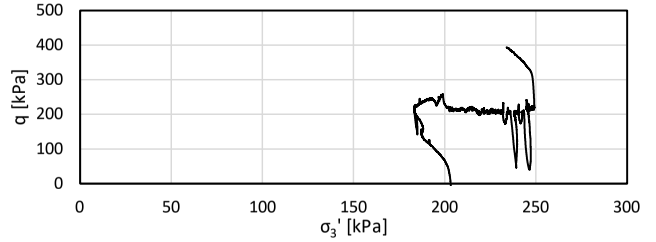

Test	Heigth	Cell pressure	Site
Undrained shear test	127 mm	200 kPa	Onsøy
Test no.	Diameter	Strain rate	Date
10	70 mm	1 / 0,2 / 5 %/h	10.02.2020
	Temperature	Depth	Remolded
	-5 °C	7 m	Yes

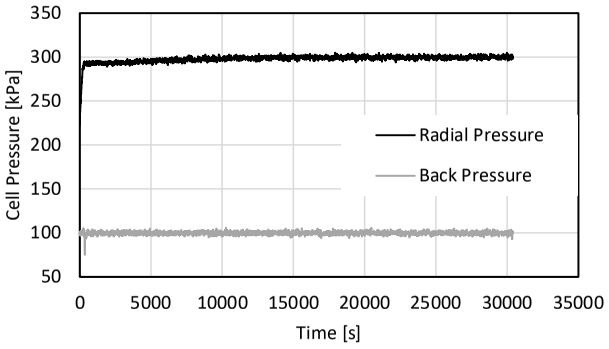

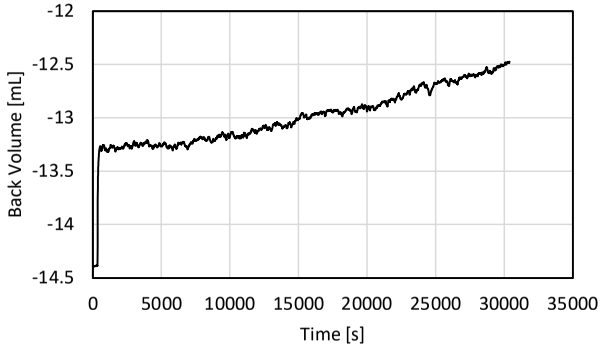

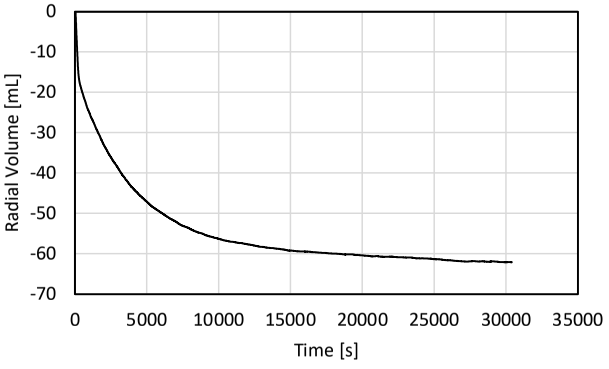

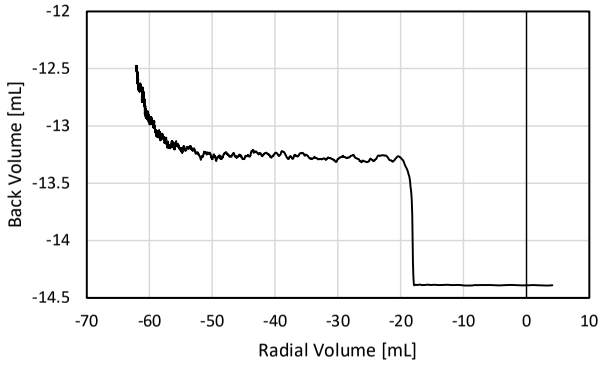

Test	Heigth	Cell pressure	Site
Undrained shear test	127 mm	200 kPa	Onsøy
	Diameter	Strain rate	Date
Test no.	70 mm	1 / 0,2 / 5 %/h	10.02.2020
10	Temperature	Depth	Remolded
	-5 °C	7 m	Yes

B.10 Test no. 11

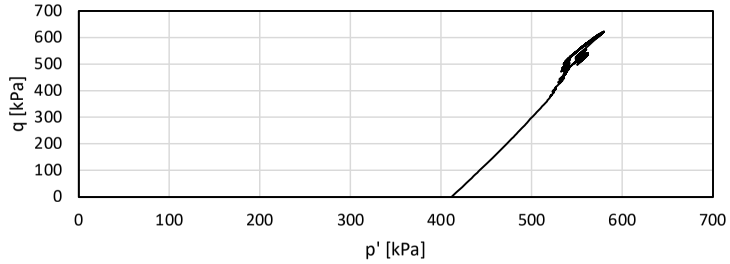

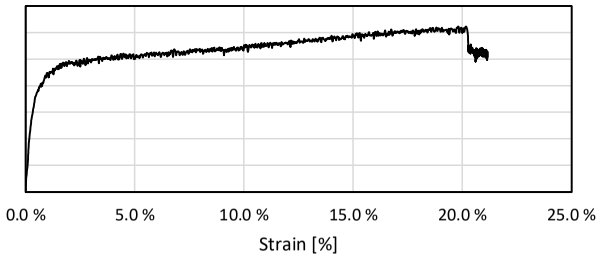

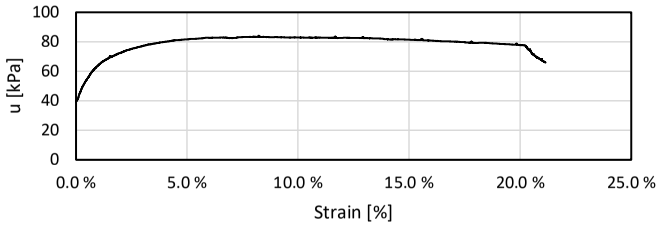

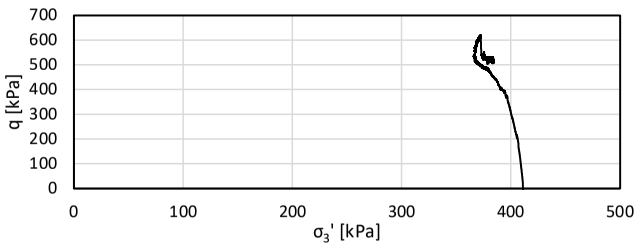

Test	Heigth	Cell pressure	Site
Undrained shear test	143 mm	400 kPa	Onsøy
	Diameter	Strain rate	Date
Test no.	73 mm	1 %/h	13.02.2020
11	Temperature	Depth	Remolded
	-5 °C	11.75 m	No

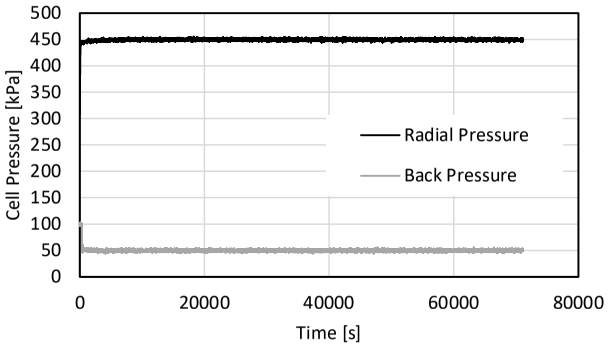

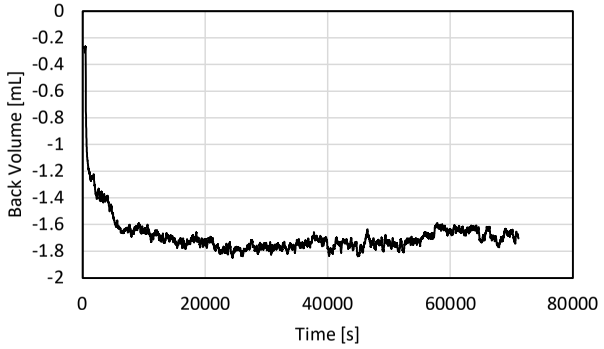

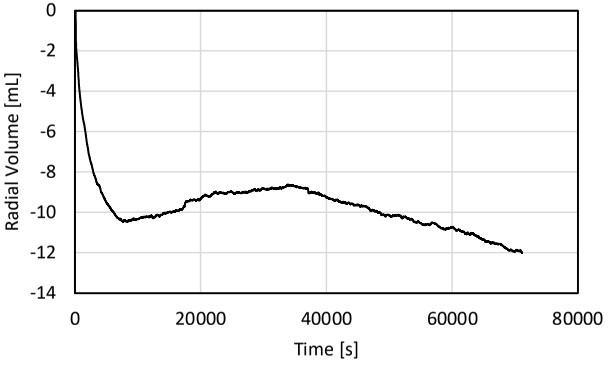

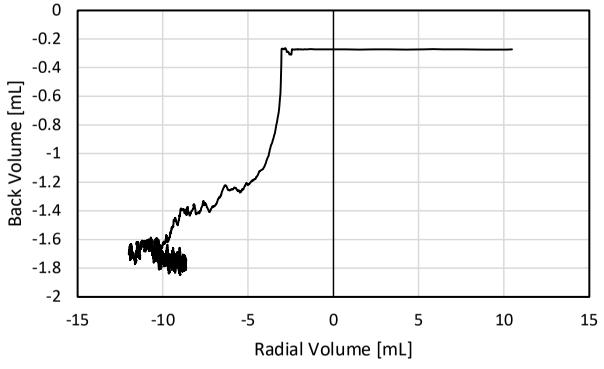

Test	Heigth	Cell pressure	Site
Undrained shear test	143 mm	400 kPa	Onsøy
	Diameter	Strain rate	Date
Test no.	73 mm	1 %/h	13.02.2020
11	Temperature	Depth	Remolded
	-5 °C	11.75 m	No

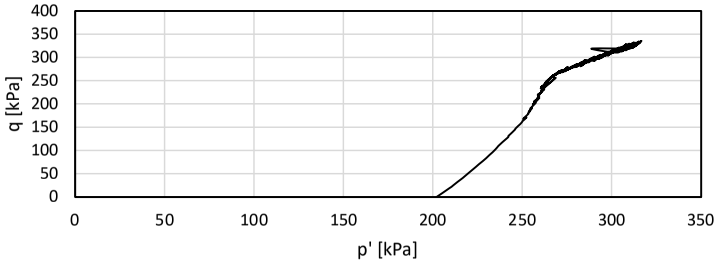

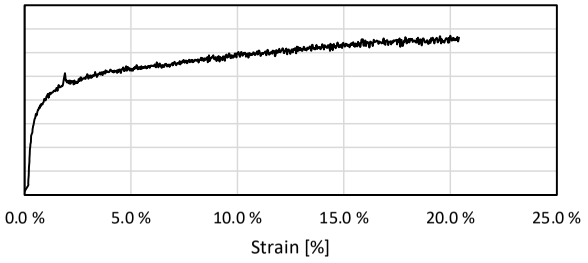

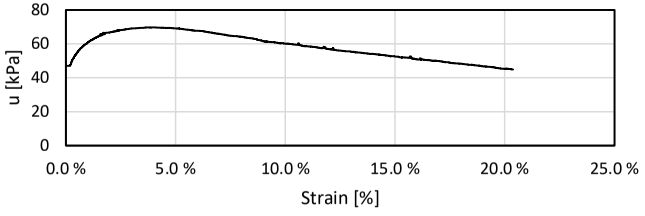

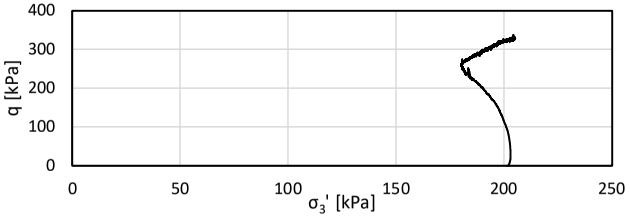

Test	Heigth	Cell pressure	Site
Undrained shear test	139 mm	250 kPa	Onsøy
	Diameter	Strain rate	Date
Test no.	70 mm	1 %/h	17.02.2020
12	Temperature	Depth	Remolded
	-5 °C	6,6-8 m	Yes

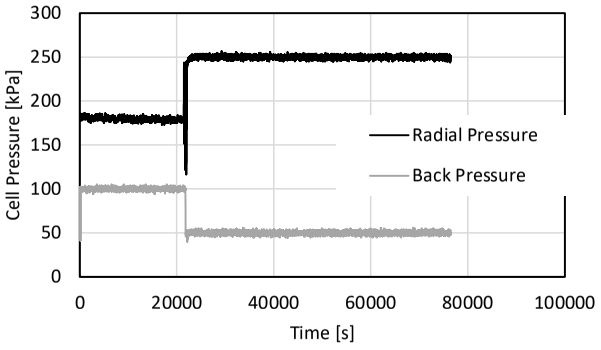

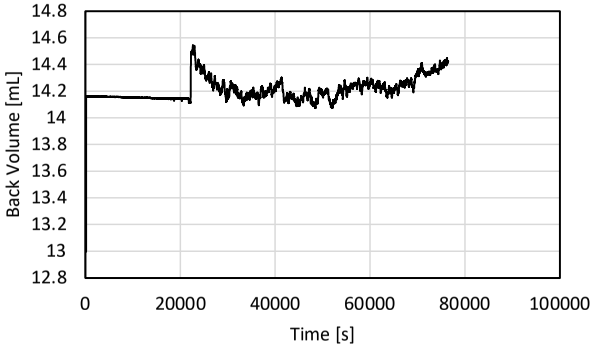

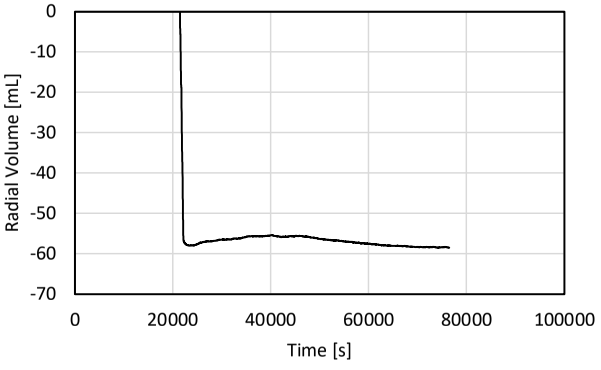

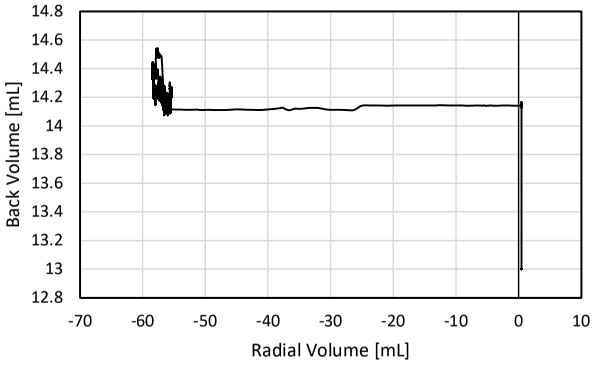

Test	Heigth	Cell pressure	Site
Undrained shear test	139 mm	250 kPa	Onsøy
	Diameter	Strain rate	Date
Test no.	70 mm	1 %/h	17.02.2020
12	Temperature	Depth	Remolded
	-5 °C	6,6-8 m	Yes

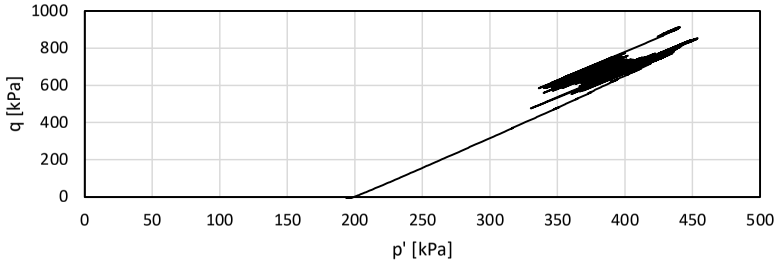

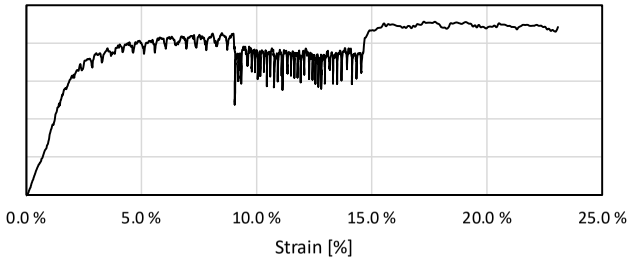

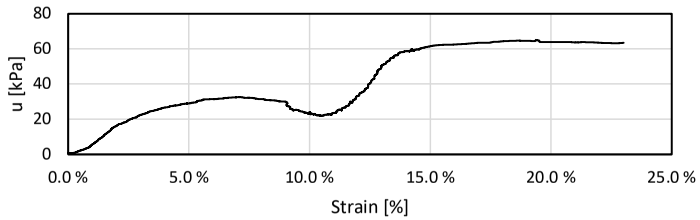

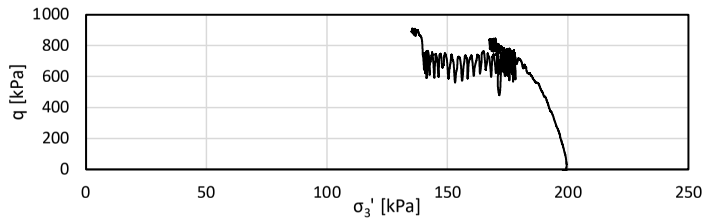

Test	Heigth	Cell pressure	Site
Undrained shear test	130 mm	200 kPa	Onsøy
	Diameter	Strain rate	Date
Test no.	70 mm	1 / 0.33 / 3 %/h	20.02.2020
13	Temperature	Depth	Remolded
	-10 °C	6.6-8.0 m	Yes

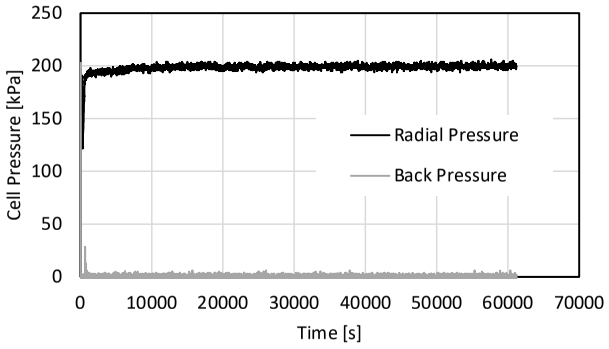

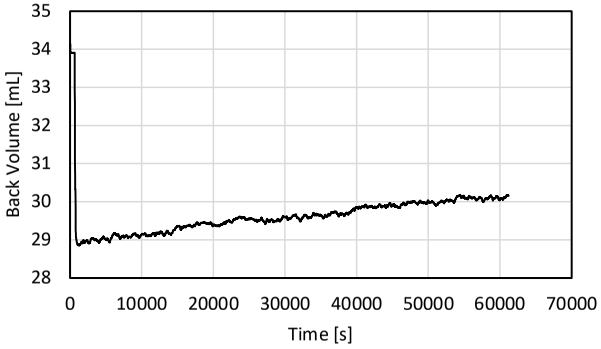

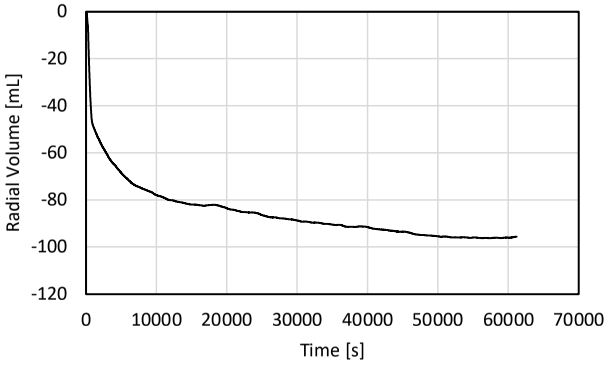

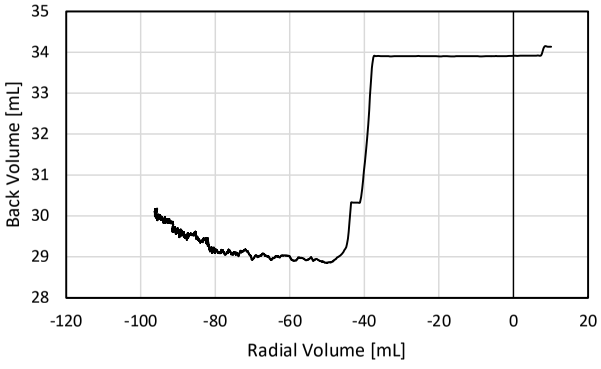

Test	Heigth	Cell pressure	Site
Undrained shear test	130 mm	200 kPa	Onsøy
	Diameter	Strain rate	Date
Test no.	70 mm	1 / 0.33 / 3 %/h	20.02.2020
13	Temperature	Depth	Remolded
	-10 °C	6.6-8.0 m	Yes

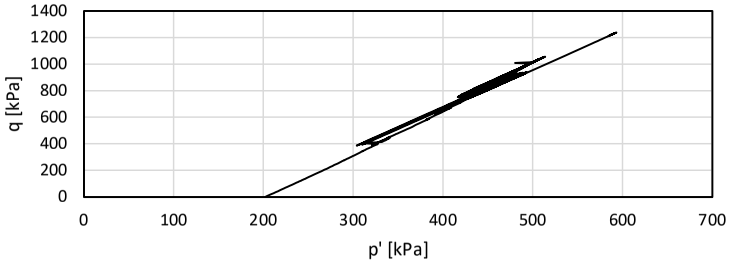

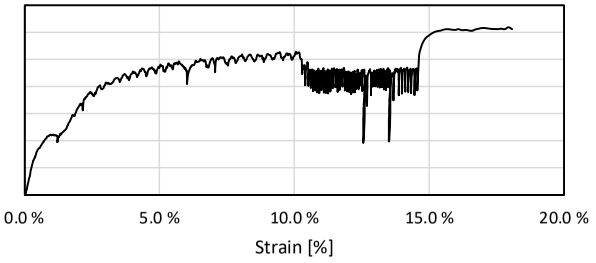

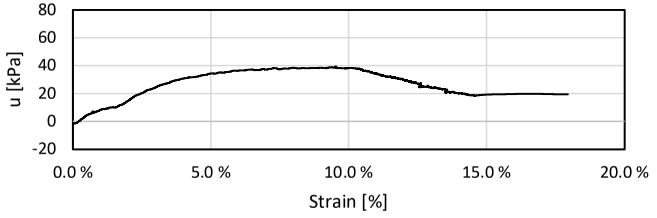

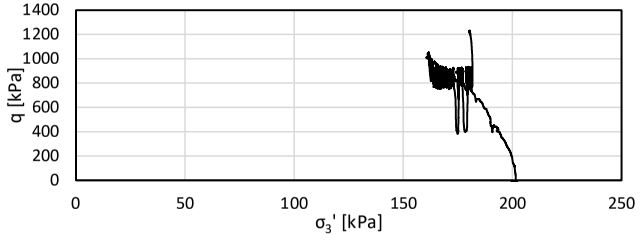

Test	Heigth	Cell pressure	Site
Undrained shear test	150 mm	200 kPa	Onsøy
Test no.	Diameter	Strain rate	Date
14	73 mm	1 / 0.2 / 5 %/h	24.02.2020
	Temperature	Depth	Remolded
	-10 °C	11-12 m	No

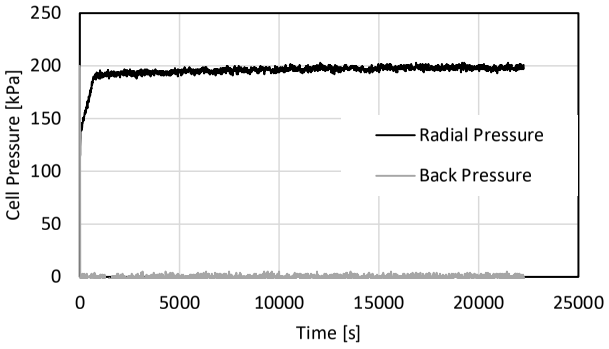

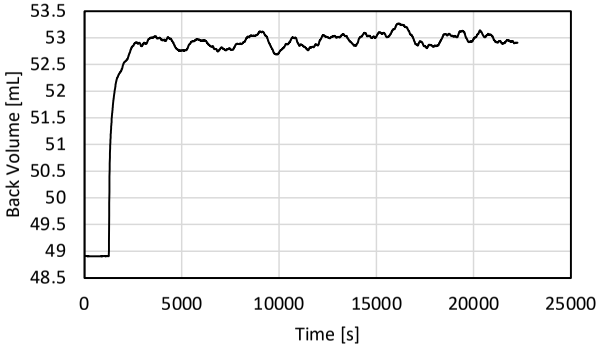

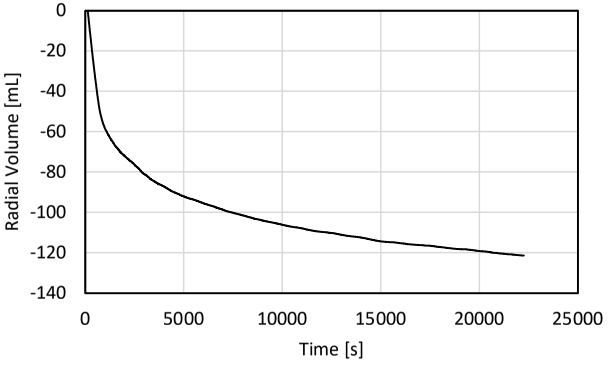

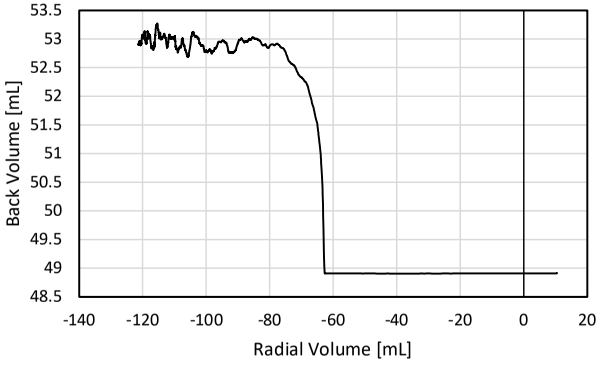

Test	Heigth	Cell pressure	Site
Undrained shear test	150 mm	200 kPa	Onsøy
	Diameter	Strain rate	Date
Test no.	73 mm	1 / 0.2 / 5 %/h	24.02.2020
14	Temperature	Depth	Remolded
	-10 °C	11-12 m	No

B.14 Test no. 15

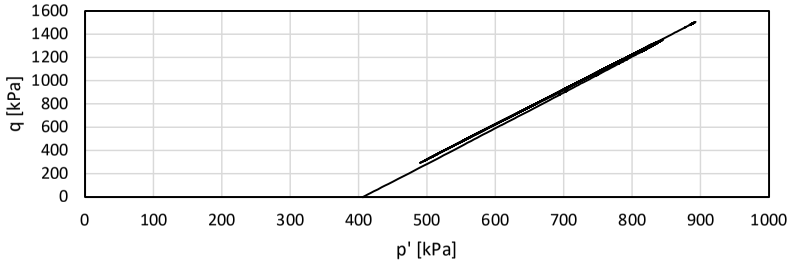

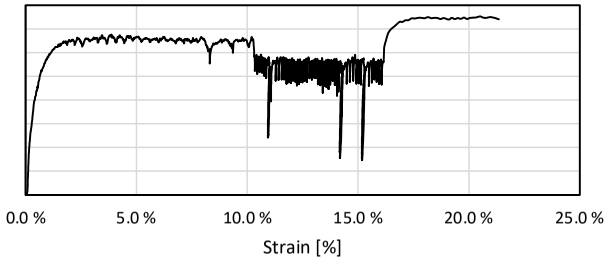

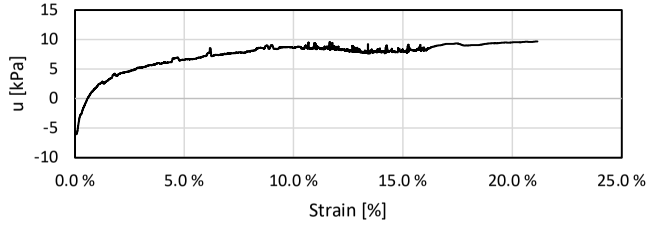

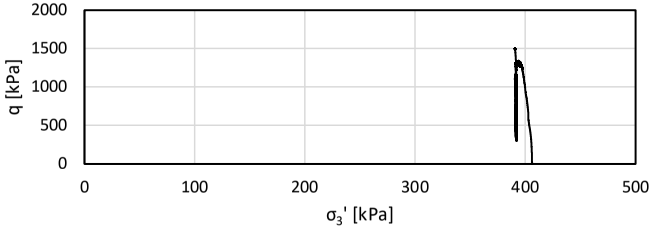

Test	Heigth	Cell pressure	Site
Undrained shear test	145 mm	400 kPa	Onsøy
	Diameter	Strain rate	Date
Test no.	73 mm	1 / 0.2 / 5 %/h	09.03.2020
15	Temperature	Depth	Remolded
	-10 °C	11-12 m	No

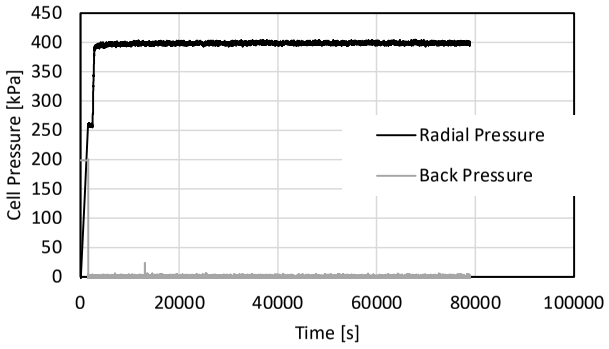

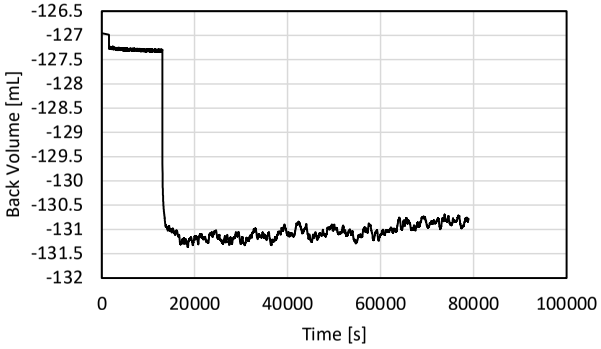

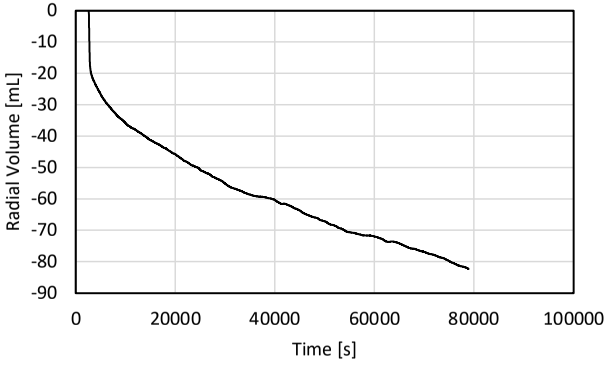

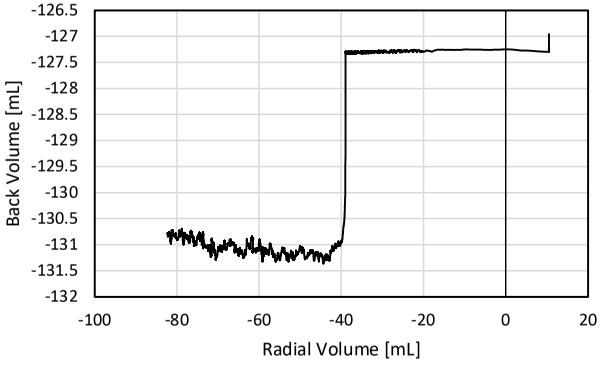

Test	Heigth	Cell pressure	Site
Undrained shear test	145 mm	400 kPa	Onsøy
	Diameter	Strain rate	Date
Test no.	73 mm	1 / 0.2 / 5 %/h	09.03.2020
15	Temperature	Depth	Remolded
	-10 °C	11-12 m	No

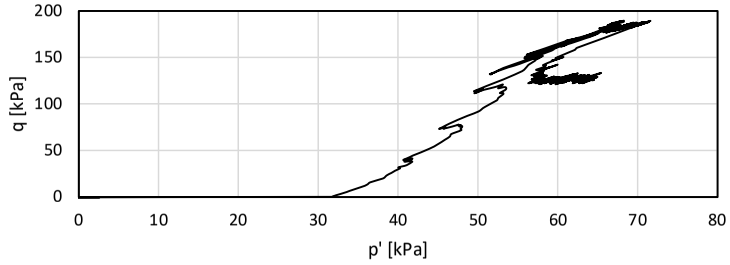

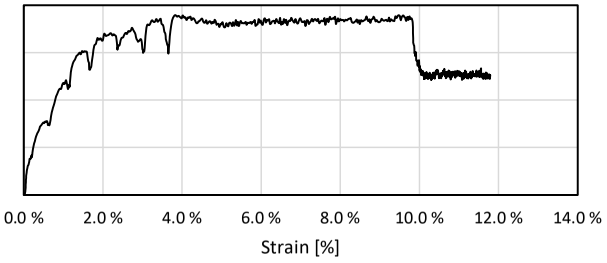

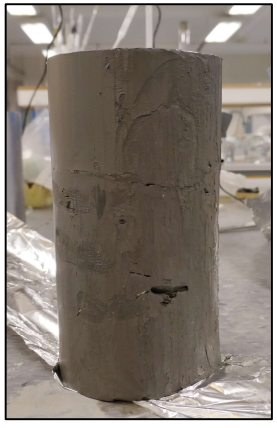

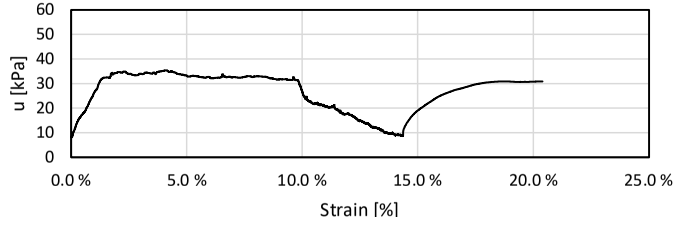

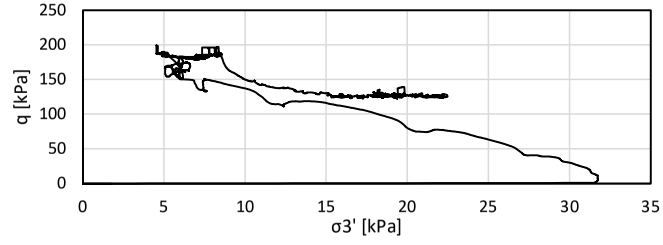

Test	Heigth	Cell pressure	Site
Undrained shear test	130 mm	20 kPa	Onsøy
Test no.	Diameter	Strain rate	Date
17	73 mm	1 / 0.2 %/h	08.05.2020
	Temperature	Depth	Remolded
	-3 °C		No

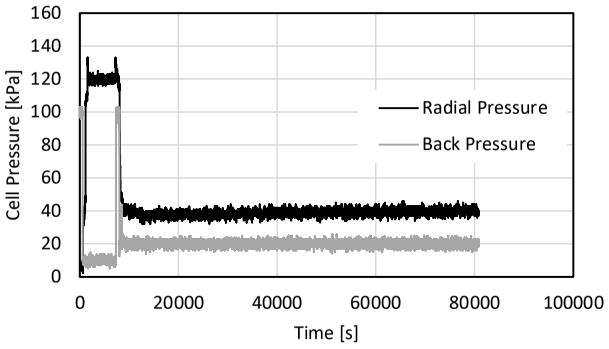

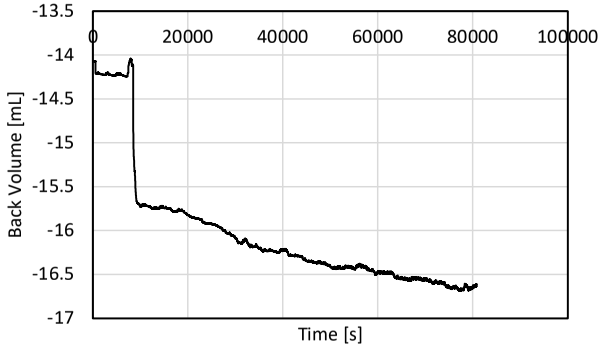

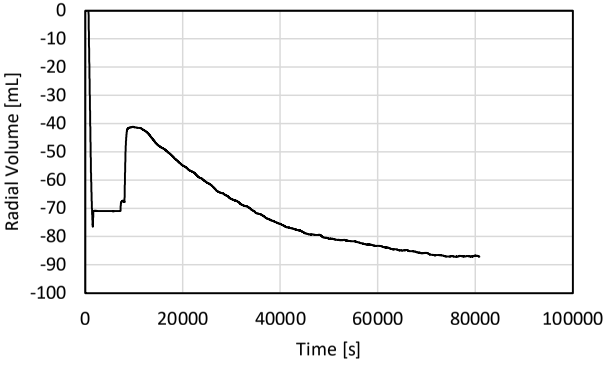

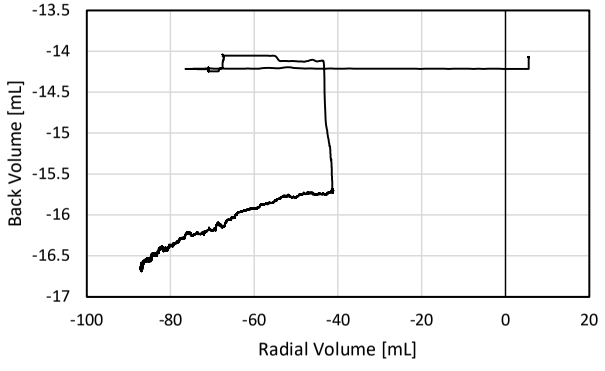

Test	Heigth	Cell pressure	Site
Undrained shear test	130 mm	20 kPa	Onsøy
	Diameter	Strain rate	Date
Test no.	73 mm	1 / 0.2 %/h	08.05.2020
17	Temperature	Depth	Remolded
	-3 °C		No

Appendix C

Computation

Equations used in calculating forces, stresses and strain in computing. Computations are done in Microsoft Excel.

Effective principle stresses,

$$\sigma_1' = \frac{F}{A} + \sigma_3 - u$$
$$\sigma_3' = \sigma_3 - u$$

Stresses,

$$q = \sigma_1' - \sigma_3'$$
$$p' = \frac{1}{3}(\sigma_1' + 2\sigma_3')$$

Vertical strain,

$$\varepsilon_a = \frac{\Delta L}{L_0}$$

Area correction,

$$A = A_0 \left(\frac{1}{1 - \varepsilon_a} \right)$$
$$h = h_0 - \varepsilon_a \cdot h_0$$
$$d = \sqrt{\frac{4 \cdot A}{\pi}}$$

Stresses are then calculated using the equations above. Height, h, and diameter, d, is used for quality assurance by comparing to measured cross-section after testing.

Appendix D

Testing Form

Experimental Table Sheet (Revised by Xin, natural clay soil testing)

General information

Date:	Density:		
Sample No:	Type:	Clay content (NGI):	
Time:	Depth:	Dimension (L×Φ):	
Water content (1): (Table below)		Salt content (1): (Table below)	
Observation: (Color……)			

Frozen natural test

Freezing method		Back pressure (kPa):	
Freezing time	—	LLVDT: Radial ☐ Vertical ☐	
Initial dimension (L×Φ):		Frozen dimension (L×Φ):	
Running sample size (L×Φ):		Running time	—
Drained ☐ Undrained ☐	σ_3 (kPa):	T (°C):	
Consolidation ☐	Time: —	Drainage (mL):	
CSR ☐	Strain rate (%/h):	CSC ☐	Load (kN):
Water content (2)		Salt content (2)	
Test issues			
MTS file		GDS file	

	Water content			Salt content	
	(1)	(2)		(1)	(2)
Mold (g)			Squeezed Liquid (g)		
Wet soil + Mold (g)			Added deion water (g)		
Dry soil + Mold (g)			Electrical Conduct. (mS)		

Note:
1. Carefully storage (aluminum and plastic foil + sealed bag);
2. Carefully mark numbers;
3. Write every detail of each test (good for back check), especially something wrong;
4. Always analyze the data immediately after test finishing:
5. Put original data, this table, sample analysis, selected typical photos into one folder;
6. Fill this table on the computer immediately after it is finished;

Details/ Action recorded	
B-test	